Volume 24, Number 2, 2024 ISSN 1562-8353

NONLINEAR DYNAMICS AND SYSTEMS THEORY
An International Journal of Research and Surveys

Volume 24 Number 2 2024

CONTENTS

 ISSN 1562-8353 Printed in Ukraine
To receive contents and abstracts by e-mail, visit our Website at: **http://www.e-ndst.kiev.ua**

NONLINEAR DYNAMICS & SYSTEMS THEORY Volume 24, No. 2, 2024

Nonlinear Dynamics and Systems Theory

An International Journal of Research and Surveys

InforMath Publishing Group
http://www.e-ndst.kiev.ua

Nonlinear Dynamics and Systems Theory
An International Journal of Research and Surveys

INSTRUCTIONS FOR CONTRIBUTORS

(1) General. Nonlinear Dynamics and Systems Theory (ND&ST) is an international journal devoted to publishing peer-refereed, high quality, original papers, brief notes and review articles focusing on nonlinear dynamics and systems theory and their practical applications in engineering, physical and life sciences. Submission of a manuscript is a representation that the submission has been approved by all of the authors and by the institution where the work was carried out. It also represents that the manuscript has not been previously published, has not been copyrighted, is not being submitted for publication elsewhere, and that the authors have agreed that the copyright in the article shall be assigned exclusively to InforMath Publishing Group by signing a transfer of copyright form. Before submission, the authors should visit the website:

http://www.e-ndst.kiev.ua

for information on the preparation of accepted manuscripts. Please download the archive Sample_NDST.zip containing example of article file (you can edit only the file Samplefilename.tex).

(2) Manuscript and Correspondence. Manuscripts should be in English and must meet common standards of usage and grammar. To submit a paper, send by e-mail a file in PDF format directly to

Professor A.A. Martynyuk, Institute of Mechanics,
Nesterov str.3, 03057, Kiev-57, Ukraine
e-mail: journalndst@gmail.com

or to one of the Regional Editors or to a member of the Editorial Board. Final version of the manuscript must typeset using LaTex program which is prepared in accordance with the style file of the Journal. Manuscript texts should contain the title of the article, name(s) of the author(s) and complete affiliations. Each article requires an abstract not exceeding 150 words. Formulas and citations should not be included in the abstract. AMS subject classifications and key words must be included in all accepted papers. Each article requires a running head (abbreviated form of the title) of no more than 30 characters. The sizes for regular papers, survey articles, brief notes, letters to editors and book reviews are: (i) 10-14 pages for regular papers, (ii) up to 24 pages for survey articles, and (iii) 2-3 pages for brief notes, letters to the editor and book reviews.

(3) Tables, Graphs and Illustrations. Each figure must be of a quality suitable for direct reproduction and must include a caption. Drawings should include all relevant details and should be drawn professionally in black ink on plain white drawing paper. In addition to a hard copy of the artwork, it is necessary to attach the electronic file of the artwork (preferably in PCX format).

(4) References. Each entry must be cited in the text by author(s) and number or by number alone. All references should be listed in their alphabetic order. Use please the following style:

Journal: [1] H. Poincare, Title of the article. *Title of the Journal* **volume** (issue) (year) pages. [Language]

Book: [2] A.M. Lyapunov, *Title of the Book.* Name of the Publishers, Town, year.

Proceeding: [3] R. Bellman, Title of the article. In: *Title of the Book.* (Eds.). Name of the Publishers, Town, year, pages. [Language]

(5) Proofs and Sample Copy. Proofs sent to authors should be returned to the Editorial Office with corrections within three days after receipt. The corresponding author will receive a sample copy of the issue of the Journal for which his/her paper is published.

(6) Editorial Policy. Every submission will undergo a stringent peer review process. An editor will be assigned to handle the review process of the paper. He/she will secure at least two reviewers' reports. The decision on acceptance, rejection or acceptance subject to revision will be made based on these reviewers' reports and the editor's own reading of the paper.

NONLINEAR DYNAMICS AND SYSTEMS THEORY
An International Journal of Research and Surveys
Published by InforMath Publishing Group since 2001

Volume 24 Number 2 2024

CONTENTS

Founded by A.A. Martynyuk in 2001.
Registered in Ukraine Number: KB No 5267 / 04.07.2001.

NONLINEAR DYNAMICS AND SYSTEMS THEORY

An International Journal of Research and Surveys

Impact Factor from SCOPUS for 2022: SJR – 0.293, SNIP – 0.784 and CiteScore – 1.5

Nonlinear Dynamics and Systems Theory (ISSN 1562–8353 (Print), ISSN 1813–7385 (Online)) is an international journal published under the auspices of the S.P. Timoshenko Institute of Mechanics of National Academy of Sciences of Ukraine and Curtin University of Technology (Perth, Australia). It aims to publish high quality original scientific papers and surveys in areas of nonlinear dynamics and systems theory and their real world applications.

AIMS AND SCOPE

Nonlinear Dynamics and Systems Theory is a multidisciplinary journal. It publishes papers focusing on proofs of important theorems as well as papers presenting new ideas and new theory, conjectures, numerical algorithms and physical experiments in areas related to nonlinear dynamics and systems theory. Papers that deal with theoretical aspects of nonlinear dynamics and/or systems theory should contain significant mathematical results with an indication of their possible applications. Papers that emphasize applications should contain new mathematical models of real world phenomena and/or description of engineering problems. They should include rigorous analysis of data used and results obtained. Papers that integrate and interrelate ideas and methods of nonlinear dynamics and systems theory will be particularly welcomed. This journal and the individual contributions published therein are protected under the copyright by International InforMath Publishing Group.

PUBLICATION AND SUBSCRIPTION INFORMATION

Nonlinear Dynamics and Systems Theory will have 6 issues in 2024, printed in hard copy (ISSN 1562–8353) and available online (ISSN 1813–7385), by InforMath Publishing Group, Nesterov str., 3, Institute of Mechanics, Kiev, MSP 680, Ukraine, 03057. Subscription prices are available upon request from the Publisher, EBSCO Information Services (`mailto:journals@ebsco.com`), or website of the Journal: `http://e-ndst.kiev.ua`. Subscriptions are accepted on a calendar year basis. Issues are sent by airmail to all countries of the world. Claims for missing issues should be made within six months of the date of dispatch.

ABSTRACTING AND INDEXING SERVICES

Papers published in this journal are indexed or abstracted in: Mathematical Reviews / MathSciNet, Zentralblatt MATH / Mathematics Abstracts, PASCAL database (INIST–CNRS) and SCOPUS.

Nonlinear Dynamics and Systems Theory, **24** (2) (2024) 111–122

Boundary Value Problem for Fractional q-Difference Equations

N. Allouch [1], S. Hamani [1*] and J. Henderson [2]

[1] *Laboratory of Pure and Applied Mathematics, Faculty of SEI, University of Mostaganem, B.P. 227, 27000, Mostaganem, Algeria.*
[2] *Department of Mathematics, Baylor University, Waco, Texas. 76798-7328, USA.*

Received: January 27, 2022; Revised: February 25, 2024

Abstract: In this paper, we study the existence of solutions for a class of boundary value problems for fractional q-difference equations involving the Caputo fractional q-difference derivative. Our results are given by applying some standard fixed point theorems. Furthermore, an example is presented to illustrate one of the main results.

Keywords: *fractional q-difference equations; Caputo fractional q-derivative; existence; fixed point; Leray-Schauder nonlinear alternative.*

Mathematics Subject Classification (2010): 26A33, 34A37, 70K05, 70K20.

1 Introduction

Fractional calculus is an important branch in mathematical analysis, currently being addressed by many researchers in various fields of science and engineering such as physics, chemistry, biology, economics, control theory, and biophysics, etc. For more details, see [15, 19, 22, 23, 27]. Recently, considerable attention has been given to the existence of solutions to the boundary value problems for fractional differential equations. See for example, the papers of Benchohra *et al.* [4, 10, 11] and references therein.

In 1910, Jackson [16, 17], the first researcher to develop q-difference calculus or quantum calculus in a systematic way, introduced the notions of the q-integral and some classical concepts.

Combining fractional calculus and q-calculus, we obtain fractional q-difference calculus. This generalizes q-calculus by defining the q-derivatives and q-integrals in an arbitrary order. The fractional q-difference calculus had its origin in the end of the

* Corresponding author: mailto:hamani_samira@yahoo.fr

sixties with the works of Al-Salam [7] and Agarwal [3]. For an extended book on the subject, we suggest to the reader the recent book [9]. Since then, there has appeared much work on the theory of fractional q-difference calculus and fractional q-difference equations, see [8, 24, 25] for example.

Moreover, fractional q-difference equations have wide applications in several fields such as engineering, economics, chemistry, physics, and so on. So, the boundary value problems for fractional q-difference equations involving the Caputo fractional q-derivative have become of importance and the existence of their solutions has been studied by a great number of researchers, see the references [1, 2, 5, 6, 26].

In this paper, motivated by the works of Benchohra *et al.* [11] and Benhamida *et al.* [12], we wish to discuss the existence of solutions of the boundary value problem for fractional q-difference equations of the form

$$({}^C D_q^\alpha y)(t) = f(t, y(t)), \text{ for a.e. } t \in J = [0, T], \quad 0 < \alpha \leq 1, \tag{1}$$

$$ay(0) + by(T) = c, \tag{2}$$

where $T > 0$, $q \in (0, 1)$, ${}^C D_q^\alpha$ is the Caputo fractional q-difference derivative of order $0 < \alpha \leq 1$, $f : [0, T] \times \mathbb{R} \to \mathbb{R}$ is a given function and a, b and c are real constants such that $a + b \neq 0$.

We give three existence results, one based on Banach's fixed point theorem, another based on Schaefer's fixed point theorem and the third based on Leray-Schauder nonlinear alternative theorem. Finally, we present an example.

2 Preliminaries

In this section, we introduce notations, definitions, and preliminary facts that will be used in the remainder of this paper.

Let $T > 0$ and define $J := [0, T]$. Consider the Banach space $C(J, \mathbb{R})$ of continuous functions from J into $\mathbb{R}$, with the norm

$$\|y\|_\infty = \sup\{|y(t)| : 0 \leq t \leq T\}.$$

Let $L^1(J, \mathbb{R})$ denote the Banach space of measurable functions $y : J \to \mathbb{R}$ which are Lebesgue integrable, with the norm

$$\|y\|_{L^1} = \int_J |y(t)| dt.$$

Now, we recall some definitions and properties of the fractional q-calculus [13, 18]. For $a \in \mathbb{R}$ and $0 < q < 1$, we set

$$[a]_q = \frac{1 - q^a}{1 - q}.$$

The q-analogue of the power $(a - b)^{(n)}$ is expressed by

$$(a - b)^{(0)} = 1, \ (a - b)^{(n)} = \prod_{k=0}^{n-1} (a - bq^k), \ a, b \in \mathbb{R}, \ n \in \mathbb{N}.$$

In general,

$$(a - b)^{(\alpha)} = a^\alpha \prod_{k=0}^{\infty} \left(\frac{a - bq^k}{a - bq^{k+\alpha}} \right), \ a, b, \alpha \in \mathbb{R}.$$

Note that if $b = 0$, then $a^{(\alpha)} = a^\alpha$.

Definition 2.1 [18] The q-gamma function is defined by

$$\Gamma_q(\alpha) = \frac{(1-q)^{(\alpha-1)}}{(1-q)^{\alpha-1}},\ \alpha \in \mathbb{R} - \{0, -1, -2, \ldots\}.$$

Notice that the q-gamma function satisfies $\Gamma_q(\alpha+1) = [\alpha]_q \Gamma_q(\alpha)$.

Definition 2.2 [18] The q-derivative of order $n \in \mathbb{N}$ of a function $f : J \to \mathbb{R}$, is defined by $(D_q^0 f)(t) = f(t)$,

$$(D_q f)(t) = (D_q^1 f)(t) = \frac{f(t) - f(qt)}{(1-q)t},\ t \neq 0,\ (D_q f)(0) = \lim_{t \to 0} (D_q f)(t),$$

and

$$(D_q^n f)(t) = (D_q^1 D_q^{n-1} f)(t),\ t \in J,\ n \in \{1, 2, \ldots\}.$$

Set $J_t := \{tq^n : n \in \mathbb{N}\} \cup \{0\}$.

Definition 2.3 [18] The q-integral of a function $f : J_t \to \mathbb{R}$, is defined by

$$(I_q f)(t) = \int_0^t f(s) d_q s = \sum_{n=0}^{\infty} t(1-q) q^n f(tq^n),$$

provided that the series converges.

We note that $(D_q I_q f)(t) = f(t)$, while if f is continuous at 0, then

$$(I_q D_q f)(t) = f(t) - f(0).$$

Definition 2.4 [3] The Riemann-Liouville fractional q-integral of order $\alpha \geq 0$ of a function $f : J \to \mathbb{R}$ is defined by $(I_q^0 f)(t) = f(t)$, and

$$(I_q^\alpha f)(t) = \int_0^t \frac{(t - qs)^{(\alpha-1)}}{\Gamma_q(\alpha)} f(s) d_q s,\ t \in J.$$

Note that for $\alpha = 1$, we have $(I_q^1 f)(t) = (I_q f)(t)$.

Lemma 2.1 *[25] For $\alpha \geq 0$ and $\beta \in (-1, +\infty)$, we have*

$$(I_q^\alpha (t-a)^{(\beta)})(t) = \frac{\Gamma_q(\beta+1)}{\Gamma_q(\alpha+\beta+1)} (t-a)^{(\alpha+\beta)},\ 0 < a < t < T.$$

In particular,

$$(I_q^\alpha 1)(t) = \frac{1}{\Gamma_q(\alpha+1)} t^{(\alpha)}.$$

Definition 2.5 [24] The Riemann-Liouville fractional q-derivative of order $\alpha \geq 0$ of a function $f : J \to \mathbb{R}$ is defined by $(D_q^0 f)(t) = f(t)$, and

$$(D_q^\alpha f)(t) = (D_q^{[\alpha]} I_q^{[\alpha]-\alpha} f)(t),\ t \in J,$$

where $[\alpha]$ is the integer part of α.

Definition 2.6 [24] The Caputo fractional q-derivative of order $\alpha \geq 0$ of a function $f : J \to \mathbb{R}$ is defined by $(D_q^0 f)(t) = f(t)$, and

$$({}^C D_q^\alpha f)(t) = (I_q^{[\alpha]-\alpha} D_q^{[\alpha]} f)(t), \ t \in J,$$

where $[\alpha]$ is the integer part of α.

Lemma 2.2 *[24] Let $\alpha, \beta \geq 0$ and let f be a function defined on J. Then the following identities hold:*

(i) $(I_q^\alpha I_q^\beta f)(t) = (I_q^{\alpha+\beta} f)(t)$,

(ii) $(D_q^\alpha I_q^\alpha f)(t) = f(t)$.

Lemma 2.3 *[24] Let $\alpha \geq 0$ and let f be a function defined on J. Then the following equality holds:*

$$(I_q^\alpha \ {}^C D_q^\alpha f)(t) = f(t) - \sum_{k=0}^{[\alpha]-1} \frac{t^k}{\Gamma_q(k+1)} (D_q^k f)(0).$$

In particular, if $\alpha \in (0,1)$, then

$$(I_q^\alpha \ {}^C D_q^\alpha f)(t) = f(t) - f(0).$$

Next, we offer a variety of fixed point theorems.

Theorem 2.1 (Banach contraction principle) [14]
Let C be a non-empty closed subset of a Banach space X, then any contraction mapping H of C into itself has a unique fixed point.

Theorem 2.2 *(Schaefer) [28] Let X be a Banach space and $H : X \to X$ be a completely continuous operator. If the set*

$$E(H) := \{y \in X : y = \lambda H(y), \ for \ \lambda \in (0,1)\}$$

is bounded, then H has a fixed point.

Theorem 2.3 *(Nonlinear alternative of Leray-Schauder) [14] Let X be a Banach space and C be a closed, convex subset of X. Let U be an open subset of C with $0 \in U$ and $H : \overline{U} \to C$ be a continuous and compact operator. Then either*

(a) H has fixed points, or

(b) There exist $y \in \partial U$ and $\lambda \in (0,1)$ with $y = \lambda H(y)$.

3 Main Results

Let us start by defining what we mean by a solution of the problem (1)-(2).

Definition 3.1 A function $y \in C(J, \mathbb{R})$ is said to be a solution of the problem (1)-(2) if y satisfies the equation $({}^C D_q^\alpha y)(t) = f(t, y(t))$ on J, and satisfies the condition $ay(0) + by(T) = c$.

For the existence of solutions to the problem (1)-(2), we need the following auxiliary lemma.

Lemma 3.1 *Let $h : J \to \mathbb{R}$ be continuous, the solution of the boundary value problem*

$$({}^C D_q^\alpha y)(t) = h(t),\ t \in J = [0,T], \quad 0 < \alpha \leq 1, \tag{3}$$

$$ay(0) + by(T) = c, \tag{4}$$

is given by

$$y(t) = \int_0^t \frac{(t-qs)^{(\alpha-1)}}{\Gamma_q(\alpha)} h(s) d_q s - \frac{b}{a+b} \int_0^T \frac{(T-qs)^{(\alpha-1)}}{\Gamma_q(\alpha)} h(s) d_q s + \frac{c}{a+b}. \tag{5}$$

Proof. Applying the Riemann-Liouville fractional q-integral of order α to both sides of equation (3), and by using Lemma 2.3, we have

$$y(t) = \int_0^t \frac{(t-qs)^{(\alpha-1)}}{\Gamma_q(\alpha)} h(s) d_q s + c_0. \tag{6}$$

Using the boundary condition of the problem in (4), we obtain

$$ay(0) + by(T) = ac_0 + b(I_q^\alpha h(T) + c_0) = c.$$

So

$$c_0 = \frac{c}{a+b} - \frac{b}{a+b} I_q^\alpha h(T).$$

Finally, by substitution of c_0 into (6), we give

$$y(t) = \int_0^t \frac{(t-qs)^{(\alpha-1)}}{\Gamma_q(\alpha)} h(s) d_q s - \frac{b}{a+b} \int_0^T \frac{(T-qs)^{(\alpha-1)}}{\Gamma_q(\alpha)} h(s) d_q s + \frac{c}{a+b}.$$

The proof is completed. □

In the following subsections we prove the existence and uniqueness results of the problem (1)-(2) by using a variety of fixed point theorems.

We consider the following hypotheses:

($H1$) The function $f : [0,T] \times \mathbb{R} \to \mathbb{R}$ is continuous.

($H2$) There exists a constant $L > 0$ such that

$$|f(t,x) - f(t,y)| \leq L|x-y|,\ for\ each\ t \in J\ and\ each\ x, y \in \mathbb{R}.$$

($H3$) There exists a constant $M > 0$ such that

$$|f(t,x)| \leq M,\ for\ each\ t \in J\ and\ each\ x \in \mathbb{R}.$$

The first result is based on the Banach contraction principle theorem (Theorem 2.1).

Theorem 3.1 *Assume that the hypothesis ($H2$) is satisfied. If*

$$\left(1 + \frac{|b|}{|a+b|}\right) \frac{LT^{(\alpha)}}{\Gamma_q(\alpha+1)} < 1, \tag{7}$$

then the problem (1)-(2) has a unique solution on $[0,T]$.

Proof. Transform the problem (1)-(2) into a fixed point problem. Consider the operator

$$H : C(J,\mathbb{R}) \longrightarrow C(J,\mathbb{R})$$

defined by

$$\begin{aligned} (Hy)(t) &= \int_0^t \frac{(t-qs)^{(\alpha-1)}}{\Gamma_q(\alpha)} f(s,y(s))d_qs \\ &\quad -\frac{b}{a+b}\int_0^T \frac{(T-qs)^{(\alpha-1)}}{\Gamma_q(\alpha)} f(s,y(s))d_qs + \frac{c}{a+b}. \end{aligned} \tag{8}$$

By Lemma 3.1, the fixed points of H are the solutions of the problem (1)-(2). We shall prove that H is a contraction mapping on $C(J,\mathbb{R})$.

For $x,y \in C(J,\mathbb{R})$ and for each $t \in J = [0,T]$, we have

$$\begin{aligned} |(Hx)(t)-(Hy)(t)| &= \Bigg| \int_0^t \frac{(t-qs)^{(\alpha-1)}}{\Gamma_q(\alpha)} \left(f(s,x(s))-f(s,y(s))\right) d_qs \\ &\quad -\frac{b}{a+b}\int_0^T \frac{(T-qs)^{(\alpha-1)}}{\Gamma_q(\alpha)} \left(f(s,x(s))-f(s,y(s))\right) d_qs \Bigg|. \end{aligned}$$

Therefore, by $(H2)$, we obtain

$$\begin{aligned} |(Hx)(t)-(Hy)(t)| &\leq \int_0^t \frac{(t-qs)^{(\alpha-1)}}{\Gamma_q(\alpha)} |f(s,x(s))-f(s,y(s))| \, d_qs \\ &\quad +\frac{|b|}{|a+b|}\int_0^T \frac{(T-qs)^{(\alpha-1)}}{\Gamma_q(\alpha)} |f(s,x(s))-f(s,y(s))| \, d_qs, \\ &\leq L\int_0^t \frac{(t-qs)^{(\alpha-1)}}{\Gamma_q(\alpha)} |x(s)-y(s)| \, d_qs \\ &\quad +\frac{L|b|}{|a+b|}\int_0^T \frac{(T-qs)^{(\alpha-1)}}{\Gamma_q(\alpha)} |x(s)-y(s)| \, d_qs. \end{aligned}$$

Hence

$$\|H(x)-H(y)\|_\infty \leq \left(1+\frac{|b|}{|a+b|}\right)\frac{LT^{(\alpha)}}{\Gamma_q(\alpha+1)}\|x-y\|_\infty.$$

By (7), H is a contraction, and by the Banach contraction principle theorem, we deduce that H has a unique fixed point, which is the unique solution of the problem (1)-(2). □

The second result is based on Schaefer's fixed point theorem (Theorem 2.2).

Theorem 3.2 *Assume that the hypotheses* ($H1$) *and* ($H3$) *hold. Then the problem (1)-(2) has at least one solution on* $[0, T]$.

Proof. We shall use Schaefer's fixed point theorem to prove that H defined by (8) has a fixed point.
The proof will be given in several steps.

Step 1: *H is continuous.*

Let $\{y_n\}_{n\in\mathbb{N}}$ be a sequence such that $y_n \to y$ in $C(J, \mathbb{R})$. Then, for each $t \in J$, we have

$$\begin{aligned} |(Hy_n)(t) - (Hy)(t)| &\leq \int_0^t \frac{(t-qs)^{(\alpha-1)}}{\Gamma_q(\alpha)} |f(s, y_n(s)) - f(s, y(s))|\, d_q s \\ &\quad + \frac{|b|}{|a+b|} \int_0^T \frac{(T-qs)^{(\alpha-1)}}{\Gamma_q(\alpha)} |f(s, y_n(s)) - f(s, y(s))|\, d_q s. \end{aligned}$$

Hence, for each $t \in J$, we find

$$\|H(y_n) - H(y)\|_\infty \leq \left(1 + \frac{|b|}{|a+b|}\right) \frac{T^{(\alpha)}}{\Gamma_q(\alpha+1)} \|f(., y_n(.)) - f(., y(.))\|_\infty.$$

Since f is continuous, we have

$$\|H(y_n) - H(y)\|_\infty \to 0 \quad as \quad n \to \infty.$$

Consequently, H is continuous on $C(J, \mathbb{R})$.

Step 2: *H maps bounded sets into bounded sets in $C(J, \mathbb{R})$.*

Indeed, it is enough to show that for any $r > 0$, there exists a positive constant R such that for each $y \in B_r = \{y \in C(J, \mathbb{R}) : \|y\|_\infty \leq r\}$, we have $\|H(y)\|_\infty \leq R$.
Let $y \in B_r$. Then, for each $t \in J$, we have

$$|(Hy)(t)| = \left| \int_0^t \frac{(t-qs)^{(\alpha-1)}}{\Gamma_q(\alpha)} f(s, y(s)) d_q s - \frac{b}{a+b} \int_0^T \frac{(T-qs)^{(\alpha-1)}}{\Gamma_q(\alpha)} f(s, y(s)) d_q s + \frac{c}{a+b} \right|.$$

By ($H3$), we obtain

$$\begin{aligned} |(Hy)(t)| &\leq \int_0^t \frac{(t-qs)^{(\alpha-1)}}{\Gamma_q(\alpha)} |f(s, y(s))| d_q s \\ &\quad + \frac{|b|}{|a+b|} \int_0^T \frac{(T-qs)^{(\alpha-1)}}{\Gamma_q(\alpha)} |f(s, y(s))| d_q s + \frac{|c|}{|a+b|}, \\ &\leq \left(1 + \frac{|b|}{|a+b|}\right) \frac{MT^{(\alpha)}}{\Gamma_q(\alpha+1)} + \frac{|c|}{|a+b|}. \end{aligned}$$

Hence

$$\|H(y)\|_\infty \leq \left(1 + \frac{|b|}{|a+b|}\right) \frac{MT^{(\alpha)}}{\Gamma_q(\alpha+1)} + \frac{|c|}{|a+b|} := R.$$

Consequently, H is uniformly bounded on B_r.

Step 3: *H maps bounded sets into equicontinuous sets of $C(J,\mathbb{R})$.*

Let $t_1, t_2 \in J$, $t_1 < t_2$ and let B_r be a bounded set of $C(J,\mathbb{R})$ as in Step 2. Let $y \in B_r$, then

$$\begin{aligned}|(Hy)(t_2) - (Hy)(t_1)| &= \left| \int_0^{t_2} \frac{(t_2 - qs)^{(\alpha-1)}}{\Gamma_q(\alpha)} f(s, y(s)) d_q s \right. \\ &\quad \left. - \int_0^{t_1} \frac{(t_1 - qs)^{(\alpha-1)}}{\Gamma_q(\alpha)} f(s, y(s)) d_q s \right|, \\ &\leq \int_0^{t_1} \frac{\left((t_2 - qs)^{(\alpha-1)} - (t_1 - qs)^{(\alpha-1)}\right)}{\Gamma_q(\alpha)} |f(s, y(s))| d_q s \\ &\quad + \int_{t_1}^{t_2} \frac{(t_2 - qs)^{(\alpha-1)}}{\Gamma_q(\alpha)} |f(s, y(s))| d_q s.\end{aligned}$$

By $(H3)$, we get

$$\begin{aligned}|(Hy)(t_2) - (Hy)(t_1)| &\leq \frac{M}{\Gamma_q(\alpha)} \int_0^{t_1} \left((t_2 - qs)^{(\alpha-1)} - (t_1 - qs)^{(\alpha-1)}\right) d_q s \\ &\quad + \frac{M}{\Gamma_q(\alpha)} \int_{t_1}^{t_2} (t_2 - qs)^{(\alpha-1)} d_q s.\end{aligned}$$

Thus

$$\|(Hy)(t_2) - (Hy)(t_1)\|_\infty \leq \frac{M}{\Gamma_q(\alpha+1)} \left(t_2^{(\alpha)} - t_1^{(\alpha)}\right).$$

As $t_1 \to t_2$, the right-hand side of the above inequality tends to zero.

As a consequence of Steps 1, 2 and 3, together with the Arzela-Ascoli theorem, we can conclude that H is completely continuous.

Step 4: *A priori bound.*

Now, we prove that the set $\Omega = \{y \in C(J,\mathbb{R}) : y = \lambda H(y), 0 < \lambda < 1\}$ is bounded. Let $y \in \Omega$. Thus, for each $t \in J$, we have

$$\begin{aligned}y(t) &= \lambda (Hy)(t), \\ &= \lambda \left(\int_0^t \frac{(t - qs)^{(\alpha-1)}}{\Gamma_q(\alpha)} f(s, y(s)) d_q s \right. \\ &\quad \left. - \frac{b}{a+b} \int_0^T \frac{(T - qs)^{(\alpha-1)}}{\Gamma_q(\alpha)} f(s, y(s)) d_q s + \frac{c}{a+b} \right).\end{aligned}$$

Then, by $(H3)$ (as in Step 2), it follows that, for each $t \in J$, we get

$$\|y(t)\|_\infty \leq \left(1 + \frac{|b|}{|a+b|}\right) \frac{MT^{(\alpha)}}{\Gamma_q(\alpha+1)} + \frac{|c|}{|a+b|}.$$

Consequently, $\|y(t)\|_\infty \leq R < \infty$, the set Ω is bounded.

As a consequence of Schaefer's fixed point theorem, we deduce that H has a fixed point which is a solution of the problem (1)-(2). □

The third result is based on the Leray-Schauder nonlinear alternative theorem (Theorem 2.3).

Theorem 3.3 *Assume that (H1) holds and the following hypotheses are satisfied:*

(H4) There exist $\phi_f \in L^1(J,\mathbb{R}_+)$ and $\psi : [0,\infty) \to (0,\infty)$ are continuous and nondecreasing such that

$$|f(t,y)| \leq \phi_f(t)\psi(|y|) \text{ for each } t \in J \text{ and each } y \in \mathbb{R}.$$

(H5) There exists a number $\nu > 0$ such that

$$\frac{\nu}{\left(1+\frac{|b|}{|a+b|}\right)\psi(\nu)(I_q^{\alpha}\phi_f)(T)+\frac{|c|}{|a+b|}} \quad > \quad 1.$$

Then the problem (1)-(2) has at least one solution on $[0,T]$.

Proof. We shall use the Leray-Schauder theorem to prove that H defined by (8) has a fixed point. As shown in Theorem 3.2, we see that the operator H is continuous and completely continuous.

Let $y \in C(J,\mathbb{R})$ such that for each $t \in [0,T]$, we have $y(t) = \lambda(Hy)(t)$ for $\lambda \in (0,1)$. Then, from $(H4)$ and for every $t \in J$, we give

$$\begin{aligned}
|y(t)| \quad &\leq \quad \int_0^t \frac{(t-qs)^{(\alpha-1)}}{\Gamma_q(\alpha)}|f(s,y(s))|d_qs \\
&\quad +\frac{|b|}{|a+b|}\int_0^T \frac{(T-qs)^{(\alpha-1)}}{\Gamma_q(\alpha)}|f(s,y(s))|d_qs+\frac{|c|}{|a+b|}, \\
&\leq \quad \int_0^t \frac{(t-qs)^{(\alpha-1)}}{\Gamma_q(\alpha)}\phi_f(s)\psi(|y|)d_qs \\
&\quad +\frac{|b|}{|a+b|}\int_0^T \frac{(T-qs)^{(\alpha-1)}}{\Gamma_q(\alpha)}\phi_f(s)\psi(|y|)d_qs+\frac{|c|}{|a+b|}.
\end{aligned}$$

Thus

$$\|y\|_\infty \quad \leq \quad \left(1+\frac{|b|}{|a+b|}\right)\psi(\|y\|_\infty)(I_q^{\alpha}\phi_f)(T)+\frac{|c|}{|a+b|}.$$

Hence

$$\frac{\|y\|_\infty}{\left(1+\frac{|b|}{|a+b|}\right)\psi(\|y\|_\infty)(I_q^{\alpha}\phi_f)(T)+\frac{|c|}{|a+b|}} \quad \leq \quad 1.$$

Then, by condition $(H5)$, there exists ν such that $\|y\|_\infty \neq \nu$. Let us set

$$U = \{y \in C(J,\mathbb{R}) : \|y\|_\infty < \nu\}.$$

The operator $H : \overline{U} \to C(J,\mathbb{R})$ is completely continuous. From the choice of U, there is no $y \in \partial U$ such that $y = \lambda H(y)$, for some $\lambda \in (0,1)$. As a result, by the nonlinear alternative of Leray-Schauder type, H has a fixed point $y \in \overline{U}$, which is a solution of the problem (1)-(2). The proof is completed. □

4 Example

Consider the boundary value problem for fractional $\frac{1}{3}$-difference equations

$$({}^C D_{\frac{1}{3}}^{\frac{1}{2}} y)(t) = \frac{e^{-t^2} y(t)}{(6+t)(1+y(t))}, \ t \in J = [0,1], \ 0 < \alpha \leq 1, \tag{9}$$

$$y(0) + y(1) = 0, \tag{10}$$

where $\alpha = \frac{1}{2}, \ q = \frac{1}{3}, \ a = 1, \ b = 1, \ c = 0, \ T = 1$, and

$$f(t,y) = \frac{e^{-t^2} y}{(6+t)(1+y)}, \ (t,y) \in J \times [0,\infty).$$

Let $x, y \in [0,\infty)$ and $t \in J$. Then we have

$$\begin{aligned} |f(t,x) - f(t,y)| &= \left| \frac{e^{-t^2}}{(6+t)} \left(\frac{x}{1+x} - \frac{y}{1+y} \right) \right|, \\ &\leq \frac{e^{-t^2}}{(6+t)} |x-y|, \\ &\leq \frac{1}{6} |x-y|. \end{aligned}$$

Hence, the condition $(H2)$ holds with $L = \frac{1}{6}$. We shall check that condition (7) is satisfied with $T = 1$. Indeed,

$$\begin{aligned} \left(1 + \frac{|b|}{|a+b|}\right) \frac{LT^{(\alpha)}}{\Gamma_q(\alpha+1)} &= \left(1 + \frac{1}{2}\right) \frac{1}{6\Gamma_q(\frac{3}{2})}, \\ &= 0.2666 < 1, \end{aligned}$$

where $\Gamma_{\frac{1}{3}}(\frac{3}{2}) \approx 0.9376$. Then, by Theorem 3.1, the problem (9)-(10) has a unique solution on $[0,1]$.

5 Conclusion

In this paper, we have presented the existence and uniqueness of solutions of the boundary value problem for fractional q-difference equations. The uniqueness result is obtained by applying the Banach contraction principle theorem, while the existence results are proved via Schaefer's fixed point theorem and the Leray-Schauder nonlinear alternative theorem. Finally, we illustrated our main results by providing an example.

Acknowledgment

The authors are grateful to the reviewers for their useful comments and suggestions that have helped to improve the present paper. The research of N. Allouch, S. Hamani and J. Henderson was supported by Mostaganem University, Mostaganem, Algeria, and Baylor University, Texas, USA.

References

[1] S. Abbas, M. Benchohra, J. Henderso. Existence and oscillation for coupled fractional q-difference systems. *Fract. Calc. Appl.* **12** (1) (2021) 143–155.

[2] S. Abbas, M. Benchohra, N. Laledj and Y. Zhou. Exictence and Ulam Stability for implicit fractional q-difference equation. *Adv. Differ. Equ.* **2019** (480) (2019) 1–12.

[3] R. Agarwal. Certain fractional q-integrals and q-derivatives. *Proc. Camb. Philos. Soc.* **66** (1969).

[4] R. P. Agarwal, M. Benchohra and S. Hamani. A survey on existence results for boundary value problems for nonlinear fractional differential equations and inclusions. *Acta. Appl. Math.* **109** (3) (2010) 973–1033.

[5] B. Ahmad. Boundary value problem for nonlinear third order q-difference equations. *Electron. J. Differ. Equ.* **2011** (94) (2011) 1–7.

[6] B. Ahmad, S. K. Ntouyas and I. K. Purnaras. Existence results for nonlocal boundary value problems of nonlinear fractional q-difference equations. *Adv. Differ. Equ.* **2011** (140) (2012) 1–15.

[7] W. Al-Salam. Some fractional q-integrals and q-derivatives. *Proc. Edinb. Math. Soc.* **15** (2) (1966–1967) 135–140.

[8] W. Al-Salam and A. Verma. A fractional Leibniz q-formula. *Pac. J. Math.* **60** (2) (1975) 1–10.

[9] M. H. Annaby and Z. S. Mansour. *q-Fractional Calculus and Equations, Lecture Notes in Mathematics.* **2056**. Springer, Heidelberg, 2012.

[10] M. Benchohra and S. Hamani. Boundary value problems for differential equations with fractional order and nonlocal conditions. *Nonlinear Anal.* **71** (2009) 2391–2396.

[11] M. Benchohra, S. Hamani and S. K. Ntouyas. Boundary value problems for differential equations with fractional order. *Surv. Math. Appl.* **3** (2008) 1–12.

[12] W. Benhamida, S. Hamani and J. Henderson. Boundary value problems for Caputo-Hadamard fractional differential equations. *Adv. Theory. Nonlinear Anal. Appl.* **2** (3) (2018) 138–145.

[13] G. Gasper and M. Rahman. *Basic Hypergeometric Series. Cambridge University Press* Cambridge, 1990.

[14] A. Granas and J. Dugundji. *Fixed Point Theory.* Springer, New York, 2003.

[15] R. Hilfer. *Applications of Fractional Calculus in Physics.* World Scientific, Singapore, 2000.

[16] F. Jackson. On q-definite integrals. *Quart. J. Pure Appl. Math.* **41** (1910) 193–203.

[17] F. Jackson. On q-functions and a certain difference operator. *Trans. R. Soc. Edinb.* **46** (1908) 253–281.

[18] V. Kac and P. Cheung. *Quantum Calculus.* Springer, New York, 2002.

[19] A. A. Kilbas, H. M. Srivastava and J. J. Trujillo. *Theory and Applications of Fractional Differential Equations.* North-Holland Mathematical Studies. **vol.204**, Elsevier Science B.V. Amsterdam, 2006.

[20] G. A. Leonov and M. M. Shumafov. *Stabilization of Linear Systems.* Cambridge Scientific Publishers, Cambridge, 2011.

[21] A. A. Martynyuk. *Stability of Motion: The Role of Multicomponent Liapunov's Functions.* Cambridge Scientific Publishers, Cambridge, 2007.

[22] K. S. Miller and B. Ross. *An Introduction to the Fractional Calculus and Differential Equations.* John Wiley, New York, 1993.

[23] I. Podlubny. *Fractional Differential Equations.* Academic Press, San Diego, 1998.

[24] P. M. Rajkovic, S. D. Marinkovic and M. S. Stankovic. On q-analogues of Caputo derivative and Mittag-Leffler function. *Fract. Calc. Appl. Anal.* **10** (4) (2007) 359–373.

[25] P. M. Rajkovic, S. D. Marinkovic and M. S. Stankovic. Fractional integrals and derivatives in q-calculus. *Appl. Anal. Discrete Math.* **1** (2007) 311–323.

[26] M. E. Samei, G. H. Khalilzadeh Ranjbar and V. Hedayati. Existence of solution for a class of Caputo fractional q-difference inclusion on multifunctios by computational results. *Kragujevac J. Math.* **45** (4) (2021) 543-570.

[27] S. G. Samko, A. A. Kilbas and O. I. Marichev. *Fractional Integrals and Derivatives. Theory and Applications.* Gordon and Breach, Yverdon, 1993.

[28] D.R. Smart. *Fixed Point Theorems.* Cambridge University Press, 1980.

Nonlinear Dynamics and Systems Theory, **24** (2) (2024) 123–134

Numerical Approach for Solving Incommensurate Higher-Order Fractional Differential Equations

Iqbal M. Batiha [1,2*], Iqbal H. Jebril [1], Shameseddin Alshorm [1], Mazin Aljazzazi [3] and Shawkat Alkhazaleh [4]

[1] *Department of Mathematics, Al Zaytoonah University of Jordan, Amman 11733, Jordan.*
[2] *Nonlinear Dynamics Research Center (NDRC), Ajman University, Ajman, UAE.*
[3] *Department of Mathematics, The University of Jordan, Amman 11942, Jordan.*
[4] *Department of Mathematics, Jadara University, Irbid, Jordan.*

Received: August 7, 2023; Revised: February 12, 2024

Abstract: In this research, we present a novel numerical approach to tackle an incommensurate system of fractional differential equations of 2α-order, where $\alpha = (\alpha_1, \alpha_2, \alpha_3, \cdots, \alpha_n)$ with $0 < \alpha_i \leq 1$, $\forall i = 1, 2, 3, \cdots, n$. Our proposed method involves reducing the system to α-fractional differential equations using a newly derived result, followed by the implementation of the Modified Fractional Euler Method (MFEM), a recent numerical technique. We demonstrate the efficacy of our approach through an illustrative example, providing validation for our proposed methodology.

Keywords: *incommensurate system; fractional differential equations; modified fractional Euler method.*

Mathematics Subject Classification (2010): 34A08, 26C10.

1 Introduction

In recent years, Fractional Differential Equations (FDEs) have been extensively studied and applied due to their ability to capture the dynamics of systems with long-range interactions, anomalous diffusion, and viscoelasticity. The fractional derivatives allow for the inclusion of memory and hereditary properties, making them suitable for modeling phenomena that exhibit memory retention and relaxation effects. While significant progress has been made in solving FDEs, there remains a challenging class of problems known as incommensurate higher-order FDEs. These equations involve fractional derivatives of different orders that are not rational multiples of each other. As a result, they

* Corresponding author: mailto:i.batiha@zuj.edu.jo

lack a common denominator, leading to difficulties in analytical solutions and numerical treatments.

In this paper, we focus on addressing incommensurate higher-order FDEs, which are characterized by having fractional derivatives of different orders. Such systems present unique challenges in numerical solutions due to their complex nature [1–4]. Our objective is to develop an efficient and accurate numerical method to handle this class of FDEs. The proposed numerical approach is based on two main steps. First, we derive a result that enables us to transform the incommensurate system into a set of α-FDEs, where $\alpha = (\alpha_1, \alpha_2, \alpha_3, \cdots, \alpha_n)$. This transformation simplifies the problem and prepares it for numerical treatment. The parameters α_i are limited to the range $0 < \alpha_i \leq 1$, for $i = 1, 2, 3, \cdots, n$, encompassing various degrees of fractional order, allowing for a comprehensive analysis of the system's behavior. Next, we employ the Modified Fractional Euler Method (MFEM), a recently developed numerical technique tailored to solve FDEs efficiently and accurately. The MFEM incorporates adaptive step-size control and higher-order approximation schemes, making it well-suited for addressing the complexities of incommensurate higher-order fractional systems.

To demonstrate the effectiveness of our numerical approach, we present two illustrative examples. The results obtained by our proposed method are compared with existing analytical solutions, showcasing the accuracy and reliability of our approach. The rest of the paper is organized as follows. Section 2 provides a brief overview of the relevant background and related works. Section 3 outlines the theoretical framework and the proposed numerical approach in detail. In Section 4, we present two numerical examples with some comparisons, and in Section 5, we conclude the whole paper.

2 Preliminaries

In this section, we recall some preliminaries and basic results related to fractional calculus. For more about FDEs and fractional calculus, see [5].

Definition 2.1 Let α be a real nonnegative number. Then the Riemann-Liouville fractional-order integrator J_a^α is defined by

$$J_a^\alpha f(x) = \frac{1}{\Gamma(\alpha)} \int_a^x (x-t)^{\alpha-1} f(t)dt, \ a \leq x \leq b. \tag{1}$$

Definition 2.2 Let $\alpha \in \mathbb{R}^+$ and $m = \lceil \alpha \rceil$ such that $m - 1 < \alpha \leq m$. Then the Caputo fractional-order differentiator of order α is given by

$$D_a^\alpha f(x) = \frac{1}{\Gamma(m-\alpha)} \int_a^x (x-t)^{m-\alpha-1} f^{(m)}(t)dt, \ x > a. \tag{2}$$

Theorem 2.1 *[6] (Generalized Taylor's Theorem). Suppose that $D_*^{k\alpha} f(x) \in C(0, b]$ for $k = 0, 1, \cdots, n+1$, where $0 < \alpha \leq 1$. Then the function f can be expanded about $x = x_0$ as*

$$f(x) = \sum_{i=0}^{n} \frac{x^{i\alpha}}{\Gamma(i\alpha+1)} D_*^{i\alpha} f(x_0) + \frac{x^{(n+1)\alpha}}{\Gamma((n+1)\alpha+1)} D_*^{(n+1)\alpha} f(\xi), \tag{3}$$

with $0 < \xi < x$, $\forall x \in (0, b]$.

Now, by using the first three terms of the generalized Taylor theorem and for $\xi \in (a, b)$, $t_i \in [a, b]$, in which the interval is divided as $a = t_0 < t_1 = t_0 + h < t_2 = t_0 + 2h < \cdots < t_n = t_0 + nh = b$ with $h = \frac{b-a}{n}$ for $i = 1, 2, \cdots, n$, we can expand $y(t)$ about $t = t_i$ to develop a new further modification for the Fractional Euler Method (FEM), called the MFEM. This formula has the form [7, 8]

$$\begin{aligned} y(t_{i+1}) = y(t_i) + \frac{h^\alpha}{\Gamma(\alpha+1)} f\left(t_i + \frac{h^\alpha}{2\Gamma(\alpha+1)}, y(t_i) + \frac{h^\alpha}{2\Gamma(\alpha+1)} f(t_i, y(t_i))\right) \\ + \frac{h^{2\alpha}}{\Gamma(2\alpha+1)} D^{2\alpha}(\xi), \end{aligned} \tag{4}$$

where $\xi \in (a, b)$.

3 Numerical Approach

In this section, we propose a novel result that can reduce the higher incommensurate fractional system of 2α-order into an α-fractional system, where $\alpha = (\alpha_1, \alpha_2, \alpha_3, \cdots, \alpha_n)$ with $0 < \alpha_i \leq 1$, $\forall i = 1, 2, 3, \cdots, n$. Then, we describe how one can deal with the produced system.

Lemma 3.1 *Any FDE of order $n\alpha, n \in \mathbb{Z}^+$ and $\alpha \in (0, 1]$, with functions possessing values in $\mathbb{R}$, can be converted into a system of FDEs of order α with values in $\mathbb{R}^{nd}$.*

Proof. To prove this result, we should first take the scalar case that takes place whenever $d = 1$ and then we will consider the remaining case that occurs when $\alpha > 1$. For this reason, we should note that the general form of the FDE of order $n\alpha$ in its scalar case can be given by

$$D^{n\alpha} y(t) = G(t, y(t), D^\alpha y(t), D^{2\alpha} y(t), \cdots, D^{(n-1)\alpha} y(t)), \tag{5}$$

where G is a continuous function defined on the subset $I \times \mathbb{R} \times \mathbb{R} \times \cdots \times \mathbb{R}$ so that it takes values in $\mathbb{R}$ for a given interval I. Now, define the function

$$\mathbf{\Psi}(t, v_0, v_1, \cdots, v_{n-1}) = (v_1, v_2, \cdots, G(t, v_0, v_1, \cdots, v_{n-1})) \tag{6}$$

as a continuous function defined on $I \times \mathbb{R} \times \mathbb{R} \times \cdots \times \mathbb{R}$ as G, but it takes the values in $\mathbb{R}^n$. In this regard, we consider the following equation:

$$D^\alpha \mathbf{Y}(t) = \mathbf{\Psi}(t, \mathbf{Y}(t)), \text{ for } t \in I. \tag{7}$$

Now, we want to show that $x : I \to \mathbb{R}$ is a solution of equation (6) if and only if the function

$$\begin{aligned} \mathbf{X} :& I \to \mathbb{R}^n, \\ & t \to (x(t), D^\alpha x(t), D^{2\alpha} x(t), \cdots, D^{(n-1)\alpha} x(t)), \end{aligned} \tag{8}$$

is a solution of equation (7). To this end, we assume that x is a solution to equation (6) such that $\mathbf{X}$ is as defined above. Then we have

$$D^\alpha \mathbf{X}(t) = \begin{pmatrix} D^\alpha x(t) \\ D^{2\alpha} x(t) \\ \vdots \\ D^{(n-1)\alpha} x(t) \\ D^{n\alpha} x(t) \end{pmatrix} = \begin{pmatrix} D^\alpha x(t) \\ D^{2\alpha} x(t) \\ \vdots \\ D^{(n-1)\alpha} x(t) \\ G(t, x(t), D^\alpha x(t), D^{2\alpha} x(t), \cdots, D^{(n-1)\alpha} x(t)) \end{pmatrix}, \tag{9}$$

i.e.,

$$D^{\alpha}\mathbf{X}(t) = \mathbf{\Psi}(t, \mathbf{X}(t)). \tag{10}$$

Herein, the converse of the above discussion is similar. Now, for the case of $\alpha > 1$, one can reread the above proof again, and substitute each occurrence of $\mathbb{R}$ by $\mathbb{R}^d$ to get the result.

Corollary 3.1 *Lemma 3.1 can hold for $\alpha = (\alpha_1, \alpha_2, \cdots, \alpha_n)$, where $0 < \alpha_i \leq 1$, for all $i = 1, 2, \cdots, n$.*

For the purpose of addressing FDEs of 2α-order, where $\alpha = (\alpha_1, \alpha_2, \cdots, \alpha_n)$ such that $0 < \alpha_i \leq 1$, for all $i = 1, 2, \cdots, n$, we consider this system has the following form:

$$\begin{aligned} &D^{2\alpha_1} y_1(t) = g_1(t, \mathbf{Y}(t), D^{2\alpha}\mathbf{Y}(t)), \\ &D^{2\alpha_2} y_2(t) = g_2(t, \mathbf{Y}(t), D^{2\alpha}\mathbf{Y}(t)), \\ &D^{2\alpha_3} y_3(t) = g_3(t, \mathbf{Y}(t), D^{2\alpha}\mathbf{Y}(t)), \\ &\vdots \\ &D^{2\alpha_n} y_n(t) = g_n(t, \mathbf{Y}(t), D^{2\alpha}\mathbf{Y}(t)) \end{aligned} \tag{11}$$

with the initial conditions

$$y_i(0) = a_i, \quad D^{\alpha} y_i(0) = b_i \tag{12}$$

such that a_i and b_i are constants for all $i = 1, 2, \cdots, n$, where

$$\mathbf{Y}(t) = (y_1(t), y_2(t), y_3(t), \cdots, y_n(t))$$

and

$$D^{2\alpha}\mathbf{Y}(t) = \left(D^{2\alpha_1} y_1(t), D^{2\alpha_2} y_2(t), D^{2\alpha_3} y_3(t), \cdots, D^{2\alpha_n} y_n(t)\right).$$

In order to obtain an approximate solution to system (11), we reduce it with the use of Lemma 3.1 into α-FDEs. In particular, we suppose that

$$\begin{aligned} &v_1(t) = D^{\alpha_1} y_1(t), \\ &v_2(t) = D^{\alpha_2} y_2(t), \\ &v_3(t) = D^{\alpha_3} y_3(t), \\ &\vdots \\ &v_n(n) = D^{\alpha_n} y_n(t). \end{aligned} \tag{13}$$

Actually, the above assumption would convert system (11) to the following form:

$$\begin{aligned} &D^{\alpha_1} y_1(t) = v_1(t) = h_1(t, \mathbf{X}(t)), \\ &D^{\alpha_1} v_1(t) = g_1(t, \mathbf{X}(t)), \\ &D^{\alpha_2} y_2(t) = v_2(t) = h_2(t, \mathbf{X}(t)), \\ &D^{\alpha_2} v_2(t) = g_2(t, \mathbf{X}(t)), \\ &D^{\alpha_3} y_3(t) = v_3(t) = h_3(t, \mathbf{X}(t)), \\ &D^{\alpha_3} v_3(t) = g_3(t, \mathbf{X}(t)), \\ &\vdots \\ &D^{\alpha_n} y_n(t) = v_n(t) = h_n(t, \mathbf{X}(t)). \\ &D^{\alpha_n} v_n(t) = g_n(t, \mathbf{X}(t)) \end{aligned} \tag{14}$$

with the initial conditions

$$y_i(0) = a_i, \quad v_i(0) = b_i, \ \forall i = 1, 2, \cdots, n, \tag{15}$$

where $\mathbf{X}(t) = (y_1(t), v_1(t), y_2(t), v_2(t), y_3(t), v_3(t), \cdots, y_n(t), v_n(t))$. Now, to solve system (14), we use the MFEM. This method divides the solutions interval $[a, b]$ as $a = t_0 < t_1 = t_0 + h < t_2 = t_0 + 2h < \cdots < t_n = t_0 + nh = b$, in which $t_i = a + ih$ are called the mesh points for $i = 1, 2, \cdots, n$, and $h = \frac{b-a}{n}$ is the step size of the algorithm. Accordingly, based on the MFEM, we obtain the following states:

$$\begin{aligned}
y_1(t_{i+1}) &= y_1(t_i) + \frac{h^{\alpha_1}}{\Gamma(\alpha_1+1)} h_1\left(t_i + \frac{h^{\alpha_1}}{2\Gamma(\alpha_1+1)}, \mathbf{X}(t_i) + \frac{h^{\alpha_1}}{\Gamma(\alpha_1+1)} h_1(t_i, \mathbf{X}(t_i))\right), \\
v_1(t_{i+1}) &= v_1(t_i) + \frac{h^{\alpha_1}}{\Gamma(\alpha_1+1)} g_1\left(t_i + \frac{h^{\alpha_1}}{2\Gamma(\alpha_1+1)}, \mathbf{X}(t_i) + \frac{h^{\alpha_1}}{\Gamma(\alpha_1+1)} g_1(t_i, \mathbf{X}(t_i))\right), \\
y_2(t_{i+1}) &= y_2(t_i) + \frac{h^{\alpha_2}}{\Gamma(\alpha_2+1)} h_2\left(t_i + \frac{h^{\alpha_2}}{2\Gamma(\alpha_2+1)}, \mathbf{X}(t_i) + \frac{h^{\alpha_2}}{\Gamma(\alpha_2+1)} h_2(t_i, \mathbf{X}(t_i))\right), \\
v_2(t_{i+1}) &= v_2(t_i) + \frac{h^{\alpha_2}}{\Gamma(\alpha_2+1)} g_2\left(t_i + \frac{h^{\alpha_2}}{2\Gamma(\alpha_2+1)}, \mathbf{X}(t_i) + \frac{h^{\alpha_2}}{\Gamma(\alpha_2+1)} g_2(t_i, \mathbf{X}(t_i))\right), \\
y_3(t_{i+1}) &= y_3(t_i) + \frac{h^{\alpha_3}}{\Gamma(\alpha_3+1)} h_3\left(t_i + \frac{h^{\alpha_3}}{2\Gamma(\alpha_3+1)}, \mathbf{X}(t_i) + \frac{h^{\alpha_3}}{\Gamma(\alpha_3+1)} h_3(t_i, \mathbf{X}(t_i))\right), \\
v_3(t_{i+1}) &= v_3(t_i) + \frac{h^{\alpha_3}}{\Gamma(\alpha_3+1)} g_3\left(t_i + \frac{h^{\alpha_3}}{2\Gamma(\alpha_3+1)}, \mathbf{X}(t_i) + \frac{h^{\alpha_3}}{\Gamma(\alpha_3+1)} g_3(t_i, \mathbf{X}(t_i))\right), \\
&\vdots \\
y_n(t_{i+1}) &= y_n(t_i) + \frac{h^{\alpha_n}}{\Gamma(\alpha_n+1)} h_n\left(t_i + \frac{h^{\alpha_n}}{2\Gamma(\alpha_n+1)}, \mathbf{X}(t_i) + \frac{h^{\alpha_n}}{\Gamma(\alpha_n+1)} h_n(t_i, \mathbf{X}(t_i))\right), \\
v_n(t_{i+1}) &= v_n(t_i) + \frac{h^{\alpha_n}}{\Gamma(\alpha_n+1)} g_n\left(t_i + \frac{h^{\alpha_n}}{2\Gamma(\alpha_n+1)}, \mathbf{X}(t_i) + \frac{h^{\alpha_n}}{\Gamma(\alpha_n+1)} g_n(t_i, \mathbf{X}(t_i))\right)
\end{aligned} \tag{16}$$

for all $i = 1, 2, \cdots, n$. As a matter of fact, formulas (16) represent an approximate solution of system (14) and therefore $(y_1(t), y_2(t), y_3(t), \cdots, y_n(t)$ is then the desired solution of system (11).

4 Illustrative Examples

In this part, we illustrate our proposed approach by considering two incommensurate systems of FDEs, each of them is of 2α-order, where $\alpha = (\alpha, \beta)$ with $0 < \alpha, \beta \leq 1$.

Example 4.1 Consider the following system:

$$\begin{aligned}
D^{2\alpha} x_1(t) + \frac{1}{2}(x_1(t) - x_2(t)) = 1, \\
D^{2\beta} x_2(t) + \frac{1}{2}(x_2(t) - x_1(t)) = 2
\end{aligned} \tag{17}$$

with the initial conditions

$$\begin{aligned}
x_1(0) = 1, D^{\alpha} x_1(0) = 0, \\
x_2(0) = \frac{1}{2}, D^{\beta} x_2(0) = 0.
\end{aligned} \tag{18}$$

To solve system (17)-(18) with the use of Lemma 3.1, we assume $u_1(t) = D^\alpha x_1(t)$ and $u_2(t) = D^\beta x_2(t)$. This would convert system (17)-(18) to be as follows:

$$\begin{aligned} D^\alpha x_1(t) &= u_1(t), \\ D^\alpha u_1(t) &= 1 - \frac{1}{2}(x_1(t) - x_2(t)), \\ D^\beta x_2(t) &= u_2(t), \\ D^\beta u_2(t) &= 2 - \frac{1}{2}(x_2(t) - x_1(t)) \end{aligned} \tag{19}$$

with the initial conditions

$$\begin{aligned} &x_1(0) = 1, u_1(0) = 0, \\ &x_2(0) = \frac{1}{2}, u_2(0) = 0. \end{aligned} \tag{20}$$

For simplicity, one might suppose

$$\begin{aligned} f_1(t, \mathbf{X}(t)) &= u_1(t), \\ f_2(t, \mathbf{X}(t)) &= 1 - \frac{1}{2}(x_1(t) - x_2(t)), \\ f_3(t, \mathbf{X}(t)) &= u_2(t), \\ f_4(t, \mathbf{X}(t)) &= 2 - \frac{1}{2}(x_2(t) - x_1(t)), \end{aligned} \tag{21}$$

where $\mathbf{X}(t) = (x_1(t), u_1(t), x_2(t), u_2(t))$. This would make system (19)-(20) to be as

$$\begin{aligned} D^\alpha x_1(t) &= f_1(t, \mathbf{X}(t)), \\ D^\alpha u_1(t) &= f_2(t, \mathbf{X}(t)), \\ D^\beta x_2(t) &= f_3(t, \mathbf{X}(t)), \\ D^\beta u_2(t) &= f_4(t, \mathbf{X}(t)) \end{aligned} \tag{22}$$

with the initial conditions

$$\begin{aligned} &x_1(0) = 1, u_1(0) = 0, \\ &x_2(0) = \frac{1}{2}, u_2(0) = 0. \end{aligned} \tag{23}$$

To solve system (22)-(23) by the MFEM, we are applying the solution's formula (16) to obtain

$$\begin{aligned} x_1(t_{i+1}) &= x_1(t_i) + \frac{h^\alpha}{\Gamma(\alpha+1)} f_1\left(t_i + \frac{h^\alpha}{2\Gamma(\alpha+1)}, \mathbf{X}(t_i) + \frac{h^\alpha}{\Gamma(\alpha+1)} f_1(t_i, \mathbf{X}(t_i))\right), \\ u_1(t_{i+1}) &= u_1(t_i) + \frac{h^\alpha}{\Gamma(\alpha+1)} f_2\left(t_i + \frac{h^\alpha}{2\Gamma(\alpha+1)}, \mathbf{X}(t_i) + \frac{h^\alpha}{\Gamma(\alpha+1)} f_2(t_i, \mathbf{X}(t_i))\right), \\ x_2(t_{i+1}) &= x_2(t_i) + \frac{h^\beta}{\Gamma(\beta+1)} f_3\left(t_i + \frac{h^\beta}{2\Gamma(\beta+1)}, \mathbf{X}(t_i) + \frac{h^\beta}{\Gamma(\beta+1)} f_3(t_i, \mathbf{X}(t_i))\right), \\ u_2(t_{i+1}) &= u_2(t_i) + \frac{h^\beta}{\Gamma(\beta+1)} f_4\left(t_i + \frac{h^\beta}{2\Gamma(\beta+1)}, \mathbf{X}(t_i) + \frac{h^\beta}{\Gamma(\beta+1)} f_4(t_i, \mathbf{X}(t_i))\right) \end{aligned} \tag{24}$$

for all $i = 1, 2, \cdots, n$. In fact, the first and third equations of system (24) represent the numerical solution of system (17). In order to see the validity of our scheme, we make some comparisons between our approximate solutions

$$\begin{aligned} x_1(t_{i+1}) &= x_1(t_i) + \frac{h^\alpha}{\Gamma(\alpha+1)} f_1\left(t_i + \frac{h^\alpha}{2\Gamma(\alpha+1)}, \mathbf{X}(t_i) + \frac{h^\alpha}{\Gamma(\alpha+1)} f_1(t_i, \mathbf{X}(t_i))\right) \\ x_2(t_{i+1}) &= x_2(t_i) + \frac{h^\beta}{\Gamma(\beta+1)} f_3\left(t_i + \frac{h^\beta}{2\Gamma(\beta+1)}, \mathbf{X}(t_i) + \frac{h^\beta}{\Gamma(\beta+1)} f_3(t_i, \mathbf{X}(t_i))\right) \end{aligned} \tag{25}$$

and the following exact solution that could be obtained when $\alpha = \beta = 1$:

$$\begin{aligned} x_1(t) &= \frac{3}{4}t^2 + \frac{3}{4}cos(t) - \frac{5}{4}, \\ x_2(t) &= \frac{3}{4}t^2 - \frac{3}{4}cos(t) + \frac{5}{4} \end{aligned} \tag{26}$$

for system (17)-(18). In particular, Figure 1 depicts a graphical comparison between the numerical solution (25) and the exact solution (26). In addition, we plot in Figures 2 and 3 the numerical solution (25) of system (17)-(18) in accordance with commensurate and incommensurate fractional-order values, respectively.

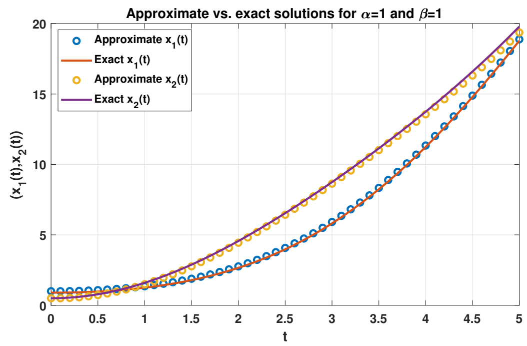

Figure 1: Approximate vs. exact solution of $(x_1(t), x_2(t))$ for $\alpha = 1$ and $\beta = 1$.

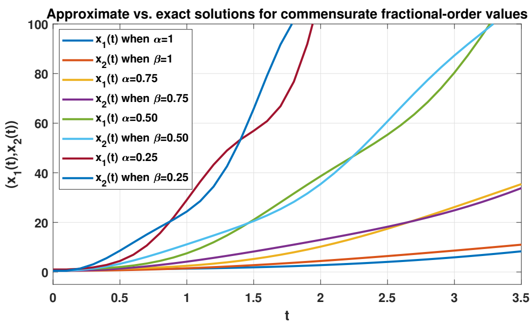

Figure 2: Approximate vs. exact solutions of $(x_1(t), x_2(t))$ for commensurate fractional-order values.

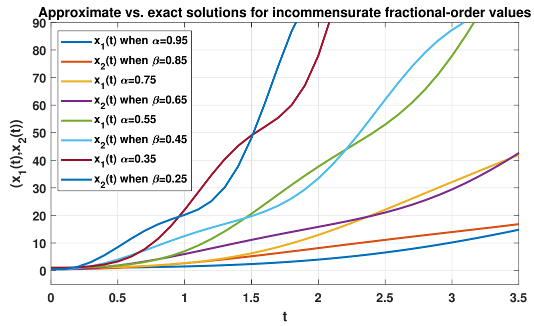

Figure 3: Approximate solutions of $(x_1(t), x_2(t))$ for incommensurate fractional-order values.

Example 4.2 Consider the following system:

$$\begin{aligned} D^{2\alpha}x_1(t) &= 3x_1(t) + 3x_2(t) - D^{\alpha}x_1(t), \\ D^{2\beta}x_2(t) &= 3x_1(t) + 3x_2(t) - D^{\beta}x_2(t) \end{aligned} \tag{27}$$

with the initial conditions

$$\begin{aligned} x_1(0) = 1, D^{\alpha}x_1(0) = 0, \\ x_2(0) = 1, D^{\beta}x_2(0) = 0. \end{aligned} \tag{28}$$

To solve system (27)-(28) with the use of Lemma 3.1, we assume $u_1(t) = D^{\alpha}x_1(t)$ and $u_2(t) = D^{\beta}x_2(t)$. This would convert system (27)-(28) to be as follows:

$$\begin{aligned} D^{\alpha}x_1(t) &= u_1(t), \\ D^{\alpha}u_1(t) &= 3x_1(t) + 3x_2(t) - u_1(t), \\ D^{\beta}x_2(t) &= u_2(t), \\ D^{\beta}u_2(t) &= 3x_1(t) + 3x_2(t) - u_2(t) \end{aligned} \tag{29}$$

with the initial conditions

$$\begin{aligned} x_1(0) = 1, u_1(0) = 0, \\ x_2(0) = 1, u_2(0) = 0. \end{aligned} \tag{30}$$

For simplicity, one might suppose

$$\begin{aligned} f_1(t, \mathbf{X}(t)) &= u_1(t), \\ f_2(t, \mathbf{X}(t)) &= 3x_1(t) + 3x_2(t) - u_1(t), \\ f_3(t, \mathbf{X}(t)) &= u_2(t), \\ f_4(t, \mathbf{X}(t)) &= 3x_1(t) + 3x_2(t) - u_2(t), \end{aligned} \tag{31}$$

where $\mathbf{X}(t) = (x_1(t), u_1(t), x_2(t), u_2(t))$. This would make system (29)-(30) to be as

$$\begin{aligned} D^{\alpha}x_1(t) &= f_1(t, \mathbf{X}(t)), \\ D^{\alpha}u_1(t) &= f_2(t, \mathbf{X}(t)), \\ D^{\beta}x_2(t) &= f_3(t, \mathbf{X}(t)), \\ D^{\beta}u_2(t) &= f_4(t, \mathbf{X}(t)) \end{aligned} \tag{32}$$

with the initial conditions

$$\begin{aligned} x_1(0) = 1, u_1(0) = 0, \\ x_2(0) = 1, u_2(0) = 0. \end{aligned} \tag{33}$$

To solve system (32)-(33) by the MFEM, we are applying the solution's formula (16) to obtain

$$\begin{aligned}
x_1(t_{i+1}) &= x_1(t_i) + \frac{h^\alpha}{\Gamma(\alpha+1)} f_1\left(t_i + \frac{h^\alpha}{2\Gamma(\alpha+1)}, \mathbf{X}(t_i) + \frac{h^\alpha}{\Gamma(\alpha+1)} f_1(t_i, \mathbf{X}(t_i))\right), \\
u_1(t_{i+1}) &= u_1(t_i) + \frac{h^\alpha}{\Gamma(\alpha+1)} f_2\left(t_i + \frac{h^\alpha}{2\Gamma(\alpha+1)}, \mathbf{X}(t_i) + \frac{h^\alpha}{\Gamma(\alpha+1)} f_2(t_i, \mathbf{X}(t_i))\right), \\
x_2(t_{i+1}) &= x_2(t_i) + \frac{h^\beta}{\Gamma(\beta+1)} f_3\left(t_i + \frac{h^\beta}{2\Gamma(\beta+1)}, \mathbf{X}(t_i) + \frac{h^\beta}{\Gamma(\beta+1)} f_3(t_i, \mathbf{X}(t_i))\right), \\
u_2(t_{i+1}) &= u_2(t_i) + \frac{h^\beta}{\Gamma(\beta+1)} f_4\left(t_i + \frac{h^\beta}{2\Gamma(\beta+1)}, \mathbf{X}(t_i) + \frac{h^\beta}{\Gamma(\beta+1)} f_4(t_i, \mathbf{X}(t_i))\right)
\end{aligned} \tag{34}$$

for all $i = 1, 2, \cdots, n$. In fact, the first and third equations of system (34) represent the numerical solution of system (27). In order to see the validity of our scheme, we make some comparisons between our approximate solutions

$$\begin{aligned}
x_1(t_{i+1}) &= x_1(t_i) + \frac{h^\alpha}{\Gamma(\alpha+1)} f_1\left(t_i + \frac{h^\alpha}{2\Gamma(\alpha+1)}, \mathbf{X}(t_i) + \frac{h^\alpha}{\Gamma(\alpha+1)} f_1(t_i, \mathbf{X}(t_i))\right) \\
x_2(t_{i+1}) &= x_2(t_i) + \frac{h^\beta}{\Gamma(\beta+1)} f_3\left(t_i + \frac{h^\beta}{2\Gamma(\beta+1)}, \mathbf{X}(t_i) + \frac{h^\beta}{\Gamma(\beta+1)} f_3(t_i, \mathbf{X}(t_i))\right)
\end{aligned} \tag{35}$$

and the following exact solution that could be obtained when $\alpha = \beta = 1$:

$$\begin{aligned}
x_1(t) &= c_1 e^{2t} + c_2 e^{-3t} + c_3 + c_4 e^{-t} \\
x_2(t) &= c_1 e^{2t} + c_2 e^{-3t} - c_3 - c_4 e^{-t}
\end{aligned} \tag{36}$$

for system (27)-(28), where $c_1 = \frac{1}{5}$, $c_2 = -\frac{1}{5}$ and $c_3 = c_4 = 0$. In particular, Figures 4 and 5 depict graphical comparisons between the numerical solutions given in (35) and the exact solution (36). In addition, we plot in Figures 6 and 7 the numerical solution (35) of system (27)-(28) in accordance with commensurate fractional-order values, and similarly, we plot in Figures 8 and 9 the numerical solution (35) of the same system according to some incommensurate fractional-order values.

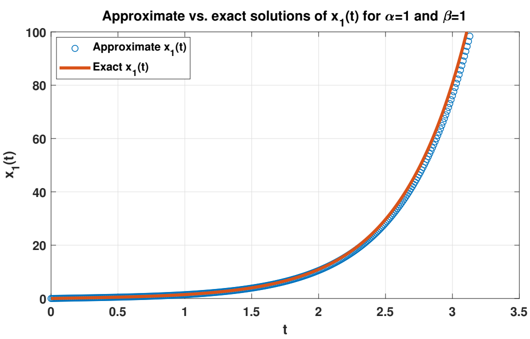

Figure 4: Approximate vs. exact solutions of $x_1(t)$ for $\alpha = 1$ and $\beta = 1$.

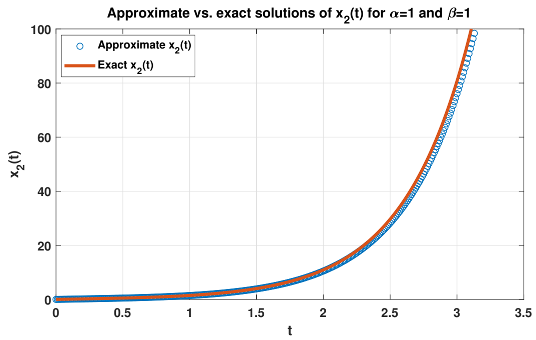

Figure 5: Approximate vs. exact solutions of $x_2(t)$ for $\alpha = 1$ and $\beta = 1$.

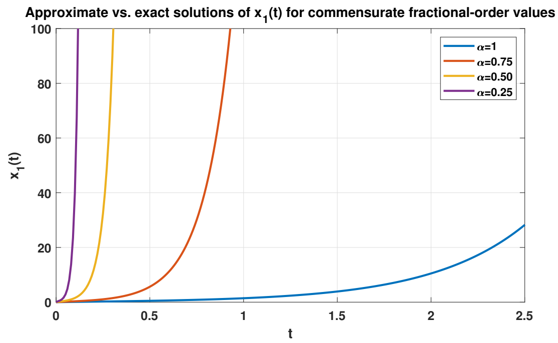

Figure 6: Approximate vs. exact solutions of $x_1(t)$ for commensurate fractional-order values.

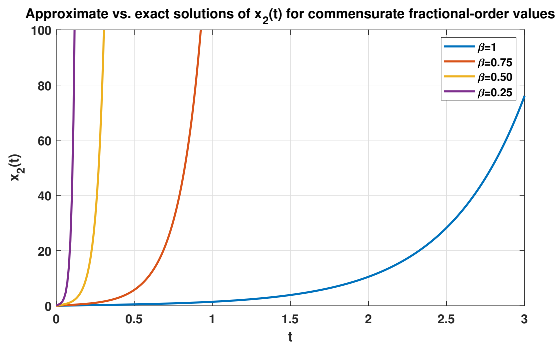

Figure 7: Approximate vs. exact solutions of $x_2(t)$ for commensurate fractional-order values.

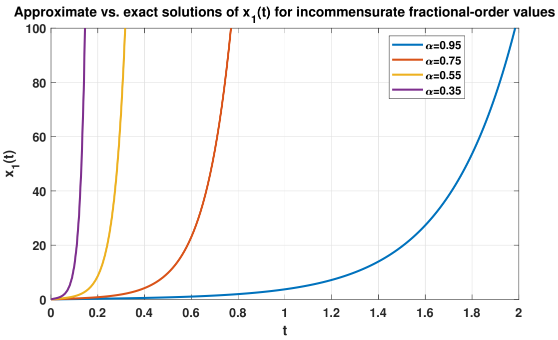

Figure 8: Approximate vs. exact solutions of $x_1(t)$ for incommensurate fractional-order values.

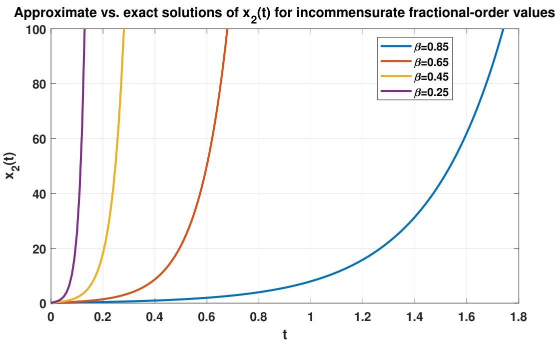

Figure 9: Approximate vs. exact solutions of $x_2(t)$ for incommensurate fractional-order values.

5 Conclusion

In conclusion, this research introduces a novel and effective numerical approach for addressing the challenges posed by incommensurate systems of fractional differential equations of 2α-order, where $\alpha = (\alpha_1, \alpha_2, \alpha_3, \cdots, \alpha_n)$ with $0 < \alpha_i \leq 1$, $\forall i = 1, 2, 3, \cdots, n$. Our proposed method offers a systematic solution by transforming the incommensurate system into a set of α-fractional differential equations using a newly derived result. Subsequently, we successfully apply the Modified Fractional Euler Method (MFEM), a recently developed numerical technique, to efficiently solve the transformed equations. Through an illustrative example, we demonstrate the practical efficacy and reliability of our numerical approach.

References

[1] N. Yizengaw. Numerical solutions of initial value ordinary differential equations using finite difference method. *Open Access Library Journal* **2** (2015) 1–7.

[2] A. Suliman. Applications of virtual modules in numerical analysis. *Open Access Library Journal* **3** (2016) 1–8.

[3] R. L. Burden and J. D. Faires. *Numerical Analysis*. Brookscole, Boston, 2011.

[4] H. Qawaqneh, M. S. Md Noorani, H. Aydi, A. Zraiqat and A. H. Ansari. On fixed point results in partial b-metric spaces. *Journal of Function Spaces* **2021** (2021) 8769190.

[5] I. Podlubny. *Fractional Differential Equations*. Academic Press, San Diego, 1999.

[6] Z. Odibat and S. Momani. An algorithm for the numerical solution of differential equations of fractional order. *Journal of Applied Mathematics & Informatics* **26** (1-2) (2008) 15–27.

[7] I. M. Batiha, B. Anwar, A. A. Al-Nana, A. Shameseddin, I. H. Jebril and Z. Amjed. A numerical scheme for dealing with fractional initial value problem. *International Journal of Innovative Computing, Information and Control* **19** (3) (2023) 763-–774.

[8] I. M. Batiha, A. A. Abubaker, I. H. Jebril, S. B. Al-Shaikh and K. Matarneh. New algorithms for dealing with fractional initial value problems. *Axioms* **12** (5) (2023) 488.

Nonlinear Dynamics and Systems Theory, **24** (2) (2024) 135–146

Derivation of Multi-Asset Black-Scholes Differential Equations

K. Fahim *, A. U. Alfajriyah and E. R. M. Putri

Department of Mathematics, Sepuluh Nopember Institute of Technology,
Sukolilo, Surabaya, Indonesia

Received: September 3, 2023; Revised: February 18, 2024

Abstract: The Black-Scholes differential equations are extensively proposed in multi-asset option prices. Modelling of the Black-Scholes differential equation is generally completed by applying a Δ-hedging method, which could first-rate be accomplished on entire markets. Another technique, which is done in this work, is by first modelling multi-asset option prices in a backward stochastic differential equation. This study starts constructing a multi-asset portfolio which is written in BSDEs. The Feynman-Kac concept offers the relation between BSDEs and the Black-Scholes differential equations. Then we obtain a theorem which explains that the solution of BSDEs of multi-asset portfolios exists and is unique. It is also a solution to the Black-Scholes differential equations. Finally, in the last part of this work, we give some simulations of multi-asset option prices which are executed in a software.

Keywords: *backward stochastic differential equations (BSDEs); Black-Scholes differential equations; Feynman-Kac theorem; multi-asset option; partial differential equations (PDEs).*

Mathematics Subject Classification (2010): 22E10, 28B05, 35R60, 93-10, 70K75.

* Corresponding author: mailto:kfahim@matematika.its.ac.id

1 Introduction

Determining the price of derivative products in the capital market is an important problem in the field of financial mathematics. Derivative products are contracts whose profit value is determined by the underlying asset. One of the derivative products are options. An option is an agreement between two parties whereby the contract holder has the right to sell or buy an amount of the underlying asset at a certain price and at a stated time. The most widely used option pricing method is the Black-Scholes differential equation since it provides an option price solution for the options of one or more underlying assets. Options with several underlying assets are termed as multi-asset options. Derivation of the Black-Scholes differential equation is generally done using the Δ-hedging theory that can only be done on a complete market by setting the stock portfolio value equal to the option value. This is called a portfolio replication. The opposite of a complete market is an incomplete market. In the incomplete market, there are only a few securities or financial products. Portfolios or wealth processes on the incomplete market can only be built using primary securities, so there is an impossibility to replicate the payoff with a portfolio of underlying assets [2]. Pricing of financial products in the incomplete market is one of the BSDEs applications.

Several previous studies stated that the Black-Scholes differential equation can be obtained through BSDEs (Backward Stochastic Differential Equations). BSDEs are a useful method for studying options pricing problems because they have several advantages. BSDEs can be used on the incomplete market. Another advantage of BSDEs is that there is no need to change the measurement to a neutral risk condition. When determining the price of options, the return value is adjusted according to the investor's risk preferences, while the discount rate differs between the investors. There is an alternative method, namely by adjusting all investors' risk preferences. This risk preference is marked with a number called the risk premium and then the expected value is calculated in the new probability measure, which is a neutral risk measure. The BSDE solution corresponds to the PDE (partial differential equation) solution. This result is given by an analogy called the Feynman-Kac theorem.

BSDEs application in financial mathematics was first introduced by El Karoui et al. [2]. This study shows that the Black-Scholes differential equation for one asset can be obtained using BSDEs [2]. Actually, the process of changing portfolio values (wealth process) can be represented in the form of BSDEs. This research was conducted on one asset options. Pricing of single asset options, non-linear in the incomplete market can also be modeled using BSDEs [2]. In the *complete market*, option prices are a BSDEs solution with a linear generator function f. On the other hand, in the incomplete market, changes in portfolio wealth are given by BSDEs with the non-linear generator function f [2]. The generalization of the Feynman-Kac theorem has an important function in the solution of parabolic PDEs including the BSDEs in option pricing.

This research begins by formulating risky asset prices and a risk-free asset. Then we construct a multi-asset portfolio that contains risky and risk-free assets. The portfolio is structured in such a way that it satisfies the system of BSDEs (6) and (14). Then the existence and uniqueness of the solution of the System (6) and (14) are proven. Using the Feynman-Kac theorem, a multi-asset Black-Scholes differential equation can be obtained. Simulation and the analysis of multi-asset option price simulation results are also carried out.

2 The Feynman-Kac Theorem

In this section, we firstly present a theorem on the existence and uniqueness of the solution to BSDE (1). Then we give the Feynman-Kac theorem which provides the relation between BSDE (1) and semilinear PDE (3). These two theorems are essential for the main result of this study and are given without proof. The complete proofs can be found in [2,9]. Let us first consider a BSDE

$$\begin{cases} -dY(t) = f\left(t, X(t), Y(t), Z(t)\right) dt - Z(t)\, dW(t),\ t \in [0,T), \\ Y_T = \xi, \end{cases} \tag{1}$$

or, equivalently,

$$Y_t = \xi + \int_t^T f(s, X_s, Y_s, Z_s) ds - \int_t^T Z_s dW_s,\ t \in [0,T), \tag{2}$$

where W is an m-dimensional Brownian motion on a probability space $(\Omega, \mathcal{F}, \{\mathcal{F}_t\}, \mathbb{P})$, the terminal condition $\xi : \Omega \mapsto \mathbb{R}$ is a random variable being $\mathcal{F}_T$-measurable, and f is a generator function from $\mathbb{R}^+ \times \mathbb{R}^n \times \mathbb{R} \times \mathbb{R}^{1\times n}$ into $\mathbb{R}$. Here, X_t is an $\mathbb{R}^n$-valued stochastic process satisfying the differential equation

$$dX(t) = \mu(X(t))dt + \sigma(X(t))dW(t).$$

Moreover, the terminal condition ξ and the generator function f are called a pair of standard parameters if they satisfy the following conditions:

1. $\xi \in L_T^2(\mathbb{R})$,
2. $f(\cdot,\cdot,0,0) \in H_T^2(\mathbb{R})$,
3. f is uniformly Lipschitz, i.e., there exists a number $M > 0$ such that

$$|f(\cdot,\cdot,y_1,z_1) - f(\cdot,\cdot,y_2,z_2)| \le M(|y_1 - y_2| + |z_1 - z_2|),\ \text{a.s. for all } y_1, y_2, z_1, z_2,$$

where $L_T^2(\mathbb{R}^d)$ is a space of d-dimensional random variables which are $\mathcal{F}_T$-measurable and square integrable, and $H_T^2(\mathbb{R}^{m\times n})$ is a space of $\mathbb{R}^{m\times n}$-valued predictable processes Y such that $\int_0^T |Y_t|^2 dt$ is an integrable random variable.

Theorem 2.1 *If (f, ξ) is a pair of standard parameters, then (1) has a unique solution (Y, Z) in $H_T^2(\mathbb{R}) \times H_T^2(\mathbb{R}^{1\times m})$.*

In the following theorem, we give the Feynman-Kac theorem which explains the relation between BSDE (1) and the semilinear PDE

$$\begin{cases} -\frac{\partial V(t,x)}{\partial t} - \mathcal{L}V(t,x) - f(t,x,V(t,x),(\bigtriangledown_x V(t,x))^T\sigma(x)) = 0,\ t \in [0,T), x \in \mathbb{R}^n, \\ V(T,x) = \zeta(x),\ x \in \mathbb{R}^n, \end{cases} \tag{3}$$

where $\mathcal{L}$ is a generator function given by

$$\mathcal{L}V(t,x) = (\bigtriangledown_x V(t,x))^T \mu(x) + \frac{1}{2} Tr(\sigma^T(x) H_x V(t,x) \sigma(x)). \tag{4}$$

Theorem 2.2 *Let V be a solution of (3) and let*

$$Y_t = V\big(t, X_t\big),\ Z_t = \big(\bigtriangledown_x V(t,X_t)\big)^T \sigma(X_t), Y_T,$$

then (Y_t, Z_t) is a solution of BSDE (1) with the terminal condition $\xi = V(T, X_T)$.

3 The BSDE of Multi-Asset Options

In this section, we will derive the BSDE of multi-asset options. But first, let us introduce the assumptions we use to derive the BSDE.

Assumption 3.1 The following statements are some assumptions:

(1) we use basket options;

(2) the payoff of basket options is a geometric mean, i.e.,

$$Payoff = (\prod_{i=1}^{n} S_i^{\alpha_i} - K)^+, \tag{5}$$

where $\Sigma\alpha_i = 1$ and $\alpha_i \geq 0$;

(3) the wealth process can be replicated;

(4) there exists a risk premium.

The equation of multi-asset options has the form of multi-dimensional parabolic partial differential equations. There are several types of multi-asset options that have different payoffs. According to Assumption 3.1 (1), we use basket options that consist of more than two underlying assets. The basket option pricing formula can be obtained from the multi-asset Black-Scholes differential equation. The multivariable problem of pricing basket options can be reduced to one dimension if the payoff of basket options satisfies Assumption 3.1 (2) (see [5]).

Multi-asset options are formed from several underlying assets consisting of risky assets and risk-free assets. In this study, stocks and bonds are used as risky and risk-free assets, respectively. Suppose S_i denotes the price of the i-th stock which satisfies the geometric Brownian motion equation as follows:

$$\frac{dS_i}{S_i} = \mu_i \, dt + \sum_{j=1}^{m} \sigma_{ij} \, dW_j, \qquad i = 1, 2, ..., n\,, \tag{6}$$

where μ_i is the i-th stock return, σ_{ij} is the volatility of the i-th stock due to the j-th Brownian motion and $W = [W_1, W_2, \ldots, W_m]^T$ is an m-dimensional Brownian motion of a probability space $(\Omega, \mathcal{F}, \{\mathcal{F}_t\}, \mathbb{P})$. The movement price of the bond P at time t satisfies the equation

$$P(t) = \upsilon \, e^{-\int_t^T r(u)\, du}$$

or

$$\begin{cases} dP(t) = P(t)\, r\, dt, & 0 \leq t < T \\ P(T) = \upsilon, \end{cases} \tag{7}$$

where r is a risk-free interest rate and T is a due time.

Here, we use a multi-asset portfolio equation to determine the option price. Once the price of options is obtained, we can construct a multi-asset portfolio of stocks that has the same value as basket options. This is called a replicating portfolio strategy. In particular, the multi-asset portfolio equation Y is made to have the equal value as the options at time $t \in [0, T]$. A portfolio with this strategy is also known as a wealth process.

A multi-asset portfolio Y consists of n stock assets and a bond asset. Suppose the stock asset S_i, $i = 1, 2, 3, \cdots, n$, has a proportion of Δ_i and a bond P has a proportion of Δ_P. The value of the portfolio at t is defined as

$$Y(t) = \sum_{i=1}^{n} \Delta_i \, S_i \, + \, \Delta_P \, P. \tag{8}$$

We assume that the value of (8) satisfies the self-financing strategy, therefore we obtain

$$dY(t) = \sum_{i=1}^{n} \Delta_i \, dS_i + \Delta_P \, dP. \tag{9}$$

Substituting (6) and (7) into (9), we get

$$dY(t) = \Bigg(Y\, r + \sum_{i=1}^{n} \Delta_i \, S_i \, (\mu_i \, - r) \, \Bigg) dt + \sum_{i=1}^{n} \sum_{j=1}^{m} \Delta_i \, S_i \, \sigma_{ij} \, dW_j \ . \tag{10}$$

From Assumption 3.1 (3), the portfolio Y can be replicated, hence there exists a risk-free portfolio Π that has the same value as the portfolio Y and satisfies

$$d\Pi = dV(S_1, S_2, \ldots, S_n, t) - \sum_{i=1}^{n} \ \Delta_i \ dS_i \, . \tag{11}$$

Using the multi-dimensional Itô formula, we obtain

$$\begin{aligned} dV(S_1, S_2, \ldots, S_n, t) = & \left(\frac{\partial V}{\partial t} + \frac{1}{2} Tr(\sigma(\mathbf{S})^T \, H_S V \, \sigma(\mathbf{S})) + \bigtriangledown_S V(t, \mathbf{S}(t))^T \mu(S) \right) dt \\ & + \ (\bigtriangledown_S V(t, \mathbf{S}(t))^T \sigma(\mathbf{S})) \, dW(t) \ , \end{aligned} \tag{12}$$

where

$$\frac{1}{2} Tr\Big(\sigma(\mathbf{S})^T \, H_S V \, \sigma(\mathbf{S}) \Big) = \sum_{i=1}^{n} \sum_{j=1}^{m} a_{ij} S_i S_j \ ,$$

$$a_{ij} = \sum_{k=1}^{m} \sigma_{ik} \, \sigma_{jk} \ ,$$

and

$$\bigtriangledown_S V \, (t, \mathbf{S}(t))^T \, \sigma(\mathbf{S})) \, d\mathbf{W_t} = \sum_{i=1}^{n} \sum_{j=1}^{m} \sigma_{ij} S_i \frac{\partial V}{\partial S_i} \, dW_j \, .$$

Substituting (6) and (12) into (11), we have

$$\begin{aligned} d\Pi = & \left(\frac{\partial V}{\partial t} \ + \frac{1}{2} \sum_{i=1}^{n} \sum_{j=1}^{m} a_{ij} \, S_i \, S_j \, \frac{\partial^2 V}{\partial S_i \partial S_j} - \sum_{i=1}^{n} \mu_i (\Delta_i \, S_i \, - \frac{\partial V}{\partial S_i}) \right) dt \\ & + \sum_{i=1}^{n} \sum_{j=1}^{m} S_i \, \sigma_{ij} \left(\Delta_i - \frac{\partial V}{\partial S_i} \right) dW_j \, . \end{aligned}$$

Since Π is a risk-free portfolio, we obtain $\Delta_i = \dfrac{\partial V}{\partial S_i}$, $(i = 1, 2, \ldots, n)$. Substituting it to (10), we get

$$-dY(t) = -\left(Y\,r + \sum_{i=1}^{n} \frac{\partial V}{\partial S_i}\, S_i\,(\mu_i - r)\right) dt - \sum_{i=1}^{n}\sum_{j=1}^{m} \frac{\partial V}{\partial S_i}\, S_i\,\sigma_{ij}\, dW_j. \tag{13}$$

According to Assumption 3.1 (4), there exists a risk premium

$$\boldsymbol{\lambda} = \begin{bmatrix} \lambda_1 \\ \lambda_2 \\ \vdots \\ \lambda_m \end{bmatrix}$$

such that

$$\begin{bmatrix} \sigma_{11} & \sigma_{12} & \ldots & \sigma_{1m} \\ \sigma_{21} & \sigma_{22} & \ldots & \sigma_{2m} \\ \vdots & \vdots & \ddots & \vdots \\ \sigma_{n1} & \sigma_{n2} & \ldots & \sigma_{nm} \end{bmatrix} \boldsymbol{\lambda} = \begin{bmatrix} \mu_1 - r \\ \mu_2 - r \\ \vdots \\ \mu_n - r \end{bmatrix}.$$

Furthermore, (13) becomes

$$\begin{aligned} -dY(t) = -\Bigg(Y\,r + \begin{bmatrix} \frac{\partial V}{\partial S_1} S_1 & \frac{\partial V}{\partial S_2} S_2 & \ldots & \frac{\partial V}{\partial S_n} S_n \end{bmatrix} \\ \times \begin{bmatrix} \sigma_{11} & \sigma_{12} & \ldots & \sigma_{1m} \\ \sigma_{21} & \sigma_{22} & \ldots & \sigma_{2m} \\ \vdots & \vdots & \ddots & \vdots \\ \sigma_{n1} & \sigma_{n2} & \ldots & \sigma_{nm} \end{bmatrix} \times \begin{bmatrix} \lambda_1 \\ \lambda_2 \\ \vdots \\ \lambda_m \end{bmatrix} \Bigg) dt \\ - \begin{bmatrix} \frac{\partial V}{\partial S_1} S_1 & \frac{\partial V}{\partial S_2} S_2 & \ldots & \frac{\partial V}{\partial S_n} S_n \end{bmatrix} \times \begin{bmatrix} \sigma_{11} & \sigma_{12} & \ldots & \sigma_{1m} \\ \sigma_{21} & \sigma_{22} & \ldots & \sigma_{2m} \\ \vdots & \vdots & \ddots & \vdots \\ \sigma_{n1} & \sigma_{n2} & \ldots & \sigma_{nm} \end{bmatrix} \\ \times \begin{bmatrix} dW_1 \\ dW_2 \\ \vdots \\ dW_m \end{bmatrix} \end{aligned}$$

and can be written as

$$-dY(t) = f(t, \mathbf{S}(t), Y(t), \mathbf{Z}(t))\, dt - \mathbf{Z}(t)\, d\mathbf{W}(t), \tag{14}$$

where

$$f(t, \mathbf{S}(t), Y(t), \mathbf{Z}(t)) = -\,Y\,r - \mathbf{Z}(t)\boldsymbol{\lambda} \tag{15}$$

with

$$\mathbf{Z}(t) = \left[\frac{\partial V}{\partial S_1} S_1 \quad \frac{\partial V}{\partial S_2} S_2 \quad \dots \quad \frac{\partial V}{\partial S_n} S_n\right] \times \begin{bmatrix} \sigma_{11} & \sigma_{12} & \dots & \sigma_{1m} \\ \sigma_{21} & \sigma_{22} & \dots & \sigma_{2m} \\ \vdots & \vdots & \ddots & \vdots \\ \sigma_{n1} & \sigma_{n2} & \dots & \sigma_{nm} \end{bmatrix}.$$

Then, based on the fact that the portfolio Y is constructed such that it has the same value as the basket option, we have the terminal condition of BSDE (14) given by

$$Y_T = (\prod_{i=1}^{n} S_i(T)^{\alpha_i} - K)^+ \ , \tag{16}$$

where $K \in \mathbb{R}^+$.

4 Existence and Uniqueness of Solution to the System (6) and (14)

This section provides a theorem on the existence and uniqueness of solution of the system (6) and (14). This theorem explains the sufficient condition under which a solution of the system (6) and (14) exists and is unique.

Theorem 4.1 *Let* (3) *with* $f(t,x,y,z) = -yr - z\lambda$ *and*

$$V(T,(x_1,x_2,\cdots,x_n)^T) = (\prod_{i=1}^{n} x_i^{\alpha_i} - K)^+$$

have solutions in $H_T^2(\mathbb{R})$*. Then there exists a unique solution of the system* (6) *and* (14) *in* $H_T^2(\mathbb{R})$*. Furthermore,* (3) *also has a unique solution in* $H_T^2(\mathbb{R})$*.*

Proof. Firstly, we will prove that the BSDE

$$d\tilde{Y}(t) = f(t,\boldsymbol{S}(t),\tilde{Y}(t),\boldsymbol{U})dt - \boldsymbol{U}(t)d\boldsymbol{W}(t) \tag{17}$$

has a unique solution when the terminal condition is given by

$$U(T) = (\prod_{i=1}^{n} S_i(T)^{\alpha_i} - K)^+.$$

The proof is given as follows.

1. In this part, we will prove that $\tilde{Y}_T \in L_T^2(\mathbb{R})$.
   The terminal condition of BSDE (17) is given by $\tilde{Y}_T = (\prod_{i=1}^n S_i(T)^{\alpha_i} - K)^+$. Since $S_i(T)$ is $\mathcal{F}_T$-measurable, we can obtain that so is $\tilde{Y}_T$. Moreover, we also have

   $$\mathbb{E}[S_i(T)^2] = S_i(0)^2 \exp\left\{2\mu T + \sum_{j=1}^{m} \sigma_{ij}^2 T\right\} < \infty \, ,$$

   hence

   $$\mathbb{E}[|\tilde{Y}_T^2|] = \mathbb{E}\left[\left|\left(\left(\prod_{i=1}^{n} S_i(T)^{\alpha_i} - K\right)^+\right)^2\right|\right] < \infty \ .$$

Therefore, we get

$$\tilde{Y}_T = \left(\prod_{i=1}^{n} S_i(T)^{\alpha_i} - K \right)^{+} \in L_T^2(\mathbb{R}) \ .$$

2. In this part, we will prove that $f(\cdot, \cdot, 0, 0) \in H_T^2(\mathbb{R})$.
   Based on (15), we obtain

$$\mathbb{E}\left[\int_0^T |f(\cdot, \cdot, 0, 0)|^2 \, dt \right] = 0 < \infty \ .$$

   Thus, $f(\cdot, \cdot, 0, 0)$ is a predictable process and we also have

$$f(\cdot, \cdot, 0, 0) \in H_T^2(\mathbb{R}).$$

3. In this last part, we prove that f is uniformly Lipschitz.
   We can observe that for $L = \max(r, |\boldsymbol{\lambda}|)$, we have

$$f(t, \mathbf{S}(t), y_1, z_1) - f(t, \mathbf{S}(t), y_1, z_1)| \leq L(|y_1 - y_2| + |z_1 - z_2|) \ .$$

   Therefore f is a uniform Lipschitz function.

Thus three conditions in Theorem 2.1 are satisfied, so (17) has a unique solution. Moreover, suppose that V is one of the solutions of (3), which is possible because we assume that (3) has a solution. According to the Feynman-Kac theorem and the uniqueness of the solution (17), we obtain that the pair $(\tilde{Y}, \boldsymbol{U})$ given by

$$\tilde{Y}(t) = V(t, \boldsymbol{S}(t)) \tag{18}$$

and

$$\boldsymbol{U}(t) = (\nabla_x V(t, \boldsymbol{S}(t)))^T \boldsymbol{\sigma}(\boldsymbol{S}(t)) \tag{19}$$

is the unique solution of (17). Consequently, by a contradiction argument, we have $Y(t) = V(t, \boldsymbol{S}(t))$ is a unique solution of the system (6) and (14). Furthermore, by a similar argument, we can also conclude that the solution of (3) is unique.

5 Simulations of Multi-Asset Option Prices

In this section, we present the simulation of pricing of the multi-asset option in the basket option. From Theorem 4.1, we obtain that the solution of the system (6) and (14) is equivalent to the solution of

$$\begin{cases} \frac{\partial V}{\partial t} + \dfrac{1}{2} \sum_{i=1}^{n} \sum_{j=1}^{m} a_{ij} \, S_i \, S_j \dfrac{\partial^2 V}{\partial S_i \, \partial S_j} + \sum_{i=1}^{n} \dfrac{\partial V}{\partial S_i} \, r \, S_i - rV = 0 \ , \\ dS_i = \mu_i S_i \, dt + \sum_{j=1}^{m} \sigma_{ij} S_i \, dW_j , \qquad i = 1, 2, ..., n \, , \\ V(T, (S_1, S_2, \cdots, S_n)^T) = (\prod_{i=1}^{n} x_i^{\alpha_i} - K)^{+} \end{cases} \tag{20}$$

if (3) has solutions in $H_T^2(\mathbb{R})$. We can see that the last equation above is the multi-asset Black-Scholes differential equation and the exact solution is given by (see [5])

$$V(S_1, \ldots, S_n, t) = e^{-\hat{q}(T-t)} \, S_1^{\alpha_1} \, S_2^{\alpha_2} \ldots \, S_n^{\alpha_n} N(\hat{d}_1) - Ke^{-r(T-t)} N(\hat{d}_2), \tag{21}$$

where

$$
\begin{aligned}
\hat{d}_1 &= \frac{\ln\left(\frac{S_1^{\alpha_1} S_2^{\alpha_2} \dots S_n^{\alpha_n}}{K}\right) + (r - \hat{q} + \frac{\hat{\sigma}^2}{2})(T-t)}{\hat{\sigma}\sqrt{T-t}}, \\
\hat{d}_2 &= \frac{\ln\left(\frac{S_1^{\alpha_1} S_2^{\alpha_2} \dots S_n^{\alpha_n}}{K}\right) + (r - \hat{q} - \frac{\hat{\sigma}^2}{2})(T-t)}{\hat{\sigma}\sqrt{T-t}} \\
&= \hat{d}_1 - \hat{\sigma}\sqrt{T-t}, \\
\hat{\sigma}^2 &= \sum_{i=1}^{n} a_{ij}\alpha_i\alpha_j, \\
q &= \sum_{i=1}^{n} \frac{a_{ii}}{2}\alpha_i + \frac{\hat{\sigma}^2}{2}.
\end{aligned}
$$

Here, we know that (21) is also the solution of the BSDE of multi-asset options (14). Simulations were carried out to determine the effect of several variables on the option price. These variables are the strike price, interest rate, maturity date, and stock volatility. The simulation is carried out on the assets of 2, 5, 10 and 30. In each option price simulation, the number of the Brownian motion used is equal to the number of stock assets, the price of each stock is 100 and the proportion of each stock in basket options has the same value.

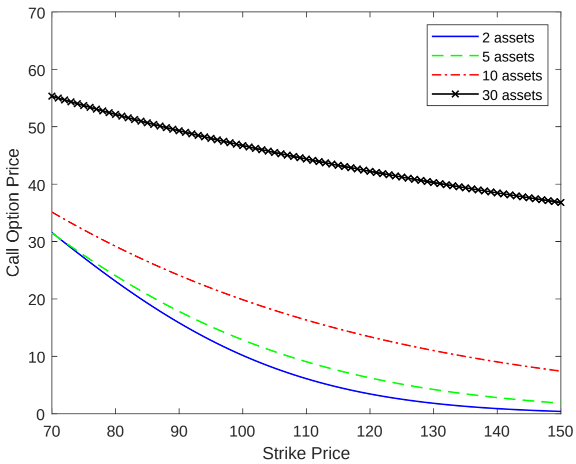

Figure 1: The effect of the strike price on the option price.

We plot the call option price influenced by different strike prices given by (21), see Figure 1. The call option price decreases when the value of strike price increases. If the call option is exercised at maturity, then the profit from the call option is the share price that exceeds the strike, $S_i^{\alpha_i} - K$. Therefore, the price of the call option is more expensive, the lower the strike price is. This also relates to the stock prices.

If the stock price is fixed, while the *strike* price is getting smaller, then the profit will be getting bigger. Therefore, the call option is more valuable as the stock price increases. Figure 1 also shows that the more assets in the call option, the higher the price of the call option.

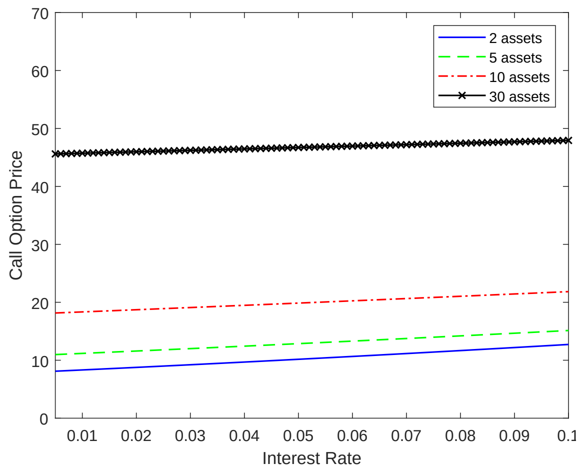

Figure 2: The effect of the interest rate on the option price.

Figure 2 shows that a higher interest rate causes a higher price of the call option. This is caused by the fact that if the interest rate in economy rises, the *return* expected by investors on stock assets tends to rise. On the other hand, the current value of funds received by the option holder is decreasing. The combination of these two causes an increase in the call option price.

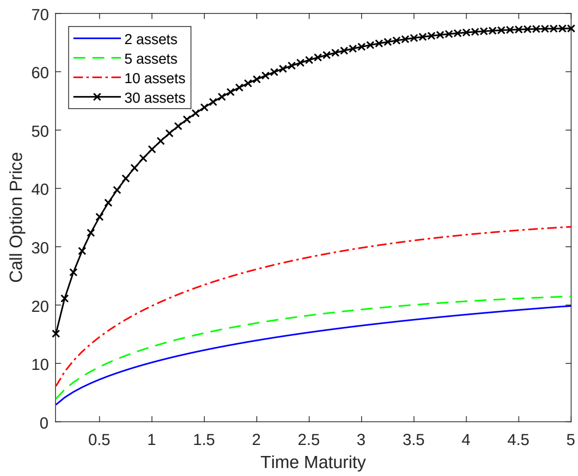

Figure 3: The effect of the time maturity on the option price.

Based on the simulation results, see Figure 3, it is found that a longer expiration time caused a higher call option price. The longer the maturity of a call option, the more opportunities the option holder gets to exercise his rights on that option. Based on Figure 4, it is found that the higher the volatility, the higher the price of the call option. Volatility shows a measure of the uncertainty of stock prices in the future. When volatility increases, stock prices also increase. As a result, the profit derived from the call option also increases. On the other hand, the loss from the call option is the price

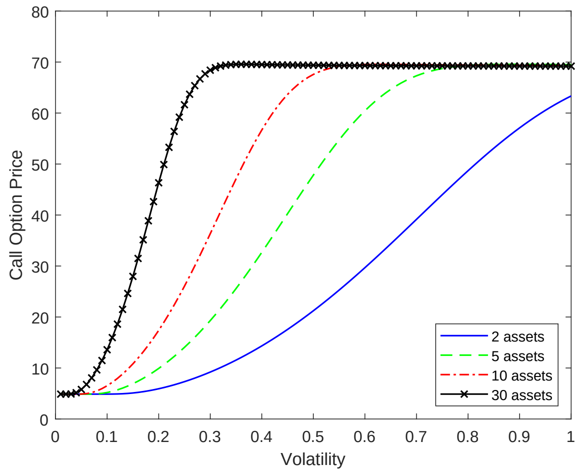

Figure 4: The effect of the volatility on the option price.

of the premium or the price of the call option paid at the beginning of the transaction. Therefore, it is found that a higher volatility resulted in a higher call option price.

6 Conclusion

In this work, we obtain a model of the multi-asset portfolio given by the system (6) and (14). The terminal condition of the BSDE is made equal to the payoff of the multi-asset option. From the theorems on the existence and uniqueness of the solution of the BSDE (see Theorem 1 and Theorem 3), we prove that there exists a unique solution of the system (6) and (14). Utilizing the Feynman-Kac theorem (Theorem 2), we can obtain the solution of the system (6) and (14), which is consistent with the multi-asset Black-Scholes differential equation's solution. In addition, there are also several factors that affect the price of multi-asset options.

Acknowledgment

The first author of this paper is fully supported by the Department of Mathematics, Institut Teknologi Sepuluh Nopember, with contract number 1367/PKS/ITS/2023.

References

[1] Z. Brzezniak and T. Zastawniak. *Basic Stochastic Processes: A Course Through Exercises*. Springer Science and Business Media, 2000.

[2] N. El Karoui, S. Peng and M. C. Quenez. Backward stochastic differential equations in finance. *Mathematical Finance* **7** (1997) 1–71.

[3] N. El Karoui , S. Hamadéne and A. Matoussi. Backward stochastic differential equations and applications. *Indifference Pricing: Theory and Applications* (2008) 267–320.

[4] J. C. Hull. *Options Futures and Other Derivatives.* Pearson Education India, 2008.

[5] L. Jiang. *Mathematical Modeling and Methods of Option Pricing.* World Scientific Publishing Company, 2005.

[6] Ning Ma, Zhen Wu and Huaizhong Zhao. Backward stochastic differential equations with Markov chains and associated PDEs. *Journal of Differential Equations* **302** (2021) 854–894.

[7] Y. Peng, B. Gong, H. Liu and B. Dai Option pricing on the GPU with backward stochastic differential equation. *2011 Fourth International Symposium on Parallel Architectures, Algorithms and Programming* (2011) 19–23.

[8] N. Perkowski. *Backward Stochastic Differential Equations: An Introduction.* https://api.semanticscholar.org/CorpusID:51816221.

[9] H. Pham. *Continuous-Time Stochastic Control and Optimization with Financial Applications.* Springer, 2009.

[10] P. Sahoo. Probability and mathematical statistics. University of Louisville, 2013.

[11] A. P. Selvadurai. *Partial Differential Equations in Mechanics 1: Fundamental, Laplace's Equation, Diffusion Equation, Wave Equation.* Springer Science and Bussiness Media, 2000.

[12] V. Shcherbakov and E. Larsson. Radial basis function partition of unity methods for pricing vanilla basket options. *Computers and Mathematics with Applications* **71** (2016) 185-200.

[13] K. Shiraya and A. Takahashi. A general control variate method for multi-dimensional SDEs: An application to multi-asset options under local stochastic volatility with jumps models in finance. *European Journal of Operational Research* **258** (2017) 358–371.

[14] F. Soleymani and A. Akgül. Improved numerical solution of multi-asset option pricing problem: A localized RBF-FD approach. *Chaos, Solitons and Fractals* **119** (2019) 298–309.

[15] L. Teng, A. Lapitckii and M. Günther. A multi-step scheme based on cubic spline for solving backward stochastic differential equations. *Applied Numerical Mathematics* **150** (2020) 117–138.

[16] B. Yu, H. Zhu and P. Wu. The closed-form approximation to price basket options under stochastic interest rate. *Finance Research Letters* **46** (2022) 102434.

Nonlinear Dynamics and Systems Theory, **24** (2) (2024) 147–158

Dynamic Analysis of a New Hyperchaotic System with Infinite Equilibria and Its Synchronization

Yasmina Ghettout [1], Lotfi Meddour [2*], Tayeb Hamaizia [2] and Rabiaa Ouahabi [2]

[1] *Laboratory of Differential Equations, Department of Mathematics, Faculty of Exact Sciences, University of Mentouri Brothers, Constantine, Algeria.*
[2] *Department of Mathematics, Faculty of Exact Sciences, University of Mentouri Brothers, Constantine, Algeria.*

Received: August 13, 2023; Revised: February 19, 2024

Abstract: In this paper, a new 4D autonomous hyperchaotic system with an infinite number of equilibrium points is introduced and analyzed. This hyperchaotic system is constructed by introducing an additional dimension with a linear state feedback controller to the third equation in the Lorenz system. The dynamical properties of the new hyperchaotic system are discussed by means of dissipation, symmetry, Lyapunov exponents, bifurcation diagrams, equilibrium points and coexisting attractors. Finally, the synchronization of the novel hyperchaotic system is discussed.

Keywords: *Lorenz system; hyperchaos; infinite equilibria; Lyapunov exponent; synchronization.*

Mathematics Subject Classification (2010): 93B52, 70K50, 34H10, 37G35, 34D06.

1 Introduction

A hyperchaotic system is a type of the dynamical system that exhibits chaotic behavior with at least two positive Lyapunov exponents, and the minimal dimension of the phase space that embeds the hyperchaotic attractor should be at least four. In 1963, Lorenz proposed a three-dimensional system with two scrolls, which is recognized as the first chaotic model reported in literature [10], it has been the subject of many studies (see, for example, [11]). Subsequently, in 1976, Rossler proposed another chaotic system like the Lorenz one, in 1979, Rossler put forward the concept of hyperchaos and proposed the

* Corresponding author: mailto:meddour_lotfi@umc.edu.dz

hyperchaotic Rossler system [13]. As a kind of behavior that is more complex than chaos, hyperchaos has greater application potential in some engineering and technological fields, which need strong complexity, including secure communications [23], nonlinear circuits, encryption, and other fields [20]. Constructing a hyperchaotic system is a real challenge because of the absence of a uniform method to generate this kind of complex systems. Until now, the main method to build a hyperchaotic system is to design it by changing an existing chaotic system. A hyperchaotic system can be generated by adding a simple state feedback controller to a regular chaotic system. The addition of feedback control introduces additional nonlinearities that can lead to more complex and richer dynamical behavior, e.g., the Lü system [14] and the Lorenz system [6].

Hyperchaotic systems with an infinite number of equilibrium points have been classified as a newly introduced class of dynamical systems with hidden attractors. This classification highlights the richness and complexity of these systems and their unique properties that were not fully understood before [21], [15], [8], [1]. The coexistence of multiple attractors in a system is indeed an exceedingly interesting phenomenon that has attracted increasing attention in the scientific community. It challenges our conventional understanding of systems having a single stable state and opens up new avenues for studying and understanding complex dynamics. The coexistence of attractors introduces the concept of multistability, where a system can exhibit different long-term behaviors depending on its initial conditions or parameters. This phenomenon has been observed in various fields of study, including physics, biology, chemistry, engineering, and social sciences. The Lorenz system is a well-known example that demonstrates the phenomenon of coexisting attractors, what makes the Lorenz system particularly interesting is that depending on the system's initial conditions, it can yield a symmetric pair of strange attractors, breaking the symmetry of the butterfly attractor. These two attractors exist simultaneously alongside each other in the system's phase space [9], [2], [22].

The synchronization of chaotic systems is a fascinating area of research that has attracted considerable attention due to its theoretical significance and practical applications, especially in the field of secure communication. Chaotic systems are highly sensitive to initial conditions, and even a tiny change in the initial state can lead to drastically different trajectories over time. Despite this sensitivity, it is possible to synchronize two or more chaotic systems in a way that they evolve with similar dynamics, exhibiting identical or correlated chaotic behaviors [16], [17], [5], [7], [18].

The rest of the paper is organized as follows. In Section 2, the novel hyperchaotic system is introduced with brief details. The dynamical system analysis and its properties are presented in Section 3. In Section 4, a synchronization control system is designed. Finally, conclusions are presented in Section 5.

2 The Novel 4D System with an Infinite Number of Equilibrium Points

The celebrated Lorenz system is described by the following equations [10]:

$$\begin{cases} \dot{x} = -a(y-x), \\ \dot{y} = -xz + cx - y, \\ \dot{z} = xy - bz, \end{cases} \tag{1}$$

where a, b, c are real parameters. When $a = 10$, $b = 8/3$, $c = 28$, it shows chaotic behavior. According to this system, a new 4D system is obtained by introducing an

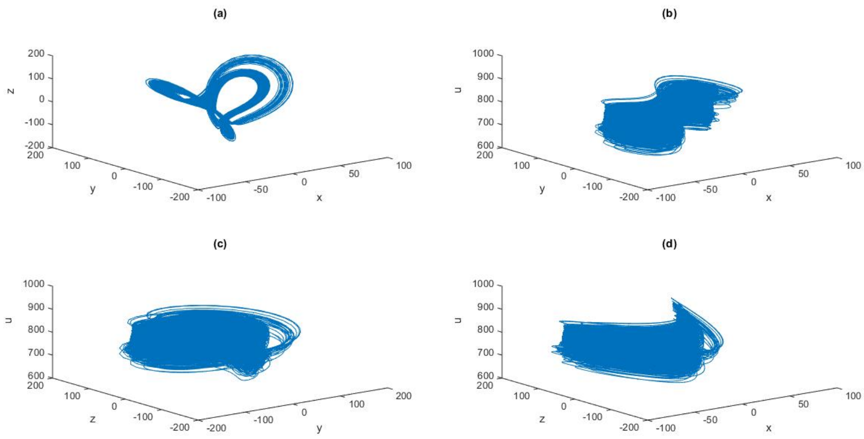

Figure 1: Three-dimensional projections of the hyperchaotic attractor of system (2): $(a, b, c, d) = (10, 5, 30, 20)$. (a) x-y-z phase space; (b) x-y-u phase space; (c) y-z-u phase space; (d) x-z-u phase space.

additional dimension with a linear state feedback controller to the third equation, and our new 4D system is given by the following dynamics:

$$\begin{cases} \dot{x} = -a(x - y), \\ \dot{y} = -xz + cx - y, \\ \dot{z} = xy - bz - u, \\ \dot{u} = dx. \end{cases} \tag{2}$$

We represent the state of the 4D system (2) by $X = (x, y, z, u)$, and a, b, c, d are positive parameters. When the parameters of system (2) are taken as $(a, b, c, d) = (10, 5, 30, 20)$ and the initial conditions $(x_0, y_0, z_0, u_0) = (0.1, 0.1, 0.1, 0.1)$, the system has a hyperchaotic attractor, and the corresponding four Lyapunov exponents can be calculated: $L_1 = 0.8289, L_2 = 0.5692, L_3 = -0.2836, L_4 = -16.9904$. The phase portraits of the new hyperchaotic system (2) are shown in Figure 1.

The Lyapunov dimension, commonly known as the Kaplan-Yorke dimension D_{KY} [3], of this system is

$$D_{KY} = j + \frac{1}{|L_{j+1}|}\sum_{i=1}^{j} L_i = 3 + \frac{L_1 + L_2 + L_3}{|L_4|},$$

$$D_{KY} = 3 + \frac{0.8289 + 0.5692 - 0.2836}{|-16.9904|} = 3.07.$$

3 Dynamical Analysis

3.1 Symmetry

The system (2) is symmetrical with respect to the z-axis for its invariance under the coordinate transformation $(x, y, z, u) \longrightarrow (-x, -y, z, -u)$.

3.2 Dissipativity and existence of attractor

For a dynamical system, the divergence of the system (2) is defined by

$$\nabla V = \frac{d\dot{x}}{dx} + \frac{d\dot{y}}{dy} + \frac{d\dot{z}}{dz} + \frac{d\dot{u}}{du} = -(a+b+1) = -16 < 0. \tag{3}$$

Therefore, the above analysis proves that our system is dissipative. The exponential contraction rate is calculated as follows:

$$V(t) = V(0)e^{-(a+b+1)t}. \tag{4}$$

It shows that each volume containing the system trajectories shrinks to zero as $t \longrightarrow \infty$ at an exponential rate $-(a+b+1)$. There exists an attractor in system (2).

3.3 Equilibrium points

The equilibria of the system (2) can be found by setting $\dot{x} = \dot{y} = \dot{z} = \dot{u} = 0$ and $a, b, c, d > 0$,

$$a(y-x) = 0, \tag{5}$$

$$-xz + cx - y = 0, \tag{6}$$

$$xy - bz - u = 0, \tag{7}$$

$$dx = 0. \tag{8}$$

Equation (8) reveals that $x = 0$. By substituting $x = 0$ into (5), we have $y = 0$, by substituting $x = 0$ and $y = 0$ into (7), we have

$$-bz - u = 0.$$

In other words, system (2) has an infinite number of equilibrium points

$$E = \{(x, y, z, u) \in R^4 | x = 0, y = 0, u = -bz\}.$$

For the equilibrium E, the Jacobian matrix of system (2) is given by

$$\mathcal{J}_E = \begin{pmatrix} -a & a & 0 & 0 \\ c-z & -1 & 0 & 0 \\ 0 & 0 & -b & -1 \\ d & 0 & 0 & 0 \end{pmatrix}.$$

The charasteristic equation of system (2) evaluated at the equilibrium E is

$$\lambda^4 + (a+b+1)\,\lambda^3 + (a + b\,(a+1) - a\,(c-z))\,\lambda^2 + b\,(a - a\,(c-z))\,\lambda = 0,$$

and the eigenvalues are

$$\begin{aligned}\lambda_1 &= 0, \lambda_2 = -b,\ \lambda_3 = -\frac{1}{2}\sqrt{4ac - 2a - 4az + a^2 + 1} - \frac{1}{2}a - \frac{1}{2},\\ \lambda_4 &= \frac{1}{2}\sqrt{4ac - 2a - 4az + a^2 + 1} - \frac{1}{2}a - \frac{1}{2}.\end{aligned}$$

Providing $z > c-1$, we have $\lambda_2 < 0$, $Re(\lambda_3) < 0$ and $Re(\lambda_4) < 0$, then the equilibrium point E is stable. Therefore, if $z < c-1$, the eigenvalue λ_4 is positive, then the equilibrium point E is unstable. Moreover, if $z = c - 1$, the system (2) reduces to the one whose dimension is less than four.

3.4 Bicurcation diagram and Lyapunov exponents

In this subsection, to explore the effect of the parameters a, b, c and d on the behavior of a new 4D system, we fixed the parameters $(a, b, c) = (10, 5, 30)$ and varied d in $[0, 25]$. Now we carry out the dynamic analysis of the system (2) numerically by its Lyapunov exponent spectrum and bifurcation diagram. Figure 2 shows the bifurcation diagram of system (2) with different values of the parameter d and the initial conditions $(x_0, y, z_0, u_0) = (1.8, 0.1, 0.79, 2.8)$. Table 1 represents the Lyapunov exponents and Lyapunov dimensions of the system (2) with different values of the parameter d .

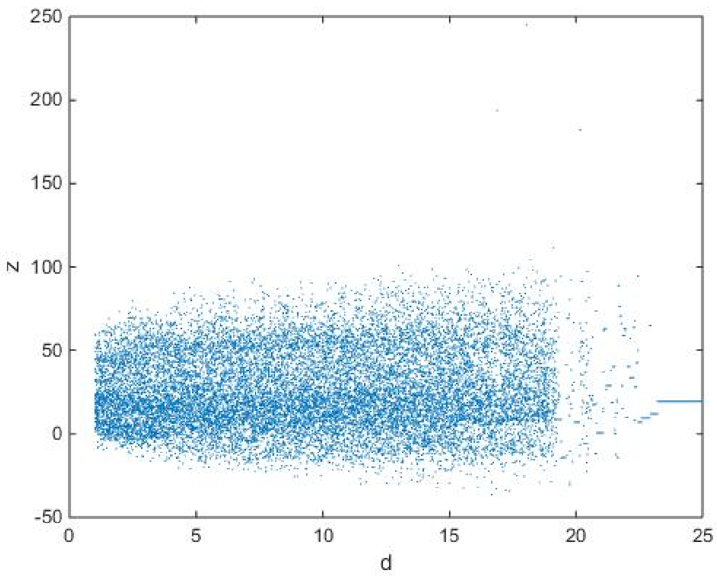

Figure 2: Bifurcation diagrams of hyperchaotic system (2) when $a = 10, b = 5, c = 30$ and d varies in $[0, 25]$.

The dynamics of system (2) changes with the increasing value of the parameter d. We can see that the results obtained from the Lyapunov spectrum agree with the results given by the bifurcation diagram in Figure 2 and the maximal Lyapunov exponents in Table 1.

Table 1: Lyapunov exponents of (2) with $(a, b, c) = (10, 5, 30)$ and different values of d.

d	L_1	L_2	L_3	L_4	Attractor type	D_{KY}
2	0	-0.7873	-0.6745	-14.5233	Periodic attractor	1
12	0.9154	0.0452	-0.0832	-16.7967	Hyperchaotic attractor	3.05
19	0.4400	-0.0128	-0.4658	-15.8353	Chaotic attractor	2.92

3.5 Coexisting attractors

The system (2) shows many complex dynamics behaviors such as hyperchaos, chaos, and periodic. Several coexisting attractors of the system (2) will be present under some appropriate parameters. A system with coexisting attractors is very sensitive to system parameters and initial values. In the event of a sudden disturbance, the state of the system can easily shift from an ideal state to another state that may be undesirable. The coexisting attractors of the system (2) satisfying different initial values can exhibit various dynamic behaviors.

Coexistence of hyperchaotic and chaotic attractors

When we fix $a = 10, b = 5, c = 30, d = 20$, and change the initial values slightly, the dynamical behaviors of the system may produce large variations in the long term:
(a) For the initial values $(0.1, 0.1, 0.1, 0.1)$, the Lyapunov exponents of the system (2) are found to be $L_1 = 0.8289, L_2 = 0.5692, L_3 = -0.2836$, and $L_4 = -16.9904$, while the fractal dimension of the system is estimated to be 3.07. A hyperchaotic attractor with an infinite number of equilibrium points can be obtained, whose 3D phase portrait is shown in Figure 3 (a).

(b) For the initial values $(-2.2, 0.1, 1, 0.1)$, the trajectories of system (2) converge to a chaotic attractor. The Lyapunov exponents of the system (2) are found to be $L_1 = 0.6775, L_2 = -0.1010, L_3 = -2.7889$, and $L_4 = -13.3054$, while the fractal dimension of the system is estimated to be 2.83, whose 3D phase portrait is shown in Figure 3(b).
Therefore, the modification of the inial conditions causes a change of the hyperchaotic behavior of the system (2). The trajectories of system (2) converge to two types of attractors (hyperchaos or chaos).

Coexistence of hyperchaotic and periodic attractors

When we fix $a = 10, b = 5, c = 30, d = 2$, and change the initial values slightly, the dynamical behaviors of the system may produce large variations in the long term:

(a) For the initial values $(-1.8, 0.1, 0.79, 2.8)$ the trajectories of system (2) converge to a hyperchaotic attractor. The Lyapunov exponents of the system (2) are found to be $L_1 = 0.5365, L_2 = 0.0710, L_3 = -0.1822$, and $L_4 = -16.3938$, while the fractal dimension of the system is estimated to be 3.03, whose 3D phase portrait is shown in Figure 4(a).

(b) For the initial values $(1.8, 0.1, 0.79, 2.8)$, the trajectories of system (2) converge to a stable periodic orbit. The Lyapunov exponents of the system (2) are found to be $L_1 = 0, L_2 = -0.7873, L_3 = -0.6745$, and $L_4 = -14.5233$, while the fractal dimension of the system is estimated to be 1, whose 3D phase portrait is shown in Figure 4(b).

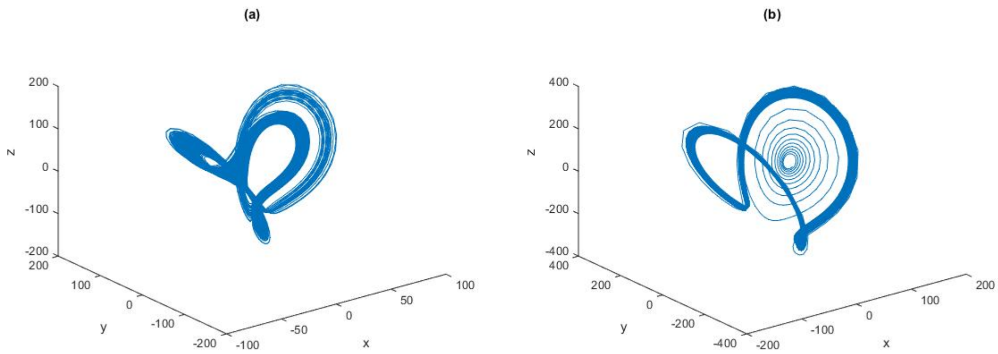

Figure 3: (a) Hyperchaotic attractor with $(a, b, c, d) = (10, 5, 30, 20)$ and $(x_0, y_0, z_0, u_0) = (0.1, 0.1, 0.1, 0.1)$. (b) Chaotic attractor with $(a, b, c, d) = (10, 5, 30, 20)$ and $(x_0, y_0, z_0, u_0) = (-2.2, 0.1, 1, 0.1)$.

A small change in the initial condition of the system causes a wide difference of trajectories. For different initial conditions, the trajectories converge to different attractors: a periodic orbit and hyperchaotic attractor.

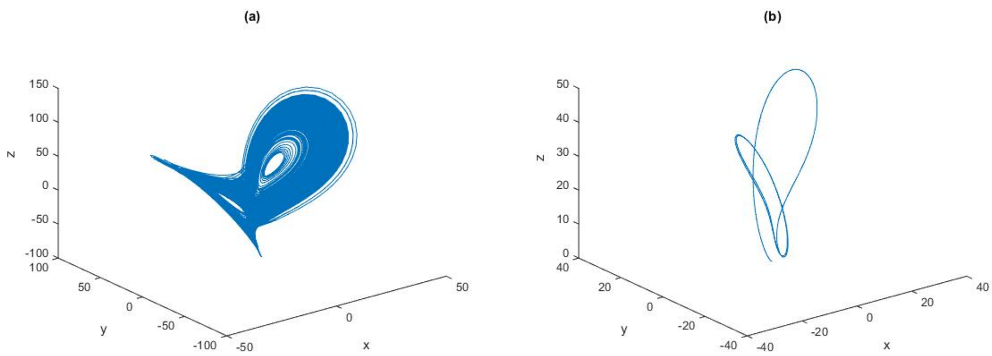

Figure 4: (a) Hyperchaotic attractor with $(a, b, c, d) = (10, 5, 30, 2)$ and $(x_0, y_0, z_0, u_0) = (-1.8, 0.1, 0.79, 2.8)$. (b) Periodic attractor with $(a, b, c, d) = (10, 5, 30, 2)$ and $(x_0, y_0, z_0, u_0) = (1.8, 0.1, 0.79, 2.8)$

4 Synchronization of a New Hyperchaotic System

In this section, the synchronization of the novel 4D hyperchaotic system (2) newly introduced is discussed. Synchronization is done between a system designed as a master one and another system as a slave one. The principle of synchronization is to apply to the slave system a control function such as the error between the two systems tends to zero. We have synchronized two identical new hyperchaotic systems with different initial conditions via the active control method.

As the master system, we consider the novel 4D hyperchaotic system (2) given by

$$\begin{cases} \dot{x_1} = -a(x_1 - x_2), \\ \dot{x_2} = -x_1x_3 + cx_1 - x_2, \\ \dot{x_3} = x_1x_2 - bx_3 - x_4, \\ \dot{x_4} = dx_1. \end{cases} \tag{9}$$

The slave system is the same system (2), with the added to it control signals $U = \{u_1, u_2, u_3, u_4\}$. It is given by

$$\begin{cases} \dot{y_1} = -a(y_1 - y_2) + u_1, \\ \dot{y_2} = -y_1y_3 + cy_1 - y_2 + u_2, \\ \dot{y_3} = y_1y_2 - by_3 - y_4 + u_3, \\ \dot{y_4} = dy_1 + u_4. \end{cases} \tag{10}$$

The synchronization error is defined by

$$\begin{cases} e_1 = y_1 - x_1, \\ e_2 = y_2 - x_2, \\ e_3 = y_3 - x_3, \\ e_4 = y_4 - x_4. \end{cases} \tag{11}$$

Then the error dynamics is expressed by

$$\begin{cases} \dot{e_1} = a(e_2 - e_1) + u_1, \\ \dot{e_2} = ce_1 - e_2 - y_1y_3 + x_1x_3 + u_2, \\ \dot{e_3} = -be_3 - e_4 + y_1y_2 - x_1x_2 + u_3, \\ \dot{e_4} = de_1 + u_4. \end{cases} \tag{12}$$

We choose the active control functions u_1, u_2, u_3, u_4 as shown in equation (13) to eliminate the nonlinear terms in (12):

$$\begin{cases} u_1 = v_1, \\ u_2 = y_1y_3 - x_1x_3 + v_2, \\ u_3 = -y_1y_2 + x_1x_2 + v3, \\ u_4 = v_4. \end{cases} \tag{13}$$

So, the system to be controlled is a linear system with a control input $\{v_1, v_2, v_3, v_4\}$

$$\begin{cases} \dot{e_1} = a(e_2 - e_1) + v_1, \\ \dot{e_2} = ce_1 - e_2 + v_2, \\ \dot{e_3} = -be_3 - e_4 + v_3, \\ \dot{e_4} = de_1 + v_4. \end{cases} \tag{14}$$

The control input v_1, v_2, v_3 and v_4 is used to force the error to converge to zero. So, the two systems (9) and (10) are synchronized.

We choose a constant matrix C which will control the error dynamics (14) such that

$$[\dot{e_1}, \dot{e_2}, \dot{e_3}, \dot{e_4}]^T = C[e_1, e_2, e_3, e_4]^T. \tag{15}$$

For the Routh-Hurwitz criterion, all eigenvalues of the chosen matrix C must be negative [19] to stabilize the synchronization between the master system (9) and the slave system (10):

$$\mathcal{C} = \begin{pmatrix} -1 & 0 & 0 & 0 \\ 0 & -1 & 0 & 0 \\ 0 & 0 & -1 & 0 \\ 0 & 0 & 0 & -1 \end{pmatrix}.$$

The eigenvalues $(\lambda_1, \lambda_2, \lambda_3, \lambda_4) = (-1, -1, -1, -1)$ of the matrix C are negative, which ensures the stability of the dynamic error. Therefore two systems (9) and (10) are synchronized.

Using (14), (15) and (16), we find the control functions

$$\begin{cases} a(e_2 - e_1) + v_1 = -e_1, \\ ce_1 - e_2 + v_2 = -e_2, \\ -be_3 - e_4 + v_3 = -e_3, \\ de_1 + v_4 = -e_4, \end{cases} \tag{16}$$

$$\begin{cases} v_1 = (a-1)e_1 - ae_2, \\ v_2 = -ce_1, \\ v_3 = (b-1)e_3 + e_4, \\ v_4 = -de_1 - e_4. \end{cases} \tag{17}$$

The control function $U = \{u_1, u_2, u_3, u_4\}$ ensures synchronization between the master system (9) and the slave system (10),

$$\begin{cases} u_1 = (a-1)e_1 - ae_2, \\ u_2 = y_1y_3 - x_1x_3 - ce_1, \\ u_3 = -y_1y_2 + x_1x_2 + (b-1)e_3 + e_4, \\ u_4 = -de_1 - e_4. \end{cases} \tag{18}$$

The initial conditions of the master system and the slave system are taken as follows:

$$(x_1, x_2, x_3, x_4) = (3, 4, 10, -8),$$

$$(y_1, y_2, y_3, y_4) = (-2, 32, -6, 12).$$

The results of simulations are depicted in Figure 5 and Figure 6, these figures show that the synchronization occurs and the errors will converge to zero exponentially after applying the active control.

5 Conclusions

In this work, we have introduced a novel hyperchaotic system with an infinite number of equilibrium points. Depending on parameter selection and initial conditions, this system can generate various types of coexisting attractors. Through theoretical analysis

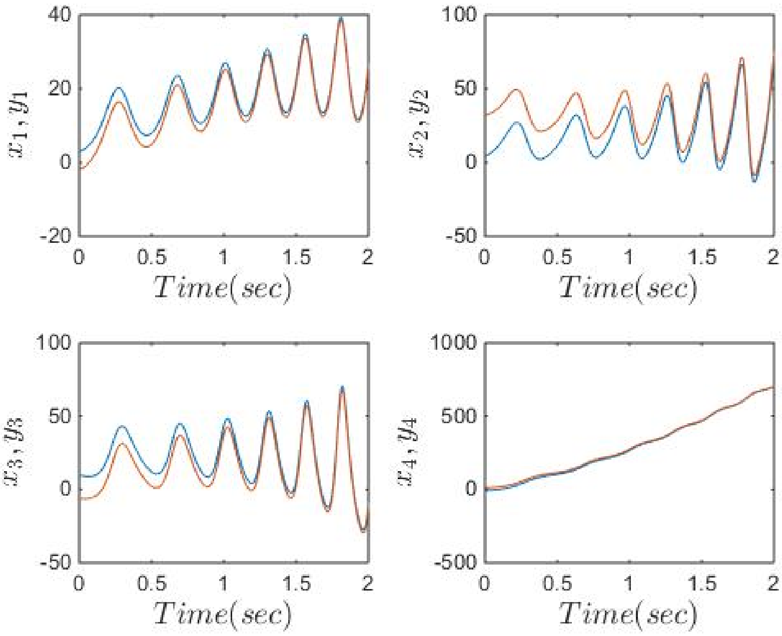

Figure 5: Synchronization of different state variables.

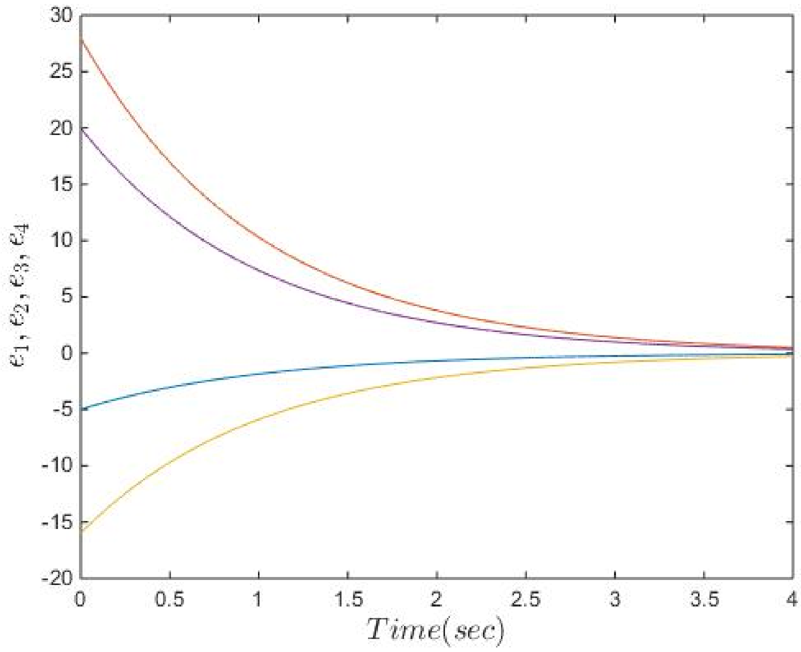

Figure 6: Errors of the synchronization system.

and numerical simulations, we investigate the dynamical behaviors of the new hyperchaotic system. This exploration encompasses dissipativity and invariance, equilibrium points and their stability, periodic orbits, as well as chaotic and hyperchaotic attractors. We conduct numerical simulations, including phase diagrams and the Lyapunov exponent spectrum, to analyze and validate the complex phenomena exhibited by our hyperchaotic system. Furthermore, we successfully achieve synchronization between this system, designed as the master one, and another system acting as the slave one, using the active control techniques.

References

[1] Y. Chen and Q.A. Yang. new Lorenz-type hyperchaotic system with a curve of equilibria. *Mathematics and Computers in Simulation* **112** (2015) 40–55.

[2] C. Dong and J. Wang. Hidden and coexisting attractors in a novel 4D hyperchaotic system with no equilibrium point. *Fractal and Fractional* **6**(6) (2022) 306.

[3] P. Frederickson, J.L. Kaplan, E.D. Yorke and J.A. Yorke. The Liapunov dimension of strange attractors. *Journal of differential equations* **49** (2) (1983) 185–207.

[4] F. Zhang, X. Liao, G. Zhang and C. Mu. Complex dynamics of a new 3D Lorenz-type autonomous chaotic system. *Pramana - J. Phys.* **89** (2017) 84.

[5] A. Ikhlef and N. Mansouri. Hyperchaotification and Synchronization of Chaotic Systems. *International Journal of Control* **2** (4) (2012) 69–74.

[6] J. Qiang. Hyperchaos generated from the Lorenz chaotic system and its control. *Physics Letters A* **366** (3) (2007) 217–222.

[7] Basil H. Jasim, Anwer Hammadi Mjily, Anwer Mossa Jassim AL-Aaragee. A novel 4 dimensional hyperchaotic system with its control, synchronization and implementation. *International Journal of Electrical and Computer Engineering* **11** (4) (2021) 2974.

[8] Sifeu Takougang Kingni, Viet-Thanh Pham, Sajad Jafari and Paul Woafo. A chaotic system with an infinite number of equilibrium points located on a line and on a hyperbola and its fractional-order form. *Chaos, Solitons & Fractals* **99** (2017) 209–218.

[9] Qiang Lai, Tsafack Nestor, Kengne Jacques and Xiao-Wen Zhao. Coexisting attractors and circuit implementation of a new 4D chaotic system with two equilibria. *Chaos, Solitons & Fractals* **107** (2018) 92–102.

[10] E.N. Lorenz. Deterministic nonperiodic flow. *Journal of atmospheric sciences* **20** (2) (1963) 130–141.

[11] L. Meddour and K. Belakrouml. On the Equivalence of Lorenz System and Li System. *Nonlinear Dynamics and Systems Theory* **22 (1)** (2022) 58–65.

[12] T. Nestor, A. Belazi, B. Abd-El-Atty, M.N. Aslam, C. Volos, D. Dieu, J. Nkapkop and A. Abd El-Latif. A new 4D hyperchaotic system with dynamics analysis, synchronization, and application to image encryption, *Symmetry* **14** (2) (2022) 424.

[13] O. Rossler. An equation for hyperchaos. *Physics Letters A* **71** (1979) 155-157.

[14] S. Pang and Y. Liu. A new hyperchaotic system from the Lü system and its control. *Journal of Computational and Applied Mathematics* **235** (8) (2011) 2775–2789.

[15] Pham, Viet-Thanh and Volos, Christos and Vaidyanathan, Sundarapandian and Wang, Xiong and others. A chaotic system with an infinitenumber of equilibrium points: dynamics, horseshoe and synchronization. *Advances in Mathematical Physics* **2016** (2016).

[16] L.M. Pecora and T.L. Carroll. Synchronization in chaotic systems. *Physical review letters* **64** (8) (1990) 821.

[17] R. Rameshbabu, K. Kavitha, P. S. Gomathi and K. Kalaichelvi A New Hidden Attractor Hyperchaotic System and Its Circuit Implementation, Adaptive Synchronization and FPGA Implementation. *Nonlinear Dynamics and Systems Theory* **23** (2) (2023) 214—226.

[18] S. Vaidyanathan and K. Rajagopal. Chaos Synchronization between Fractional-Order Lesser Date Moth Chaotic System and Integer-Order Chaotic System via Active Control. *Nonlinear Dynamics and Systems Theory* **22** (4) (2022) 407–413.

[19] S. Vaidyanathan and K. Rajagopal. Anti-Synchronization of Tigan and Li Systems with Unknown Parameters via Adaptive Control. *An International Journal of Optimization and Control: Theories & Applications* **2** (2012) 17–28.

[20] Z. Wang, F. Min and E. Wang. A new hyperchaotic circuit with two memristors and its application in image encryption. *Aip Advances* **6** (9) (2016) 095316.

[21] H. Wang and X. Li. A novel hyperchaotic system withinfinitely many heteroclinic orbits coined. *Chaos, Solitons & Fractals* **106** (2018) 5–15.

[22] Z. Wei, R. Wang and A. Liu. A new finding of the existence of hidden hyperchaotic attractors with no equilibria. *Mathematics and Computers in Simulation* **100** (2014) 13–23.

[23] S. Zhang and T. Gao. A coding and substitution frame based on hyper-chaotic systems for secure communication. *Nonlinear Dynamics* **84** (2016) 833–849.

Nonlinear Dynamics and Systems Theory, **24** (2) (2024) 159–167

Conformable Fractional Inverse Gamma Distribution

Mamon Abu Hammad, Shameseddin Alshorm *, Sondos Rasem and Lena Abed

Department of Mathematics, Al Zaytoonah University, Amman 11733, Jordan.

Received: September 7, 2023; Revised: March 4, 2024

Abstract: In this paper, we will study the Inverse Gamma distribution to introduce the Conformable Fractional Inverse Gamma Distribution (CFIGD) with a study of the entropy measures in the fractional case. The CFIGD's CDF, survival function, and hazard function are defined to shed light on its behavior and suggest possible uses for it in reliability and risk analysis. It is possible to better understand the central tendencies and higher-order characteristics of statistics by using the conformable fractional analogs of statistical measures like the expected values, r-th moments, mean, variance, skewness, and kurtosis. In addition, the conformable fractional analogs of well-known entropy measures like the Shannon, Renyi, and Tsallis entropy are introduced, offering useful instruments for estimating uncertainty and randomness.

Keywords: *probability distribution functions; conformable fractional; conformable derivative; entropy.*

Mathematics Subject Classification (2010): 26A33, 34A08, 34K37, 70K75, 70K99.

1 Introduction

The Conformable Fractional Inverse Gamma Distribution (CFIGD), which offers an avant-garde framework for simulating various real-world phenomena, has emerged as a promising statistical tool [1,2]. The development of sophisticated tools to model complex phenomena and derive meaningful insights is made possible by advancements in probability theory and statistical analysis [3,4]. The CFIGD stands out among these tools as a potent and ground-breaking idea, providing a new viewpoint on probability distributions and their applications. The CFIGD and its numerous applications in various fields will be thoroughly explored in this research paper.

* Corresponding author: alshormanshams@gmail.com

The foundation of the CFIGD is the inverse gamma distribution, which is well-known for its importance in Bayesian statistics. This family of distributions is the reciprocal of a variable that follows a gamma distribution and operates on positive real numbers. By extending conventional statistical measures to conformable fractional analogs, the CFIGD introduces a novel approach. Our comprehension of the distribution's central tendencies, higher-order properties, and quantification of uncertainty is greatly improved by these analogs [5, 7, 8].

The paper aims to clarify the fundamental characteristics of the CFIGD, namely the cumulative distribution function (CDF), survival function, and hazard function. In addition to these, we investigate the conformable fractional analogs of fundamental statistical quantities like the expected values, r-th moments, mean, variance, skewness, and kurtosis. The theoretical framework of the CFIGD is built on this thorough analysis.

Nonlinear dynamics plays a pivotal role in understanding complex systems, where traditional linear models fall short. In recent years, there has been a growing interest in exploring non-conventional probability distributions and statistical measures to enhance our comprehension of intricate systems and phenomena. This paper delves into the realm of nonlinear dynamics by introducing a novel statistical distribution, the Conformable Fractional Inverse Gamma Distribution (CFIGD) and studying its properties in the context of entropy measures in the fractional case.

Nonlinear systems, characterized by their sensitivity to initial conditions and intricate feedback loops, necessitate sophisticated statistical tools for accurate modeling and analysis. The Inverse Gamma distribution has proven to be invaluable in various fields, especially in reliability and risk analysis, where understanding the underlying probabilistic nature of events is paramount. The extension of this distribution to its fractional counterpart, as explored in this paper, opens new avenues for studying nonlinear systems with fractional dynamics, providing a more nuanced understanding of their behavior.

The organization of this paper is listed as follows. In the following section, we will introduce the basic definitions and remarks on conformable fractional derivatives. In Section 3, we will introduce a fractional inverse gamma distribution, this part is followed by Section 4 with the conclusion for this paper and references.

2 Conformable Fractional Derivative

Fractional calculus is a branch of mathematics that deals with fractional derivatives and integrals, and it has numerous applications in a variety of scientific and engineering disciplines. A current framework for describing non-local and memory-dependent complex processes is offered by fractional derivatives. One of the fascinating developments in this field is the idea of a "conformable fractional derivative", introduced by Khalil et al. [6] in 2014.

When applied to phenomena with non-differentiable or non-smooth behavior, integer-order derivatives, which are frequently used in classical calculus, have some limitations. Fractional derivatives, however, overcome these limitations by taking into account non-integer orders, which better capture a variety of natural and artificial systems utilizing the notion of conformable fractional derivative. This new concept provides a different perspective on fractional derivatives and their applications [9–11]. The conformable fractional derivative, while retaining the advantages of fractional calculus, offers an intriguing framework for modeling complex phenomena that exhibit conformability to prevailing physical laws [12–15].

Definition 2.1 Let α be a real nonnegative number. For a positive integer m such that $m-1<\alpha\leq m$, the Riemann-Liouville fractional-order differential operator of a function f of order α is defined by

$$D_a^\alpha f(x)=\frac{1}{\Gamma(m-\alpha)}\frac{d^m}{dx^m}\int_a^x (x-t)^{m-\alpha-1}f(t)dt. \tag{1}$$

Definition 2.2 Let $\alpha\in\mathbb{R}$ and $m=\lceil\alpha\rceil$. The Caputo fractional-order derivative operator D_a^α is defined by

$$D_a^\alpha f=J_a^{m-\alpha}D^m f. \tag{2}$$

Definition 2.3 Let $\alpha\in\mathbb{R}^+$ and $m=\lceil\alpha\rceil$ such that $m-1<\alpha\leq m$. Then the Caputo fractional-order deivative operator of order α is given by

$$D_a^\alpha f(x)=\frac{1}{\Gamma(m-\alpha)}\int_a^x (x-t)^{m-\alpha-1}f^{(m)}(t)dt,\ x>a. \tag{3}$$

It should be noted that if $a=0$ in Equation (3), one can get the most reliable version of the Caputo fractional-order derivative operator. That is,

$$D_*^\alpha f(x)=\frac{1}{\Gamma(m-\alpha)}\int_0^x (x-t)^{m-\alpha-1}f^{(m)}(t)dt,\ x>0. \tag{4}$$

Definition 2.4 Let $\omega:[0,\infty)\to\mathbb{R}$ and $t>0$, then given ω of order α, the conformable fractional derivative is defined as

$$D_\alpha(\omega)(t)=\lim_{\epsilon\to 0}\frac{\omega(t+\epsilon t^{1-\alpha})-\omega(t)}{\epsilon} \tag{5}$$

for all $t>0$ and $\alpha\in(0,1)$. If ω is α-differentiable in some $(0,a)$, $a>0$ and $\lim_{t\to 0^+}\omega^{(\alpha)}(t)$ exists, then specify $\omega^{(\alpha)}(0)=\lim_{t\to 0^+}\omega^{(\alpha)}(t)$.

Remark 2.1 The conformable fractional derivatives of ω of order α are denoted by $\omega^{(\alpha)}(t)$ for $D_\alpha(\omega)(t)$. Furthermore, we simply state ω is α-differentiable if the conformable fractional derivative of ω of order α exists, where $D_\alpha(t^p)=pt^{p-\alpha}$.

Remark 2.2 The integral departs from the standard Riemann integral and instead involves an erroneous version. The parameter α takes values in the interval (0, 1). The conformable derivative, while maintaining all the conventional characteristics of the ordinary first derivative, is under consideration. Furthermore, the derivative gives rise to correct propositions according to the context presented.

- $D_\alpha(a\omega+b\varphi)=aD_\alpha(\omega)+bD_\alpha(\varphi)$,
- $D_\alpha(t^p)=pt^{p-\alpha}$, for all $p\in\mathbb{R}$,
- $D_\alpha(\omega\varphi)=\omega D_\alpha(\varphi)+\varphi D_\alpha(\omega)$,
- $D_\alpha(\frac{\omega}{\varphi})=\frac{\varphi D_\alpha(\omega)-\omega D_\alpha(\varphi)}{\varphi^2}$.

3 Fractional Inverse Gamma Distribution

The Inverse Gamma distribution, denoted as $IG(\delta, \beta)$, is a two-parameter family of continuous probability distributions defined on the positive real line. The Cumulative Distribution Function (CDF) of the Inverse Gamma distribution is given by

$$G(x; \delta, \beta) = 1 - \frac{\beta^\delta}{\Gamma(\delta)} \int_0^x t^{\delta+1} e^{-\beta/t} dt, \tag{6}$$

where $\delta > 0$ and $\beta > 0$ are the shape and scale parameters, respectively, and $\Gamma(\delta)$ represents the Gamma function.

The Probability Density Function (PDF) of the Inverse Gamma distribution is defined as

$$g(x; \delta, \beta) = \frac{\beta^\delta}{\Gamma(\delta)} x^{-(\delta+1)} e^{-\beta/x}, \tag{7}$$

where $\delta > 0$ and $\beta > 0$ are the shape and scale parameters, respectively, and $\Gamma(\delta)$ represents the Gamma function.

In this section, we will introduce the CFIGD defined as follows:

$$\begin{aligned} &x^{2\alpha} D^\alpha y + (bx^\alpha - \beta + x^\alpha) y = 0, \\ &g_\alpha(x) = \frac{\alpha^2 (\frac{\beta}{\alpha})^{(b+1)/\alpha}}{\beta \Gamma(\frac{(b-\alpha-1)}{\alpha})} x^{-(b+1)} e^{\frac{-\beta}{(\alpha x^\alpha)}}. \end{aligned} \tag{8}$$

Consequently,

$$\lim_{\alpha \to 1^-} g_\alpha(x) = \frac{\beta^b}{\Gamma(b)} x^{-(b+1)} e^{\frac{-\beta}{x}}. \tag{9}$$

This represents the PDF of the Inverse Gamma distribution. Consequently, the CPDF $g_\alpha(x)$ can be seen as an extension or generalization of the PDF for the Inverse Gamma distribution as the following Figure 1 shows, and for more about fractional distributions, see [16–21]. For the Inverse Gamma distribution, α refers to the shape parameter. The

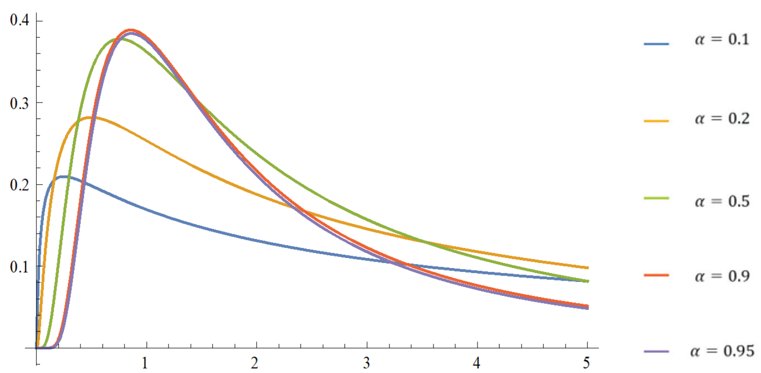

Figure 1: The CPDF of the inverse gamma distribution for different values of α.

shape parameter α is a crucial parameter that governs the shape of the distribution. It determines the skewness and tail behavior of the distribution.

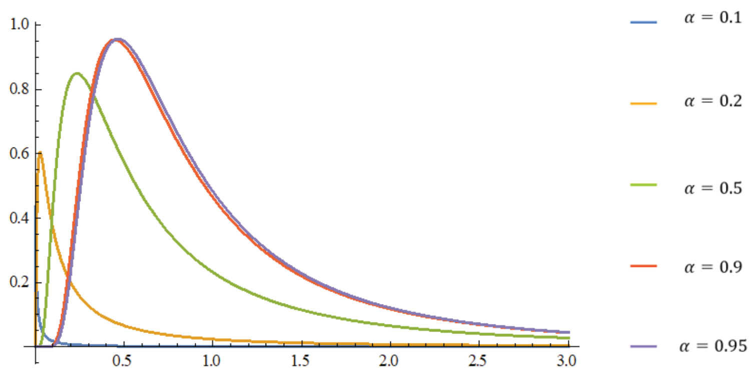

Figure 2: The CFSF of the inverse gamma distribution for different values of α.

A higher value of α results in a distribution that is more concentrated around its mean, with lighter tails. On the other hand, a lower value of α leads to a more spread-out distribution with heavier tails. Note that α must be greater than 0.

Definition 3.1 The Conformable α-Inverse Gamma Distribution (CFCDF) is defined as

$$\begin{aligned} G_\alpha(x) &= \int_0^x g_\alpha(t) d^\alpha t, \\ G_\alpha(x) &= \frac{(\frac{\alpha}{\beta})^{\frac{(2+b-\alpha)(-1+\alpha)}{\alpha}} \Gamma(2+b-\frac{1}{\alpha}-\alpha, \frac{x^{-\alpha\beta}}{\alpha})}{\Gamma(\frac{1+b-\alpha}{\alpha})}. \end{aligned} \tag{10}$$

Definition 3.2 The Conformable Fractional Survival Function (CFSF) of X, (S_α) is defined as

$$\begin{aligned} S_\alpha(x) &= 1 - G_\alpha(X) \\ S_\alpha(x) &= 1 - \frac{(\frac{\alpha}{\beta})^{\frac{(2+b-\alpha)(-1+\alpha)}{\alpha}} \Gamma(2+b-\frac{1}{\alpha}-\alpha, \frac{x^{-\alpha\beta}}{\alpha})}{\Gamma(\frac{1+b-\alpha}{\alpha})}. \end{aligned} \tag{11}$$

Definition 3.3 The Conformable Fractional Hazard Function (CFHF) X, (H_α) is defined as

$$\begin{aligned} H_\alpha &= \frac{S_\alpha(x)}{g_\alpha(x)}, \\ H_\alpha(x) &= \frac{e^{\frac{-x^{-\alpha\beta}}{\alpha}} x^{-1-b} \alpha^{\frac{-1-b+2\alpha}{\alpha}} \beta^{\frac{1+b-2\alpha}{\alpha}}}{\Gamma(\frac{1+b-\alpha}{\alpha}) - (\frac{\alpha}{\beta})^{\frac{(2+b-\alpha)(-1+\alpha)}{\alpha}} \Gamma(2+b-\frac{1}{\alpha}-\alpha, \frac{x^{-\alpha\beta}}{\alpha})}. \end{aligned} \tag{12}$$

Definition 3.4 The conformable fractional expectation E_α for the function $v(x)$ is defined as follows:

$$\begin{aligned} E_\alpha v(X) &= \int v(x) g_\alpha(x) d^\alpha x, \\ E_\alpha(X^r) &= \frac{\alpha^{\frac{-r}{\alpha}} \beta^{\frac{r}{\alpha}} \Gamma(\frac{1+b-r-\alpha}{\alpha})}{\Gamma(\frac{1+b-\alpha}{\alpha})}. \end{aligned} \tag{13}$$

To find the conformable fractional variance, conformable fractional standard deviation, conformable fractional skewness, and conformable fractional kurtosis, we will find the $E_\alpha(X^r)$ for $r = 1, 2, 3, 4$ as follows:

$$\begin{aligned}
E_\alpha(X) = \mu_\alpha &= \frac{(\frac{\alpha}{\beta})^{\frac{-1}{\alpha}}\Gamma(-1+\frac{b}{\alpha})}{\Gamma(\frac{1+b-r-\alpha}{\alpha})},\\
E_\alpha(X^2) &= \frac{(\frac{\alpha}{\beta})^{\frac{-2}{\alpha}}\Gamma(\frac{-1+b-\alpha}{\alpha})}{\Gamma(\frac{1+b-\alpha}{\alpha})},\\
E_\alpha(X^3) &= \frac{(\frac{\alpha}{\beta})^{1-\frac{1+b}{\alpha}}\beta(\frac{\beta}{\alpha})^{\frac{2-b}{\alpha}}\Gamma(-1+\frac{-2+b}{\alpha})}{\alpha\Gamma(-1+\frac{1+b}{\alpha})},\\
E_\alpha(X^4) &= \frac{(\frac{\alpha}{\beta})^{1-\frac{1+b}{\alpha}}\beta(\frac{\beta}{\alpha})^{\frac{3-b}{\alpha}}\Gamma(-1+\frac{-3+b}{\alpha})}{\alpha\Gamma(-1+\frac{1+b}{\alpha})}.
\end{aligned} \tag{14}$$

Definition 3.5 The conformable fractional variance is defined as follows:

$$\begin{aligned}
\alpha\sigma^2 &= E_\alpha(X^2) - (\mu_\alpha)^2,\\
\alpha\sigma^2 &= \frac{\alpha^{\frac{-2}{\alpha}}\beta^{\frac{2}{\alpha}}\Big(-\Gamma(-1+\frac{b}{\alpha})^2+\Gamma(\frac{-1+b-\alpha}{\alpha})\Gamma(\frac{1+b-\alpha}{\alpha})\Big)}{\Gamma(\frac{1+b-\alpha}{\alpha})^2}.
\end{aligned} \tag{15}$$

Definition 3.6 The conformable fractional standard deviation is defined as follows:

$$\alpha\sigma = \sqrt{\frac{\alpha^{\frac{-2}{\alpha}}\beta^{\frac{2}{\alpha}}\Big(-\Gamma(-1+\frac{b}{\alpha})^2+\Gamma(\frac{-1+b-\alpha}{\alpha})\Gamma(\frac{1+b-\alpha}{\alpha})\Big)}{\Gamma(\frac{1+b-\alpha}{\alpha})^2}}. \tag{16}$$

Definition 3.7 The conformable fractional skewness is defined as follows:

$$\alpha sk = \frac{E_\alpha(X-\mu)^3}{\alpha\sigma^3}, \tag{17}$$

and the conformable fractional skewness for CFIGD is defined as

$$sk = \frac{\Big(2\Gamma(-1+\frac{b}{\alpha})^3 - 3\Gamma(-1+\frac{b}{\alpha})\Gamma(\frac{-1+b-\alpha}{\alpha})\Gamma(\frac{1+b-\alpha}{\alpha})+\Gamma(\frac{-2+b-\alpha}{\alpha})\Gamma(\frac{1+b-\alpha}{\alpha})^2\Big)}{\Big(-\Gamma(-1+\frac{b}{\alpha})^2+\Gamma(\frac{-1+b-\alpha}{\alpha})\Gamma(\frac{1+b-\alpha}{\alpha})\Big)^{\frac{3}{2}}}. \tag{18}$$

Definition 3.8 The conformable fractional kurtosis is defined as follows:

$$\alpha ku = \frac{E_\alpha(X-\mu)^4}{\alpha\sigma^4}, \tag{19}$$

and the conformable fractional kurtosis for CFIGD is defined as

$$\begin{aligned}
\alpha ku = &\frac{-3\Gamma(-1+\frac{b}{\alpha})^4+6\Gamma(-1+\frac{b}{\alpha})^2\Gamma(\frac{-1+b-\alpha}{\alpha})\Gamma(\frac{1+b-\alpha}{\alpha})}{\Big(\Gamma(-1+\frac{b}{\alpha})^2-\Gamma(\frac{-1+b-\alpha}{\alpha})\Gamma(\frac{1+b-\alpha}{\alpha})\Big)^2}\\
&-\frac{4\Gamma(-1+\frac{b}{\alpha})\Gamma(\frac{-2+b-\alpha}{\alpha})\Gamma(\frac{1+b-\alpha}{\alpha})^2+\Gamma(\frac{-3+b-\alpha}{\alpha})\Gamma(\frac{1+b-\alpha}{\alpha})^3}{\Big(\Gamma(-1+\frac{b}{\alpha})^2-\Gamma(\frac{-1+b-\alpha}{\alpha})\Gamma(\frac{1+b-\alpha}{\alpha})\Big)^2}.
\end{aligned} \tag{20}$$

Definition 3.9 The conformable fractional Shannon entropy of a random variable x for the CFIGD is defined as follows:

$$SH_\alpha(x) = -E_\alpha \log g_\alpha(X),$$

$$SH_\alpha(x) = \frac{1+b-\alpha-2\alpha\log(\alpha)+\alpha\log(\beta)+\alpha\log(\Gamma(\frac{1+b-\alpha}{\alpha}))-(1+b)\Psi(0,\frac{1+b-\alpha}{\alpha})}{\alpha}. \tag{21}$$

Definition 3.10 The conformable fractional Tsallis entropy of a random variable x for the CFIGD is defined as follows:

$$SH_{T,\xi}(x) = \frac{1}{1-\xi}\log(E_\alpha(g_\alpha(X))^{\xi-1}-1),$$
$$SH_{T,\xi}(x) = \frac{-1+\alpha^{-2+2\xi}\beta^{1-\xi}\xi^{1-\frac{(1+b)\xi}{\alpha}}\Gamma(\frac{1+b-\alpha}{\alpha})^{-\xi}\Gamma(\frac{-\alpha+\xi+b\xi}{\alpha})}{1-\xi}. \tag{22}$$

In Table 1, the quantiles of the distribution are classified by α in the rows and q in the columns, the parameters of the distribution are $\beta = 0.85$ and $b = 2.51$.

$\alpha \setminus q$	25	50	75
0.1	0.037	0.181	0.298
0.2	0.144	0.393	0.534
0.3	0.363	0.646	0.771
0.4	0.767	0.952	1.023
0.5	1.5	1.333	1.302
0.6	2.85	1.823	1.624
0.7	5.5	2.491	2.019
0.8	11.456	3.49	2.546
0.9	29.883	5.34	3.394

Table 1: Quantiles of the distribution.

The percentiles of the distribution are classified by α in the rows and q in the columns, the parameters of the distribution are $\beta = 0.70$ and $b = 1.51$.

Corollary 3.1 *Hence* $\lim_{\xi\to 1} SH_{T,\alpha,\xi}(x) = SH_\alpha(x)$. *We get that the limit of the conformable fractional Tsallis entropy is equal to the conformable fractional Shannon entropy.*

Definition 3.11 The conformable fractional Renyi entropy of a random variable x for the CFIGD is defined as follows:

$$SH_{R,\alpha,\xi} = \frac{1}{1-\xi}\log(E_\alpha(g_\alpha(X))^{\xi-1}),$$
$$SH_{R,\alpha,\xi} = \frac{1}{\alpha(-1+\xi)}\Big(-2\alpha(-1+\xi)\log(\alpha)+\alpha(-1+\xi)\log(\beta)-\alpha\log(\xi)$$
$$+\xi\log(\xi)+b\xi\log(\xi)+\alpha\xi\log(\Gamma(-1+\frac{1+b}{\alpha}))-\alpha\log(\Gamma(-1+\frac{(1+b)\xi}{\alpha}))\Big). \tag{23}$$

Corollary 3.2 *Hence* $\lim_{\xi\to 1} SH_{R,\alpha,\xi} = SH_\alpha(x)$. *We get that the limit of the conformable fractional Renyi entropy is equal to the conformable fractional Shannon entropy.*

$\alpha \setminus q$	10	20	30	40	50	60	70	80	90
0.1	0.001	0.006	0.023	0.05	0.084	0.12	0.158	0.196	0.233
0.2	0.002	0.022	0.069	0.128	0.19	0.249	0.306	0.357	0.404
0.3	0.004	0.053	0.138	0.23	0.315	0.391	0.458	0.516	0.567
0.4	0.01	0.104	0.236	0.36	0.464	0.551	0.622	0.681	0.73
0.5	0.023	0.187	0.374	0.526	0.644	0.734	0.804	0.859	0.903
0.6	0.052	0.322	0.57	0.746	0.868	0.953	1.014	1.059	1.093
0.7	0.12	0.556	0.866	1.049	1.159	1.227	1.269	1.296	1.313
0.8	0.301	1.004	1.353	1.508	1.575	1.601	1.606	1.601	1.59
0.9	0.982	2.112	2.359	2.359	2.294	2.215	2.139	2.068	2.004

Table 2: Percentiles of the distribution.

4 Conclusion

The paper defines the Cumulative Distribution Function (CDF), survival function, and hazard function of the CFIGD, offering valuable insights into its behavior and potential applications in reliability and risk analysis. Statistical measures such as the expected values, r-th moments, mean, variance, skewness, and kurtosis are introduced as conformable fractional analogs, facilitating a deeper understanding of its central tendencies and higher-order characteristics. Additionally, this research reveals the conformable fractional analogs of popular entropy measures like the Shannon, Renyi, and Tsallis entropy, providing useful tools for quantifying uncertainty and randomness.

References

[1] John D. Cook. Inverse gamma distribution. *online:*`http://www.johndcook.com/inverse_gamma.pdf`*, Tech. Rep.*, 2008.

[2] M. E. Mead. Generalized inverse gamma distribution and its application in reliability. *Communications in Statistics - Theory and Methods* **44** (7) (2015) 1426–1435.

[3] A. M. Mousa, M. Kh Hassan and A. Fathi. A new non-parametric estimator for Pdf based on inverse gamma distribution. *Communications in Statistics - Theory and Methods* **45** (23) (2016) 7002–7010.

[4] Ma'mon Abu Hammad and Adnan Mohammad Awad. Distribution of Shannon statistic from normal sample. *METRON* **65** (3) (2007) 259–275.

[5] Alvaro H. Salas, Mamon Abu Hammad, Badriah M. Alotaibi, Lamiaa S. El-Sherif and S. A. El-Tantawy. Analytical and numerical approximations to some coupled forced damped duffing oscillators. *Symmetry* **14** (11) (2022) 1–13.

[6] Roshdi R. Khalil, Mohammed Al Horani, Abdelrahman Yousef and Mohammad Sababheh. A new definition of fractional derivative. *Journal of computational and applied mathematics* (264) (2014) 65–70.

[7] Iqbal Batiha, Shameseddin Alshorm, IqbalL H. Jebril and Mamon Abu Hammad. A Brief Review about Fractional Calculus. *Int. J. Open Problems Compt. Math.* **15** (4) (2022) 39–56.

[8] Ma'mon Abu Hammad, Iqbal Jebril and Roshdi Khalil. Large Fractional Linear Type Differential Equations. *Int. J. Anal. Appl.* **21** (2023) 1–8.

[9] Ma'mon Abu Hammad and R. Khalil. Systems of linear fractional differential equations. *Asian Journal of Mathematics and Computer Research* **12** (2) (2016) 120–126.

[10] Andrew G. Glen. On the inverse gamma as a survival distribution. *Computational probability applications* (2017) 15–30.

[11] Ma'mon Abu Hammad, Iqbal H. Jebril, Shameseddin Alshorm, Iqbal M. Batiha and Nancy Abu Hammad. Numerical Solution for Fractional-Order Mathematical Model of Immune-Chemotherapeutic Treatment for Breast Cancer Using Modified Fractional Formula. *Int. J. Anal. Appl.* **21** (2023).

[12] Hideaki Hayashi, Akira Furui, Yuichi Kurita and Toshio Tsuji. A variance distribution model of surface EMG signals based on inverse gamma distribution. *IEEE Transactions on Biomedical Engineering* **64** (11) (2017) 2672–2681.

[13] Rania Saadeh, Bayan Ghazal and Aliaa Burqan. A study of double general transform for solving fractional partial differential equations. *Mathematical Methods in the Applied Sciences* **46** (16) (2023) 17158–17176.

[14] W. Alshanti. Riemann-Stieltjes Integrals and Some Ostrowski Type Inequalities. *The Australian Journal of Mathematical Analysis and Applications* **18** (1) (2021) 1–11.

[15] Sondos Rasem, Amer Dabahneh and Ma'mon Abu Hammad. Applications of Conformable Fractional Weibull Distribution. *International Conference on Mathematics and Computations* (2022) 139–147.

[16] Iqbal Jebril, Duha AbuJudeh, Yousef Dalahmeh and Siham Ali Abrikah. Properties of conformable fractional Rayleigh probability distribution. *International Conference on Information Technology (ICIT)* (2021) 13–15.

[17] Iqbal Jebril, Eman Nouh, Rahaf Hamidi, Yousef Dalahmeh and Salemah Almutlak. Properties of conformable fractional gamma with two parameters probability distribution. *International Conference on Information Technology (ICIT)* (2021) 16–18.

[18] Abu Hammad, A. Awad and R. Khalil. Properties of conformable fractional chi-square probability distribution. *J. Math. Comput. Sci.* **10** (4) (2020) 1239–1250.

[19] Dana Amr and Ma'mon Abu Hammad. Application of Conformable Fractional Nakagami Distribution. *International Conference on Mathematics and Computations* (2022) 229–237.

[20] Mamon Abu Hammad, Iqbal H. Jebril, Shameseddin Alshorm, Iqbal M. Batiha and Nancy Abu Hammad. Numerical Solution for Fractional-Order Mathematical Model of Immune-Chemotherapeutic Treatment for Breast Cancer Using Modified Fractional Formula. *International Journal of Analysis and Applications* **21** (2023) 89–89.

[21] Amjed Zraiqat and Laith K. Al-Hwawcha. On exact solutions of second order nonlinear ordinary differential equations. *Applied mathematics* **6** (6) (2015).

[22] Ma'mon Abu Hammad, Oualid Zentar, Shameseddin Alshorm, Mohamed Ziane and Ismail Zitouni. Theoretical analysis of a class of α-Caputo fractional differential equations in Banach space. *AIMS Mathematics* **9** (3) 2024 6411–6423.

Nonlinear Dynamics and Systems Theory, **24** (2) (2024) 168–180

Analysis of Water Depth Variation Impact on CALM Buoy Performance for Shallow Water Condition

T. Herlambang [1], D. B. Magfira [1], R. K. Wibowo [2], K. Oktafianto [3], A. A. Firdaus [4*] and H. Arof [5]

[1] *Department of Information System, Universitas Nahdlatul Ulama Surabaya, Indonesia.*
[2] *Post Gradute Program of Technology Management, Institute of Teknologi Sepuluh Nopember, Indonesia.*
[3] *Department of Mathematics, University of PGRI Ronggolawe, Indonesia.*
[4] *Department of Engineering, Faculty of Vocational Studies, Airlangga University, Indonesia.*
[5] *Department of Electrical Engineering, University of Malaya, Malaysia.*

Received: August 2, 2023; Revised: March 5, 2024

Abstract: The SPM CALM Buoy is an offshore facility for loading/unloading crude oil. The SPM CALM Buoy in Indonesia is mostly operated in shallow water, so an analysis of the depth variation impact on the performance of the CALM Buoy is of necessity. The results of the analysis of the ship motion in free floating condition under the conditions of regular waves and spectral response show that the surge, sway, and yaw motions are influenced by depth variations, while the heave, roll, and pitch are influenced by frequency. For the CALM Buoy, all movements are affected by the depth variations. The results of the analysis in mooring condition show that the tension on the mooring line and offset on the CALM Buoy are affected by variations in depth and not affected by the towing force of the ship. The deeper the water area, the higher the values of the tension and offset. At a depth of 21 m to 42 m, a pre-tension of 10% of MBL is used, while at a depth of 50 m, a pre-tension of 15% of MBL is used since the initial pre-tension of 10% is unable to accommodate the movement of the CALM Buoy. This is because the second order wave load has a greater influence on moored structures such as the CALM Buoy.

Keywords: *CALM Buoy; offset; shallow water; second order; tension.*

Mathematics Subject Classification (2010): 76E07, 76E09.

* Corresponding author: mailto:aa.firdaus@vokasi.unair.ac.id

1 Introduction

Petroleum remains the main choice for addressing the needs for energy sources, that is, fuel for motor vehicles, industry, and power plants. Indonesia's production capacity of only around 800,000 barrels per day cannot meet the need for oil consumption reaching more than 2 million barrels per day [1]. This is because Indonesia only relies on its production from the old wells on land, that are of the colonial era. Based on the data from the Ministry of Energy and Mineral Resources, Indonesia still has oil reserves of 320 billion barrels situated off the west coast of Aceh. With the discovery of offshore oil reserves, offshore exploitation technology is needed to reap the advantage out of the potential of such discovery.

Since the petroleum exploitation is done offshore, it is necessary that a floating structure be built so as to be able to exploit and distribute petroleum. There are two ways to distribute the petroleum, that is, by flowing it through subsea pipelines and by using tankers. Distribution through subsea pipelines is considered not economical enough due to its high costs if the pipes should be installed in deep waters. So, distribution by using tankers is preferred because it is more economical.

The process of transporting crude oil from the drilling site to tankers is called offloading. Tankers require stability criteria during the offloading period, so a mooring system is required to maintain the motion limit of the ship against wave excitation. There are many configurations of mooring systems, among others, spread mooring, turret mooring, and single point mooring. The single point mooring type is a mooring system that can follow environmental conditions so that tankers can move following the waves without having to stop the offloading process.

One of the single point mooring types is SBM (Single Buoy Mooring) [2]. Single buoy mooring is a type of single point mooring using a buoy useful for mooring and connecting the riser to the tanker. Single Buoy Mooring mostly operates in shallow water because its function is to distribute oil from ships to storage depots. The buoys used for mooring systems greatly affect the strength and stability of the mooring system. The size of the buoy used must be in accordance with the size of the ship used during the offloading period because the incorrect motion response from the ship is a significant factor in influencing the stability of the buoy. The problems raised in this study include: what is the behavior of the CALM Buoy and tanker in free floating condition?, how does the difference in depth affect the tension on the mooring line and the offset on the Buoy? and what is the trend of the influence of depth variation on the level of the tension on the mooring line? The purpose of this study is to answer these three problems, the results are considered to be useful later as reference information for the interested companies.

2 Experiment

2.1 Instruments and materials

All segments of the Mooring Line are made of chains. For a long time, the chain has been the main choice in offshore operations because the chain has more strength than seabed aberration and makes a very significant contribution to anchor grip. All segments of the Mooring Line are made of a wire rope. Basically, this wire rope is lighter than the chain, therefore the wire rope has a higher restoring force in deep sea waters and requires lower pre-tension than the chain. To avoid lifting the anchor on the wire rope, a longer wire rope is needed than when using a chain. The wire rope is more susceptible to corrosion attack, therefore it requires extra care because mechanical damage due to corrosion is a more common factor causing failure. The Mooring Line is a combination of more than one chain segment and the wire rope. By combining the Mooring Line into more than one segment, namely the chain and wire rope, one will obtain the following advantages: a low pre-tension, high restoring force, larger holding anchor and resistance to aberration. These advantages make the Mooring Line with combined segments very suitable for application in the deep sea.

2.2 Work procedures

2.2.1 Theory

Various literatures and related theoretical basis are employed to support this research, starting from the effect of depth on the response of SPAR motion in deep water [3]. Based on the research, there is no significant change in depth variation when the object operates in deep water. However, when it is in shallow water, the change in depth variation has a significant effect on the response of the structure due to the energy difference (surge wave force) resulted from the difference in depth [4], [5], [6]. The difference in the response value of the structure movement in the free floating condition was analyzed by the frequency domain analysis method using the equation

$$M_{(\omega)}r + C_{(\omega)}r + K_{(\omega)}r = Xe^{i\omega t}, \tag{1}$$

where
$M_{(\omega)}$: mass matrix of frequency function (tons),
$C_{(\omega)}$: damping matrix of frequency function (ton/s),
$K_{(\omega)}$: stiffness matrix of frequency function (kN/m),
X : complex load vector giving information on load amplitude and phase at all degrees of freedom. The pattern $e^{i\omega t}$ sets the variation harmonics of the sample load with frequency.
r : displacement vector (m).

After the response value of the frequency-based structure movement is obtained, the response value of the structure in mooring state is found by the time domain analysis method using the equation

$$[m + A(\omega)]\ddot{x} + C(\omega)\dot{x} + D_1\dot{x} + D_2 f(\dot{x}) + Kx = q_{W1} + q^1_{WA} + q^2_{WA} + q_{CU} + q_{xet}, \tag{2}$$

where q_{W1} is the wind drag force, q^1_{WA} is the wave drift of first order, q^2_{WA} is the wave drift force of second order, q_{CU} is the current force, q_{xet} is the other external force.

When a time-based analysis (time domain analysis) is made, several outputs are obtained in the form of tension from the mooring line and hawser. In addition, the offset, heave, and roll/pitch of CALM Buoy are obtained [7], [8], [9], [10]. To find out the value of the tension occuring due to the holding back of the response of the structure resulted from wave excitation, the equation below is used.

$$T_{max} = T_H + wh, \tag{3}$$

where T_{max} is the maximum tension of the mooring rope (tons), T_H is the horizontal pre-tension (tons), w is the chain weight in water (ton/m), h is the water depth (m).

The tension value is affected by the ratio of the length of the mooring line to the depth of the water. In this analysis, the magnitude of the pre-tension value for each depth is made the same, which is 10% of the MBL [11].

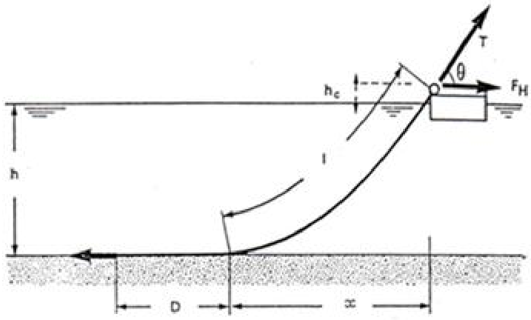

Figure 1: Setup of the Mooring Line.

The movement of the floating structure in the moored condition can be considered as a first order high frequency movement and a second order low frequency movement divided separately. The motion equation of the wave frequency [12] for the FPSO is

$$(M_{ij} + \mu_{ij})\ddot{x}_j^{(1)} + \int_0^\infty K_{ij}(\tau)\dot{x}_j^{(1)}(t-\tau)d\tau + C_{ij}x_j^{(1)} = F_i^{moor} + F_i^{wave(1)}, \qquad (4)$$

where
$x_i^{(1)}$ is the wave frequency motion, $F^{wave(1)}$ is the first order wave force, F^{moor} is the mooring force, M is the inertia matrix FPSO.

The equation of low frequency motion of FPSO [12] is as below:

$$\begin{aligned}
(m+\mu_{11})\ddot{x}_1^{(2)} + \mu_{12}\ddot{x}_2^{(2)} + \mu_{16}\ddot{x}_2^{(2)} + (B_{11}+B_{wdd})\dot{x}_1^{(2)} &= F_1^{wind} + F_1^{current} + F_1^{wave(2)} + F_1^{moor} \\
\mu_{21}\ddot{x}_1^{(2)} + (m+\mu_{22})\ddot{x}_2^{(2)} + \mu_{26}\ddot{x}_6^{(2)} + B_{22}\dot{x}_2^{(2)} &= F_2^{wind} + F_2^{current} + F_2^{wave(2)} + F_2^{moor} \\
\mu_{61}\ddot{x}_1^{(2)} + \mu_{62}\ddot{x}_2^{(2)} + (I+\mu_{66})\ddot{x}_6^{(2)} + B_{66}\dot{x}_6^{(2)} &= F_6^{wind} + F_6^{current} + F_6^{wave(2)} + F_6^{moor}
\end{aligned} \qquad (5)$$

where $x^{(2)}$ is the low frequency motion, B_{11}, B_{22}, B_{33} are the damping coeficients, B_{wdd} is the wave drift damping coeficient in the direction of the x-axis, $F_i^{current}$ is the current force, F_i^{wind} is the wind force, F_i^{moor} is the mooring force, $F_i^{wave(2)}$ is the second order wave drift force.

2.2.2 CALM Buoy

The CALM Buoy is a mooring system commonly used for loading/unloading processes as a connector between tankers and the fuel transit terminal. The #SPM150 CALM Buoy is one of the SPM owned by PT. Pertamina, operating off the coast of Tuban, having a configuration of 6 symmetrical mooring lines, a hull size of 11 m, an outer skirt diameter of 15 m, a water draft of 2.95 m, and an ability to accommodate vessels with a capacity of up to 150,000 DWT.

2.2.3 Environmental data

The environmental data used in this study are the data taken from the Tuban offshore environment, obtained from Sofec with a significant wave height of Hs = 3.1 m, a wave period of Tp = 6.9 sec, a wind speed of 11 knots, and a surface current speed of 0.75 m/sec. The depth variation is obtained from the calculation of environmental parameters, that is, the ratio of the wave number to the depth or non-dimensional water depth (kh) and based on structural parameters, that is, the ratio of depth to draft (D/T) [13].

Depth (m)	21	23	25	27	30	33	37	42	50
kh	1.3	1.4	1.5	1.6	1.8	2.0	2.2	2.5	3.0
D/T	1.2	1.3	1.4	1.5	1.7	1.9	2.1	2.4	2.9

Table 1: Calculation of Depth Variation.

The results of the calculation of depth variation for this study can be seen in Table 1. The selection of a low interval at the initial depth and a high interval at the final depth is due to the authors' desire to know a more specific downward trend when in shallow waters.

2.2.4 Structure modeling

The modeling of the ship structure and CALM Buoy in this study uses the software, while the analysis of the motion of the structure during mooring condition uses the Ariane software. For the modeling of the software, structural coordinate data are used to create a meshing to be used for hydrodynamic analysis. The meshing form of the ship structure and the CALM Buoy can be seen in the image below.

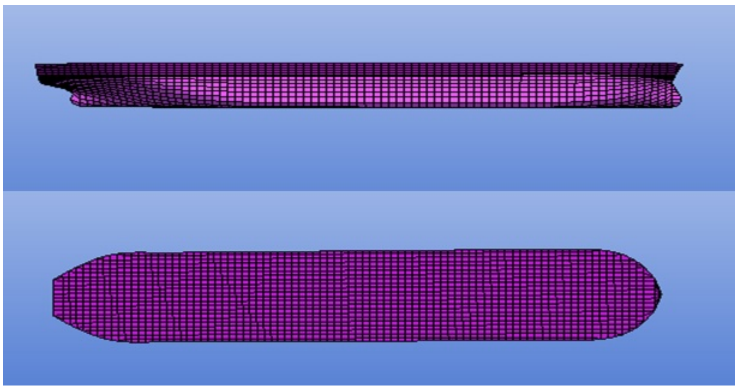

Figure 2: The results of modeling the structure of the ship on the software.

The analysis carried out on software is only to find out the characteristics of the object's motion in free-floating condition [14]. For further analysis, that is, the analysis of the mooring condition, mooring software is used. The analysis of mooring conditions is carried out under two conditions, that is, the inline mooring condition and between-line mooring conditions [15]. From Figure 4 below, the inline condition can be described as the ship is in a floating position parallel to the mooring line. This position indicates that there is only one mooring line that holds the ship when the ship is subjected to environmental loading in the form of waves or currents coming from the front of the

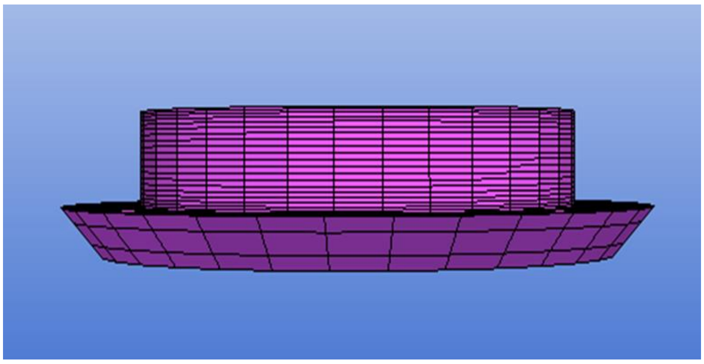

Figure 3: CALM Buoy modeling results on the software.

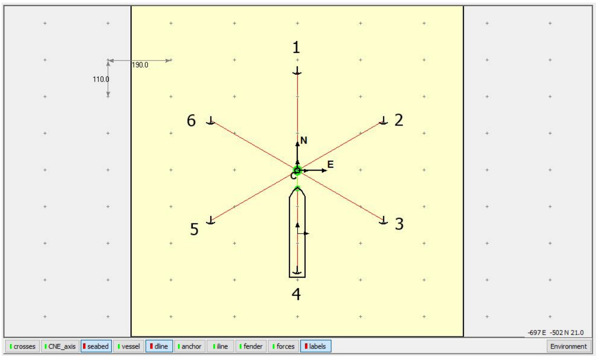

Figure 4: Inline conditions moored modeling on mooring software.

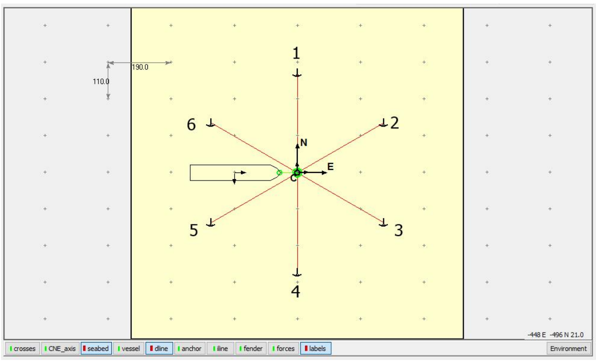

Figure 5: Inline conditions moored modeling on mooring software.

ship. From Figure 5, the between-line condition can be described as the ship is in a floating position between two mooring lines. This position indicates that there are two mooring lines that hold the ship when the ship is subjected to environmental loading in the form of waves or currents coming from the front of the ship. Therefore, the tension received by the mooring line in the between-line condition is smaller than in the inline condition because the load is distributed to two mooring lines.

2.2.5 Model validation

The validation criteria used refer to ABS (American Bureau of Shipping) of which the maximum value for displacement validation is 2% and, for other provisions, the maximum value is 1%.

3 Results and Discussion

After going through the data processing stage, the results and discussion are as follows. The discussion is to find out the effect of the depth variation on the performance of the CALM Buoy in offloading conditions. The performance of the CALM Buoy can be analyzed in terms of the magnitude of the tension on the mooring line, the offset, heave, and roll/pitch of the buoy. The CALM Buoy performance analysis is carried out with the help of mooring software using the time domain analysis method. The output data in the form of time history is then processed to obtain significant values to be used in the performance analysis.

3.1 Research location

The research site as shown in Figure 6 is in the Main Transit Terminal Facility, offshore of Tuban Regency, East Java Province, at the coordinates of 111°56′21″ east longitude and 06°42′48" south latitude. From Figure 6 below, it is known that the CALM Buoy

Figure 6: The Research Location in Tuban.

and the ship are located off the coast of Tuban not too far from the mainland and not too deep.

3.2 Motion analysis of free floating conditions

The motion analysis of the ship and CALM Buoy in free-floating condition was made to determine the behavior or characteristics of structural motion on regular waves. The

RAO analysis was carried out at the depth referring to Table 1. For the ship's RAO, the highest values of the surge, sway, and yaw motions were affected by the depth of the water, while the highest values of the heave, roll, and pitch motions were affected by the magnitude of the frequency. For the RAO of the CALM Buoy, all the motions were affected by the depth variation condition.

3.3 Response analysis on random waves

The response analysis on random waves resulted in the same conclusion as that in the free-floating condition. This was because the results of the analysis on random waves follow those of the analysis in the free-floating condition.

3.4 Tension analysis on mooring line

The tension analysis on the mooring line was carried out in two conditions, using the time domain analysis method, that is, inline condition and between-line condition.

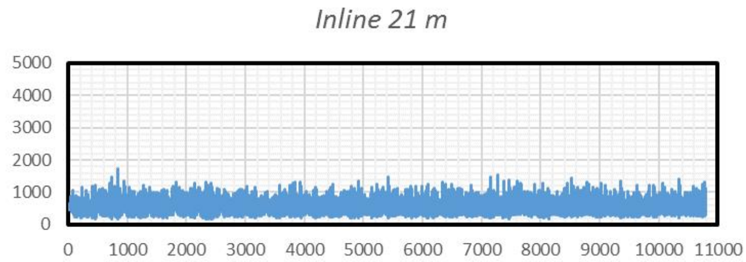

Figure 7: Example of value measurement of time history.

In the inline condition, the analysis was made only for the mooring line number 1. In the between-line condition, the analysis was made for the mooring lines number 2 and 3. This was due to the condition of the mooring line configuration in which, for both conditions, an analysis was made just for the mooring line having the greatest tension. The tension value for mooring line 1 can be seen in Table 2. For mooring lines 2 and 3, it can be seen in Table 3 and Table 4.

Description	Depth (m)								
	21	23	25	27	30	33	37	42	50
MEAN (KN))	541.19	552.05	450.72	553.27	567.14	568.91	586.61	617.26	664.37
Tension 1/3 highest (KN)	762.45	791.99	813.69	819.85	856.93	885.86	947.15	1043.80	1084.50
Tension 1/10 highest (KN)	912.88	960.47	995.54	1016.60	1089.20	1134.86	1232.90	1411.00	1500.00
Tension 1/100 highest (KN)	1175.60	1268.80	1320.00	1381.00	1520.00	1603.00	1788.20	2229.20	2483.00
MAX (KN)	1719.83	1841.95	1560.51	2033.80	2283.89	2536.75	2712.01	3612.01	4470.45
MIN (KN)	171.20	161.32	148.19	157.50	147.60	152.54	151.95	156.40	171.83

Table 2: Calculation of the Value of Tension on Mooring Line 1.

The tension values in inline and between-line conditions increased due to variation in depth. The significant value of tension for inline condition at a depth of 21 m to that of 50 m increased by 29%. The significant value of the tension for the between-line

Description	Depth (m)								
	21	23	25	27	30	33	37	42	50
MEAN (KN))	540.12	552.77	535.96	546.28	566.35	540.85	583.31	596.22	871.56
Tension 1/3 highest (KN)	708.58	719.22	742.62	764.88	780.27	801.65	868.36	905.53	1177.90
Tension 1/10 highest (KN)	853.13	854.21	886.41	922.96	1009.90	987.69	1084.80	1156.30	1421.70
Tension 1/100 highest (KN)	1080.50	1096.20	1150.00	1208.00	1385.50	1290.50	1468.00	1670.30	2071.00
MAX (KN)	1739.28	1832.96	1555.38	1804.56	2185.98	2134.09	2348.60	2679.82	4476.58
MIN (KN)	198.60	179.48	179.25	176.16	179.49	178.16	184.18	171.17	347.60

Table 3: Calculation of the Value of Tension on Mooring Line 2.

Description	Depth (m)								
	21	23	25	27	30	33	37	42	50
MEAN (KN))	539.33	546.34	531.79	542.31	558.72	540.78	579.78	598.78	875.14
Tension 1/3 highest (KN)	702.25	715.35	736.03	756.77	788.52	802.03	863.30	909.10	1189.10
Tension 1/10 highest (KN)	847.73	850.84	874.64	912.02	996.14	986.56	1078.80	1156.60	1449.20
Tension 1/100 highest (KN)	1057.80	1100.00	1120.00	1194.40	1356.40	1302.30	1494.80	1650.40	2162.00
MAX (KN)	1426.31	1824.89	1538.04	1727.19	2038.19	2524.84	2310.40	3026.76	4322.85
MIN (KN)	201.78	180.82	180.63	173.92	180.39	183.15	168.84	181.78	351.48

Table 4: Calculation of the Value of Tension on Mooring Line 3.

condition on the mooring line 2 and mooring line 3 at a depth of 21 m to that of 50 m increased by 39%. At a depth of 50 m, the tension value for the between-line condition was greater than that for the inline condition because the pre-tension value changed from 10% MBL to 15% MBL (minimum breaking load)

3.5 Calm Buoy offset analysis

The offset analysis for the mooring line was made under two conditions, that is, the inline condition and between-line condition. The offset for the inline condition can be seen in Table 5, and that for the between-line condition can be seen in Table 6.

Description	Depth (m)								
	21	23	25	27	30	33	37	42	50
MEAN (m))	0.37	0.44	0.55	0.56	0.69	0.80	1.01	1.30	1.49
Offset 1/3 highest (m)	0.71	0.85	0.99	1.08	1.32	1.53	1.92	2.43	2.84
Offset 1/10 highest (m)	0.92	1.11	1.27	1.40	1.71	1.96	2.44	3.08	3.67
Offset 1/100 highest (m)	1.21	1.47	1.66	1.88	2.28	2.60	3.19	4.00	4.83
MAX (m)	1.60	1.97	2.17	2.64	2.99	3.59	4.12	5.13	5.84

Table 5: Inline condition offset calculation.

The buoy offset in inline and between-line conditions increased due to depth variation. In the inline condition, at a depth of 21 m, the significant offset was 0.71 m, and it continued to increase to 2.84 m at a depth of 50 m. In the between-line condition, at a depth of 21 m, the value was 0.68 m and continued to increase up to 2.04 m at a depth

Description	Depth (m)								
	21	23	25	27	30	33	37	42	50
MEAN (m))	0.35	0.40	0.45	0.52	0.67	0.72	0.9	1.05	0.85
Offset 1/3 highest (m)	0.68	0.77	0.86	1.00	1.27	1.36	1.72	2.04	1.61
Offset 1/10 highest (m)	0.88	0.98	1.12	1.31	1.63	1.74	2.23	2.66	2.07
Offset 1/100 highest (m)	1.18	1.37	1.50	1.80	2.17	2.28	2.94	3.59	2.76
MAX (m)	1.55	1.99	1.97	2.54	2.8	3.53	3.89	4.47	3.70

Table 6: Between-line condition offset calculation.

of 42 m, then decreased at a depth of 50 m to 1.16 m. The significant decrease in the tension value was due to the difference in the pre-tension values, that is, from 10% MBL to 15% MBL.

3.6 Motion response analysis of Calm Buoy in moored condition

The analysis of the motion response of the CALM Buoy in moored condition covered heave and roll/pitch motions. These motions were the performance parameters of the CALM Buoy. The values of these motions can be seen in Table 7 and Table 8.

Description	Depth (m)								
	21	23	25	27	30	33	37	42	50
MEAN (m))	0.84	0.87	0.92	0.96	1.02	1.08	1.15	1.23	1.45
Heave 1/3 highest (m)	0.91	0.95	1.00	1.04	1.10	1.17	1.25	1.37	1.62
Heave 1/10 highest (m)	0.95	0.99	1.04	1.08	1.15	1.21	1.31	1.45	1.72
Heave 1/100 highest (m)	1.00	1.05	1.10	1.14	1.21	1.29	1.40	1.58	1.88
MAX (m)	1.13	1.12	1.19	1.23	1.34	1.48	1.92	1.77	2.10

Table 7: Calculation of the value of heave of the Calm Buoy.

The heave value had an upward trend based on depth variation. At a depth of 50 m it showed a decrease due to difference in pre-tension values.

3.7 Tension trend based on depth variation

For the inline condition, the trend of significant tension values was only analyzed for mooring line 1. Whereas for the between-line condition, the analysis was made for mooring lines 2 and 3 because the trend value was based on the mooring line with the greatest tension. The trend of significant changes in tension values based on the depth variation can be seen in Figure 8, Figure 9 and Figure 10.

Description	Depth (m)								
	21	23	25	27	30	33	37	42	50
MEAN (deg))	6.80	8.26	8.85	8.90	9.75	9.80	11.10	12.90	10.20
Roll/Pitch 1/3 highest (deg)	12.80	16.06	16.95	17.37	18.50	18.62	21.20	25.74	20.10
Roll/Pitch 1/10 highest (deg)	16.60	20.59	21.71	22.18	23.87	24.25	27.24	34.50	26.22
Roll/Pitch 1/100 highest (deg)	21.90	26.39	27.56	28.31	31.44	34.70	35.90	46.98	35.11
MAX (deg)	29.40	33.22	33.50	33.80	40.27	45.00	48.78	59.50	44.00

Table 8: Calculation of roll/pitch of the Calm Buoy.

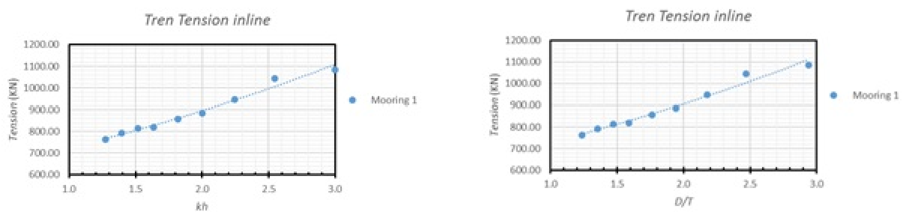

Figure 8: Tension on mooring line 1, the trendline in inline condition based on kh and D/T.

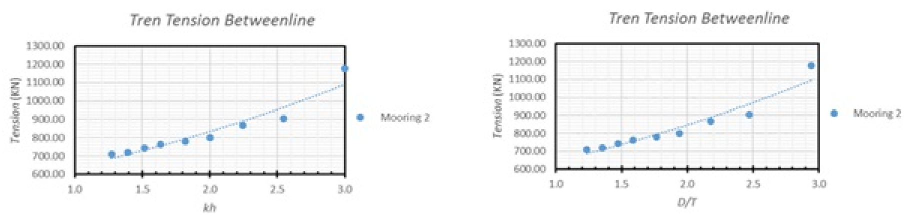

Figure 9: Tension on mooring line 2, the trendline in between-line condition based on kh and D/T.

Figure 10: Tension on mooring line 3, the trendline in between-line condition based on kh and D/T.

The significant tension value in the inline condition based on both environmental and structural parameters has an upward trend based on depth variation. The tension trend in inline condition starts to look steady within a depth of 42 m up to that of 50 m. For the significant tension value in the between-line condition, it is not known at what depth the tension trend starts to stabilize because at a depth of 50 m, a pre-tension value different from that of the previous depth is used.

4 Conclusion

The maximum value of the ship's RAO motion varies in accordance with the depth of the water. The maximum values of the surge, sway, and yaw motions are affected by the difference in depth, while the heave, pitch, and roll are affected by the frequency. The maximum RAO value of all motions of the CALM Buoy is affected by the difference in depth.

The value of the ship's response in the random waves for the surge, sway, and heave motions is affected by the depth variation, while for roll, pitch and yaw motions, it is not affected by the depth variation. The response value follows that of the RAO value. The response value of the CALM Buoy in the random waves for all motions is affected by variation in depth because the response value follows that of the RAO value, whereas the CALM Buoy motion is not affected by changes in depth.

The tension on the mooring line for both inline and between-line conditions is affected by variation in depth. If in the analysis of the movement of the structure, the deeper the water area, the smaller the movement of the structure, then in the analysis of the tension on the mooring line, it has the opposite value. The tension in the inline condition from a depth of 21 m to 50 m increased by 29%, while for the between-line condition, it increased by 39%. This is because the resulting tension is caused by the increase in the heave and offset values at depth variation.

The offset of the CALM Buoy in both inline and between-line conditions is affected by variation in depth. The highest offset in inline condition occurs at a depth of 50 m up to 5.84 m. At the same time the farthest offset in the between-line condition occurs at a depth of 48 m up to 4.47 m, this is because in the between-line condition, at a depth of 50 m, a pre-tension of 15% MBL is used. The tension in the mooring line for both inline and between-line conditions has a trend of increasing values along with increasing depth. The significant tension value in the inline condition at a depth of 21 m is 762.45 KN and continues to increase until a depth of 50 m, at which the significant tension is 1084.5 KN. The significant tension value in between-line condition at a depth of 21 m is 708.58 KN, and it continues to rise, at a depth of 50 m, the significant tension reaches 1189.1 KN. For the inline condition, the tension value starts to stay steady at a depth of 42 m up to 50 m. For the between-line condition, it is not known at what depth the tension trend starts to be steady because at a depth of 50 m, a pre-tension is different from that at the previous depth so that the tension trend seems to increase significantly.

References

[1] ESDM. *Pengendalian Konsumsi BBM Untuk Ketahanan Energi Nasional.* Jakarta, 2015.

[2] API RP 2SK Fourth Edition. *Design and Analysis of Station Keeping Systems for Floating Offshore Structures.* Washington DC: API, 1996.

[3] Z. Lin. Influence of Water Depth Variation on the Hydrodynamics of Deep-Water Mooring. *Journal of Ocean Engineering* **109** (2015) 553–566.

[4] M. Folley. The Performance of a Wave Energy Converter in Shallow Water. *6-th European Wave and Tidal Energy Conference*. Glasgow, 2005.

[5] K. Oktafianto, A. Z. Arifin, E. F. Kurniawati, T. Tafrikan, T. Herlambang and F. Yudianto. Tsunami Wave Simulation in the Presense of a Barrier. *Nonlinear Dynamics and Systems Theory* **23** (1) (2023) 69–78.

[6] M. M. Ahmad. Analysis on the Effect of Buoy Variation In the Performance of Mooring System for FPSO Brotojoyo. *Tugas Akhir Jurusan Teknik Kelautan*. Institut Teknologi Sepuluh Nopember, Surabaya, 2013.

[7] T. Herlambang, H. Nurhadi, A. Muhith, A. Suryowinoto and K. Oktafianto. Estimation of Forefinger Motion with Multi-DOF Using Advanced Kalman Filter. *Nonlinear Dynamics and Systems Theory* **23** (1) (2023) 24–33.

[8] T. Herlambang, F. A. Susanto, D. Adzkiya, A. Suryowinoto and K. Oktafianto. Design of Navigation and Guidance Control System of Mobile Robot with Position Estimation Using Ensemble Kalman Filter (EnKF) and Square Root Ensemble Kalman Filter (SR-EnKF). *Nonlinear Dynamics and Systems Theory* **22** (4) (2022) 390–399.

[9] F. A. Susanto, M. Y. Anshori, D. Rahmalia, K. Oktafianto, D. Adzkiya, P. Katias and T. Herlambang. Estimation of Closed Hotels and Restaurants in Jakarta as Impact of Corona Virus Disease (Covid-19) Spread Using Backpropagation Neural Network. *Nonlinear Dynamics and Systems Theory* **22** (4) (2022) 457–467.

[10] M. Y. Anshori, I. H. Santoso, T. Herlambang, D. Rahmalia, K. Oktafianto and P. Katias. Forecasting of Occupied Rooms in the Hotel Using Linear Support Vector Machine. *Nonlinear Dynamics and Systems Theory* **23** (2) (2023) 129–140.

[11] J. Cozijin. Coupled Mooring Analysis for Deep Water Calm Buoy. *23rd International Conference on Offshore Mechanics and Arctic Engineering*. Vancouver, 2004.

[12] J. E. W. Wichers. *A Simulation Model for a Single Point Moored Tanker*. Research Institute Netherlands, Wageningen:Maritime, 1988.

[13] O. M. Faltinsen. *Sea Loads On Ships And Offshore Structures*. United Kingdom: Cambridge University Press, 1990.

[14] D. J. Wang. An Analytical Solution of Wave Exciting Loads on CALM Buoy with Skirt. *Applied Mechanics and Materials* **477-478** (2014) 254–258.

[15] D. Krismanto. *Variasi Floater Pada MORING Line Single Buoy Mooring*. Surabaya: ITS Press, 2011.

Nonlinear Dynamics and Systems Theory, **24** (2) (2024) 181–192

The Twin-Well Duffing Equation: Escape Phenomena, Bistability, Jumps, and Other Bifurcations

J. Kyzioł and A. Okniński *

Politechnika Świętokrzyska, Al. 1000–lecia PP 7, 25-314 Kielce, Poland.

Received: August 3, 2023; Revised: February 24, 2024

Abstract: In this work, we investigate the escape phenomenon, the onset of bistability, jumps, as well as other bifurcations present in the twin-well Duffing equation. Based on the known steady-state asymptotic solution – the amplitude-frequency implicit function – and using the theory of differential properties of implicit functions, we compute the singular and critical points of this function. This enables us to predict several bifurcations present in the dynamical system under study. The main result is the calculation of the escape bifurcation set – the set of parameters for which escape phenomena occur, and equations to compute the onset of bistability.

Keywords: *metamorphoses of amplitude-frequency curves; bifurcations.*

Mathematics Subject Classification (2010): 34C05, 34C25, 34E05, 37G35, 70K20, 70K30, 70K50.

1 Introduction and Motivation

We study the dynamics of a vibrating system governed by the Duffing equation with negative linear stiffness [1, 2]:

$$\frac{d^2x}{dt^2} + k\frac{dx}{dt} - \alpha x + \gamma x^3 = f\cos\omega t \qquad (k,\ \alpha,\ \gamma > 0)\,. \tag{1}$$

After rescaling the variables as in [2]:

$$\tau = t\sqrt{\alpha},\ y = \alpha x,\ h = k/\sqrt{\alpha} > 0,\ c = \gamma/\alpha^3 > 0,\ \Omega = \omega/\sqrt{\alpha}, \tag{2}$$

we obtain the nondimensional Duffing equation

* Corresponding author: mailto:fizao@tu.kielce.pl

$$\frac{d^2y}{d\tau^2} + h\frac{dy}{d\tau} - y + cy^3 = f\cos\Omega\tau \qquad (h,\ c > 0)\,, \tag{3}$$

which is a twin-well potential system with a potential function $V(y) = \frac{1}{2}y^2 - \frac{1}{4}cy^4 + C$ (note that for $h = 2\zeta$, $c = \gamma$, we get equation (7.1.2) of [2]). Equation (3) appears in many physical problems, in early applications, it was used to model buckled beam dynamics [3,4], see also [5] and references therein.

Many bifurcations of dynamics occurring in equation (3) were described before [1,2]. The motivation of this work is to find and classify all bifurcations of the dynamics by studying qualitative changes in the differential properties of the approximate asymptotic solution (metamorphoses) of the Duffing equation (3).

Our main aim is to investigate an escape phenomenon, i.e., a transition from one well to cross-well motion under a smooth transition of a control parameter. This is an important problem since such a transition can result in a sudden increase in the amplitude of vibration with serious consequences for a vibrating construction. Moreover, we also aim at determining the onset of bistability and emergence of jump phenomena.

In the next section, we describe the methods used to find approximate asymptotic solutions of Eq.(3) and to study their differential properties. The equations for singular points and vertical tangencies are solved in Sections 3 and 4, respectively. In Section 5, we verify our analytical calculations by solving Eq.(3) numerically and summarize our results in the last section.

2 Methods

Our approach is based on: (i) the asymptotic solutions of nonlinear differential equations and (ii) the differential properties of implicit functions, see [6] and references therein. The idea to use the Implicit Function Theorem to "define and find different branches intersecting at the singular points of amplitude profiles" was proposed in [7].

Let us now look how the 1 : 1 resonance can be computed within the asymptotic approach [8–10]. For small nonzero ε, the asymptotic solutions of Eq.(3) are assumed in the form

$$y(\tau) = A_0 + A\cos(\Omega\tau + \varphi) + \varepsilon y_1(A_0, A, \varphi, \tau) + \ldots. \tag{4}$$

Working in the spirit of [10], Section 13.5, we get the following conditions for the steady-states:

$$K_1(A_0, A) = A_0\left(\tfrac{3}{2}A^2c + cA_0^2 - 1\right) = 0, \tag{5a}$$

$$K_2(A_0, A, \Omega) = h^2A^2\Omega^2 + A^2\left(\Omega^2 + 1 - 3cA_0^2 - \tfrac{3}{4}cA^2\right)^2 - f^2 = 0. \tag{5b}$$

Furthermore, following [10] again, we can solve Eq.(5a) for A_0 and substitute to (5b) obtaining the Type I (small orbits) solutions

$$L_1(A, \Omega) = h^2A^2\Omega^2 + A^2\left(\Omega^2 - 2 + \tfrac{15}{4}cA^2\right)^2 - f^2 = 0 \quad \left(cA_0^2 = 1 - \tfrac{3}{2}A^2c > 0\right), \tag{6}$$

and the Type II (large orbits) ones

$$L_2(A, \Omega) = h^2A^2\Omega^2 + A^2\left(\Omega^2 + 1 - \tfrac{3}{4}cA^2\right)^2 - f^2 = 0 \quad (A_0 = 0)\,. \tag{7}$$

We now start our analysis of the differential properties of implicit functions K_1, K_2, see Eqs.(5). Equations (5) describe a curve in the three-dimensional (3D) space (A_0, A, Ω), being an intersection of two surfaces, $K_1(A_0, A) = 0$ and $K_2(A_0, A, \Omega) = 0$.

The singular points of this curve are computed from the following equations [11, 12]:

$$\left.\begin{array}{r} K_1\left(A_0,\ A\right)=0 \\ K_2\left(A_0,\ A,\ \Omega\right)=0 \\ \det\begin{pmatrix} \frac{\partial K_1}{\partial A_0} & \frac{\partial K_2}{\partial A_0} \\ \frac{\partial K_1}{\partial A} & \frac{\partial K_2}{\partial A} \end{pmatrix}=0 \\ \det\begin{pmatrix} \frac{\partial K_1}{\partial A_0} & \frac{\partial K_2}{\partial A_0} \\ \frac{\partial K_1}{\partial \Omega} & \frac{\partial K_2}{\partial \Omega} \end{pmatrix}=0 \\ \det\begin{pmatrix} \frac{\partial K_1}{\partial A} & \frac{\partial K_2}{\partial A} \\ \frac{\partial K_1}{\partial \Omega} & \frac{\partial K_2}{\partial \Omega} \end{pmatrix}=0 \end{array}\right\}. \tag{8}$$

The determinant conditions in (8) mean that at a singular point, the continuous and differentiable functions $A_0\left(\Omega\right),\ A\left(\Omega\right)$, and $A_0\left(A\right),\ \Omega\left(A\right)$, as well as $A\left(A_0\right), \Omega\left(A_0\right)$ do not exist.

In the neighborhood of a singular point $(A_{0*},\ A_*,\ \Omega_*;\ h_*,\ c_*,\ f_*)$, the 3D curve, defined by Eqs.(5), changes its form. Accordingly, the bifurcation diagram changes its form as well, i.e., the dynamics undergoes a bifurcation.

Alternatively, we analyze simpler 2D curves defined in Eqs.(6), (7). The conditions for singular points are [11, 13]

$$\left.\begin{array}{r} L_i\left(A,\Omega;h,c,f\right)=0 \\ \dfrac{\partial L_i\left(A,\Omega;h,c,f\right)}{\partial\Omega}=0 \\ \dfrac{\partial L_i\left(A,\Omega;h,c,f\right)}{\partial A}=0 \end{array}\right\}, \tag{9}$$

where $i=1,\ 2$ and the functions $L_1,\ L_2$ are defined in Eqs.(6), (7), respectively.

The second and third conditions in (9) entail that at a singular point, the continuous and differentiable functions $\Omega\left(A\right)$ or $A\left(\Omega\right)$ do not exist. Accordingly, the amplitude response curve $L_i\left(A,\Omega;h,c,f\right)=0$ changes its differential properties at a singular point $(\Omega_*, A_*; h_*, c_*, f_*)$.

The metamorphoses of the amplitude-frequency curves (i.e., the changes of differential properties) can also occur in a non-singular setting. More precisely, a metamorphosis of this kind occurs when a smooth change of parameters leads to the formation of vertical tangential points of an amplitude [14–16]. It follows that the equations guaranteeing the formation of a (non-singular) vertical tangential point $(A_*,\ \Omega_*)$ are

$$\left.\begin{array}{r} L_i\left(A,\Omega;h,c,f\right)=0 \\ \dfrac{\partial L_i\left(A,\Omega;h,c,f\right)}{\partial A}=0 \end{array}\right\} \quad (i=1,2)\,. \tag{10}$$

More precisely, the second of conditions (10) entails that the function $A\left(\Omega\right)$ has a vertical tangency (the continuous and differentiable function $A\left(\Omega\right)$ does not exist).

Finally, the equations

$$\left.\begin{array}{r} L_i\left(A,\Omega;h,c,f\right)=0 \\ \dfrac{\partial L_i\left(A,\Omega;h,c,f\right)}{\partial\Omega}=0 \end{array}\right\} \quad (i=1,2)\,, \tag{11}$$

are conditions for the maxima, minima, and inflection points of the function $A(\Omega)$ [11] (the function $\Omega(A)$ has a vertical tangency at any of these points).

Equations (8), (9), (10), (11) are general and permit the prediction of the diverse metamorphoses of amplitude-frequency response implicit functions, see [17] in the context of Eqs.(8) and [6] and references therein for a review of the applications of Eqs.(9), (10).

However, in simple cases such as the Duffing equation, the metamorphoses of amplitude profiles, induced by a change of parameters, were predicted without invoking the differential theory of implicit curves in pioneering papers [14–16, 18].

For example, jumps were computed algebraically in [14] (in the framework of Catastrophe Theory) and in [19]. Moreover, a differential condition for jumps was obtained in [15, 16]. Furthermore, the merging of two parts of the amplitude-frequency response curve, equivalent to a singularity, was computed in [18] (see also [16] and references therein).

While the changes in the differential properties of asymptotic solutions are important, the stability of the solutions is another essential factor shaping the dynamics.

3 Singular Points

A solution of Eqs.(8) is a curve in the 3D space of state variables $A_0,\ A,\ \Omega$, with the parameters $h,\ c,\ f$. Therefore, we shall look for the singular points of this curve in the most general 3D setting. The physical solutions of Eqs.(8) are shown in Table 1,

Type I (small orbits)	Type II (large orbits)
$A_0 = \frac{\sqrt{15c}}{15c}\sqrt{11-2\Omega^2}$	$A_0 = 0$
$A = \frac{2\sqrt{5c}}{15c}\sqrt{\Omega^2+2} \leq \sqrt{\frac{2}{3c}}$	$A = \sqrt{\frac{2}{3c}}$
$h = \frac{2\sqrt{6}}{3}\sqrt{1-\Omega^2}$	h – arbitrary
$f = \frac{4\left(\Omega^2+2\right)\sqrt{10c}}{45c}\sqrt{1-\Omega^2}$	$f = \frac{\sqrt{6c}}{6c}\sqrt{4\Omega^4+4\left(h^2+1\right)\Omega^2+1}$
$c > 0$	$c > 0$
$\lvert\Omega\rvert \leq 1$	Ω – arbitrary

Table 1: Singular points: physical solutions of Eqs.(8).

where inequality (7) was used in the second row of the first column. There are also other, borderline physical solutions of Eqs.(8) with $h = f = 0$, see Table 2.

Type I (small orbits)	Type II (large orbits)
$A_0 \neq 0$	$A_0 = 0$
$A = 2A_0\sqrt{\frac{2-\Omega^2}{6\Omega^2+3}}$	$A = 2\sqrt{\frac{\Omega^2+1}{3c}}$
$h = 0$	$h = 0$
$f = 0$	$f = 0$
$c = \frac{2\Omega^2+1}{5A_0^2}$	$c \neq 0$
$\lvert\Omega\rvert \leq \sqrt{2}$	Ω – arbitrary

Table 2: Borderline physical solutions of Eqs.(8).

Alternatively, we look for singular points in a simpler, less general 2D formulation (9).

It turns out that there are physical singular points of the 2D implicit curve $L_1(A, \Omega; h, c, f) = 0$, equivalent to the solution in the first column shown in Table 1. On the other hand, the implicit curve $L_2(A, \Omega; h, c, f) = 0$ has no physical singular points. There are, however, borderline singular points listed in Table 2, see Section 5.

It follows that the solutions displayed in the second column of Table 1 can be obtained in the 3D formulation only. These solutions describe, as we shall show below, a transition between small and large orbits. The bifurcation set, the set of parameters, for a given value of Ω, for which there is a Type II solution displayed in Table 1,

$$4\Omega^4 + 4\left(h^2+1\right)\Omega^2 + 1 = 6cf^2, \tag{12}$$

cf. the 4th row of the Table, is shown in Fig.1.

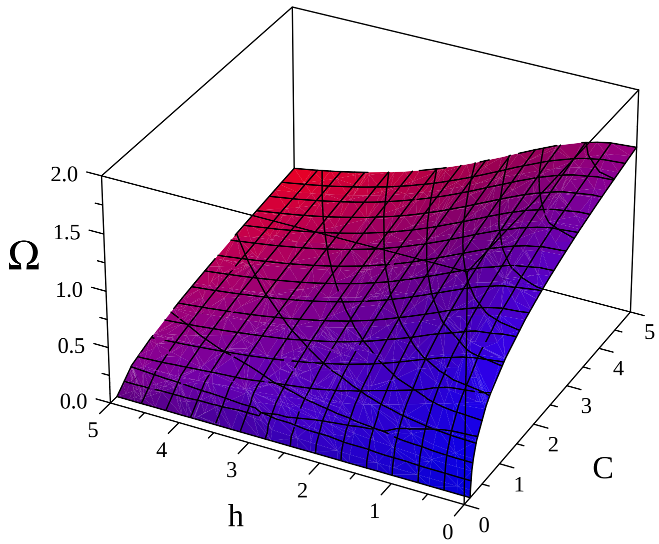

Figure 1: The bifurcation set, $4\Omega^4 + 4\left(h^2+1\right)\Omega^2 + 1 = 6C$, $C = cf^2$.

4 Jumps, Singular Points, and the Onset of Bistability

The jump equations (10) can be simplified. More precisely, we compute from (10) the equation for the amplitude A only,

$$\left.\begin{array}{l} \beta_5^{(i)}c^3h^2Z^5 + \beta_4^{(i)}c^2h^2Z^4 + \beta_3^{(i)}c^2f^2Z^3 + \beta_2^{(i)}ch^2f^2Z^2 + 16f^4 = 0, \\ \quad \beta_5^{(1)} = -3375, \quad \beta_4^{(1)} = 1800, \quad \beta_3^{(1)} = -900, \quad \beta_2^{(1)} = -120, \\ \quad \beta_5^{(2)} = 27, \qquad \beta_4^{(2)} = -36, \quad \beta_3^{(2)} = -36, \quad \beta_2^{(2)} = 24, \end{array}\right\} \tag{13}$$

$Z = A^2$, and, after a value of A is calculated, an equation for the frequency Ω is obtained:

$$\left.\begin{array}{l} \gamma_6^{(i)}c^2h^2Z^3 + \gamma_4^{(i)}ch^2Z^2 + \gamma_2^{(i)}cf^2Z + 8\gamma_0^{(i)}f^2 + 8f^2\Omega^2 = 0, \\ \quad \gamma_3^{(1)} = 225, \quad \gamma_2^{(1)} = -120, \quad \gamma_1^{(1)} = 90, \quad \gamma_0^{(1)} = h^2-2, \\ \quad \gamma_3^{(2)} = 9, \qquad \gamma_2^{(2)} = -12, \quad \gamma_1^{(2)} = -18, \quad \gamma_0^{(2)} = h^2+1, \end{array}\right\} \tag{14}$$

where $i=1$ means that we solve Eqs.(10) for the function L_1, while $i=2$ means that we solve Eqs.(10) for the function L_2, with the functions L_1, L_2 defined in equations (6) and (7), respectively.

The physical ($A>0$, $\Omega>0$) single roots of Eqs.(10) describe jumps. We now consider an important case of the double (multiple) roots of (10).

The multiple roots of Eqs.(13) occur at the parameter values for which the discriminants D_i of polynomials in Eqs.(13) vanish. The discriminant of a polynomial can be computed as a determinant of the corresponding 9×9 Sylvester matrix, see [20] and Eq.(13) in [6]. In the case of small orbits ($i=1$), we have

$$\begin{aligned} D_1(h,c,f) &= p_1(h,c,f)\, q_1(h,c,f) = 0, && \text{(15a)}\\ p_1(h,c,f) &= h^6 - 16h^4 + 64h^2 - 240f^2c, && \text{(15b)}\\ q_1(h,c,f) &= \left(12\,960f^2c - 8192\right)h^6 + 25\,920cf^2h^4 + 6075c^2f^4. && \text{(15c)} \end{aligned}$$

The singular points of small orbits are given by the equation $p_1(h,c,f)=0$, which has the physical solutions listed in the first column of Table 1. The onset of bistability, corresponding to a double root of Eq.(13), is given by the equation $q_1(h,c,f)=0$.

In the case of large orbits ($i=2$), the determinant is

$$\begin{aligned} D_2(h,c,f) &= p_2(h,c,f)\, q_2(h,c,f) = 0, && \text{(16a)}\\ p_2(h,c,f) &= h^6 + 8h^4 + 16h^2 + 48f^2c, && \text{(16b)}\\ q_2(h,c,f) &= \left(1024 - 2592f^2c\right)h^6 + 2592cf^2h^4 + 243c^2f^4. && \text{(16c)} \end{aligned}$$

The singular points of the large orbit are given by the equation $p_2(h,c,f)=0$, which has no real solutions for $c>0$. Therefore, a large orbit has the singular points listed in the second column of Table 1 only. Furthermore, the equation $q_2(h,c,f)=0$ determines the onset of bistability.

5 Numerical Verification and Analysis of the Analytical Results

5.1 Small orbits: singular points and the onset of bistability

The formulas for the Type I singular points are listed in the first column of Table 1. We choose $c=1$, $\Omega=0.8$. Then the equations listed in the first column of Table 1 yield $h=0.979\,796$, $f=0.445\,249$, and $A_0=0.804\,984$, $A=0.484\,424$.

Now, we plot the implicit function $L_1(A,\Omega)=0$, defined in Eq.(6), for $h=0.979\,796$, $c=1$, and three values of f: $f=0.44$ (green), $f=0.445\,249$ (red, analytical critical), $f=0.46$ (blue), see Fig.2. The amplitude-frequency curve has a singular point – an intersection. Therefore, we can expect a rupture of a stable branch of solution (4), corresponding to the green line in Fig.2.

The corresponding bifurcation diagrams, computed from Eq.(3) for $h=0.979\,796$, $c=1$, and two values of f: $f=0.599\,00$ (below the numerical critical value), $f=0.599\,14$ (above the numerical critical value), are shown in Fig.3. Blue and green colors in Figure 3 correspond to blue and green branches in Fig.2.

Indeed, it follows that the upper blue branch in Fig.2 is continuous, see the upper blue curve in Fig.3. On the other hand, after the metamorphosis, see the red curve, the upper green curve in Fig.3 must be ruptured since the green branches in Fig.2 are disconnected. Note that, while the gap in the green branch in Fig.3 occurs near the critical value

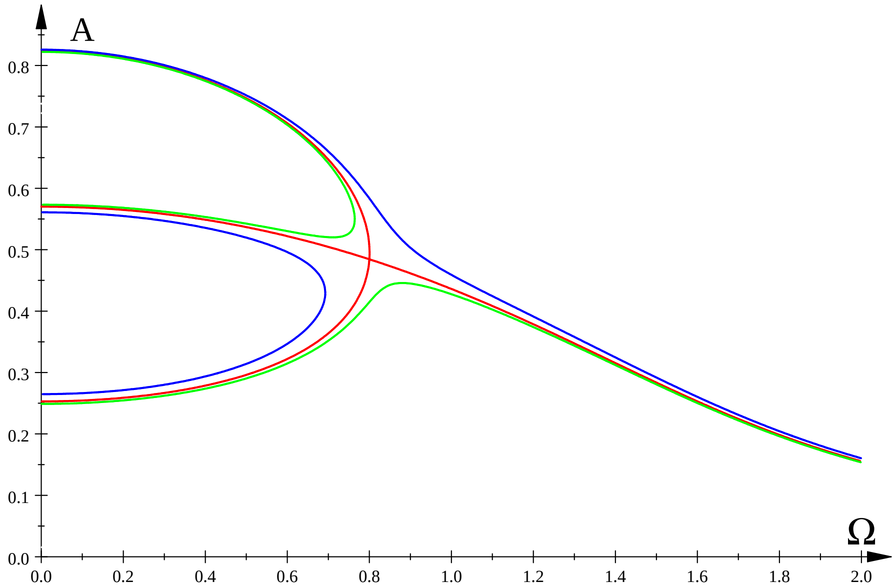

Figure 2: Implicit functions $L_1(A, \Omega; h, c, f) = 0$: $h = 0.979\,796$, $c = 1$, $f = 0.44$ (green), $f = 0.445\,249$ (red), $f = 0.46$ (blue).

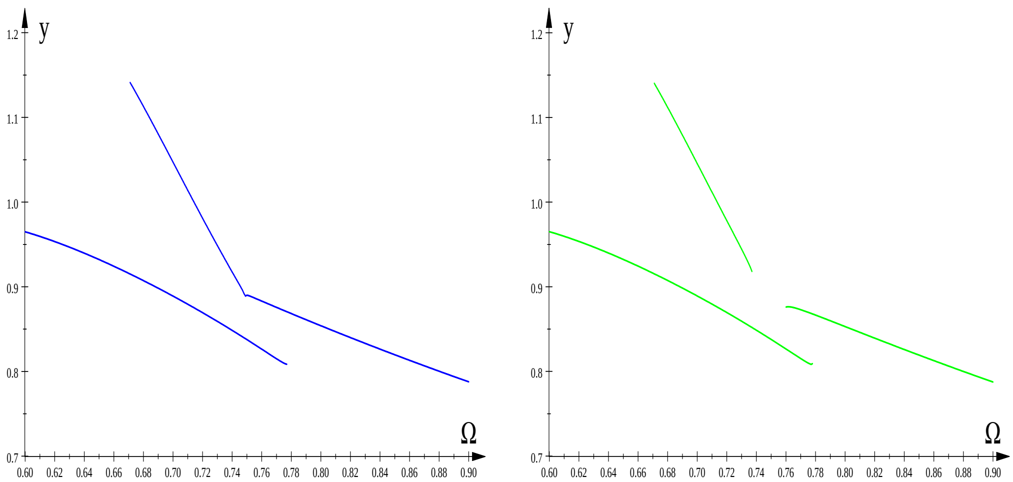

Figure 3: Bifurcation diagrams $y(\Omega)$ for Eq.(3): $h = 0.979\,796$, $c = 1$, $f = 0.599\,14$ (blue), and $f = 0.599\,00$ (green).

$\Omega = 0.8$, the numerical critical value of the parameter f, $f \in (0.599\,00,\ 0.599\,14)$, is quite far from the analytical value $f = 0.445\,249$.

We now use equations (15) from Section 4 to study jump phenomena.

Let $h = 0.1$, $c = 1$. Then the equation $p_1(h,\ c,\ f) = 0$ yields the real solution $f = 0.051\,575$, corresponding to a singular point. On the other hand, the equation $q_1(h,\ c,\ f) = 0$ has the real solution $f = 0.031\,088$ which determines the onset of bistability. In the left Figure 4, the amplitude-frequency curves are shown and the right Figure 4 shows the bifurcation diagram computed for Eq.(3).

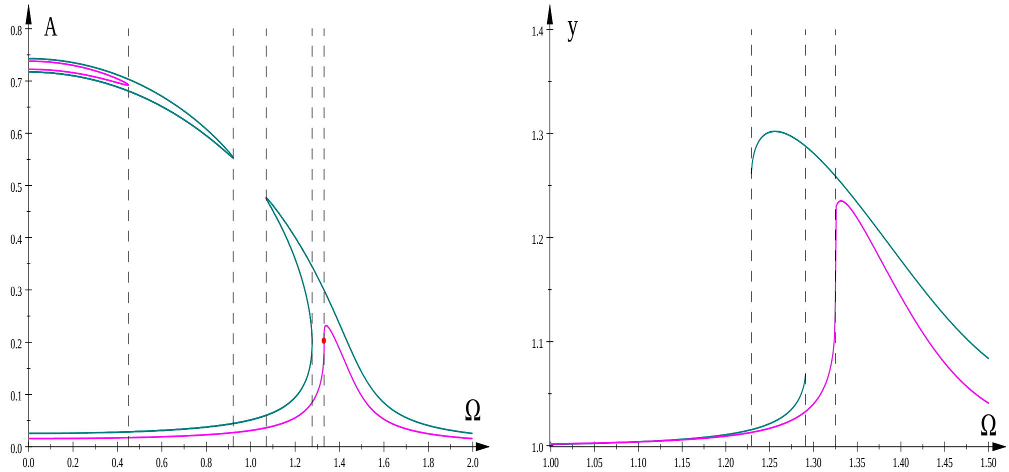

Figure 4: Functions $L_1(A, \Omega) = 0$: $h = 0.1$, $c = 1$, $f = 0.031\,088$ (magenta) and $f = 0.51$ (blue-green); bifurcation diagrams $y(\Omega)$: $f = 0.037$ (magenta) and $f = 0.51$ (blue-green).

5.2 Large orbits: singular points, jumps, and escape phenomena

The Type II singular points can be computed from the expressions listed in Table 1.

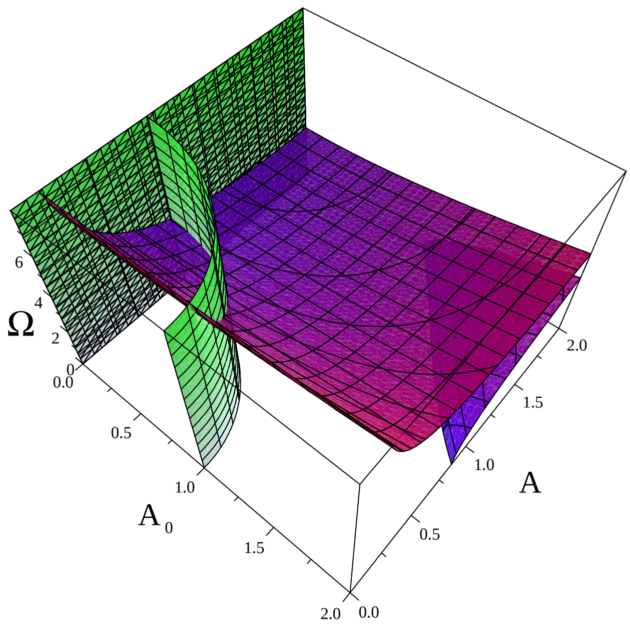

Figure 5: Intersection of surfaces: $K_1(A_0,\ A) = 0$ (green) and $K_2(A_0,\ A,\ \Omega) = 0$ (blue and red), $h = 0.5$, $c = 0.5$, $f = 10$.

The surfaces $K_1(A_0,\ A) = 0$ (green) and $K_2(A_0,\ A,\ \Omega) = 0$ (blue and red) are shown in Fig.5 for $h = 0.5$, $c = 0.5$, $f = 10$. For these parameter values, we compute, from the formulas listed in Table 1, $\Omega = 2.836$, $A = 1.155$. Therefore, the intersection point of green (two patches) and blue and red surfaces has the coordinates $(A_0,\ A,\ \Omega) = (0,\ 1.155,\ 2.836)$ in Fig.5 and $(A,\ \Omega) = (1.155,\ 2.836)$ in Fig.6, see the red dot denoted as "1". The black dashed line denotes the borderline solution of Table 2.

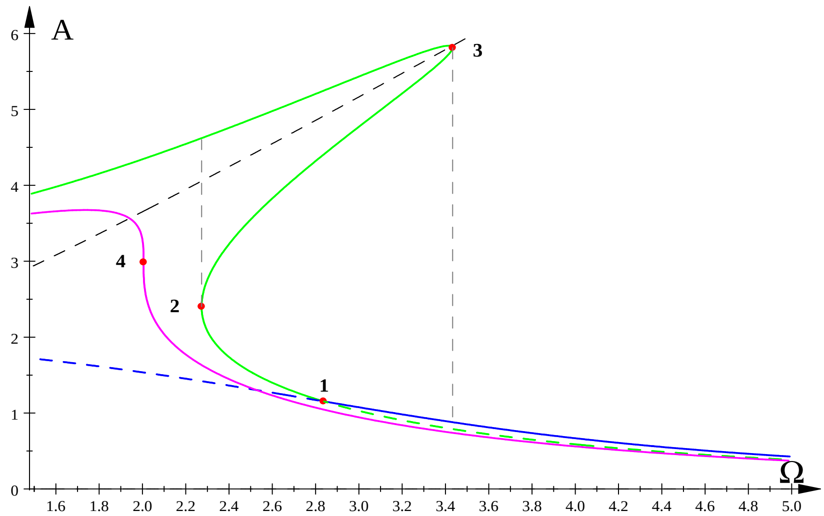

Figure 6: Implicit functions: $L_1(A, \Omega;\ 0.5, 0.5, 10) = 0$ (blue), $L_2(A, \Omega;\ 0.5, 0.5, 10) = 0$ (green), $L_2(A, \Omega;\ 1.446, 0.5, 10) = 0$ (magenta), and $L_2(A, \Omega;\ 0, 0.5, 0) = 0$ (black, dashed).

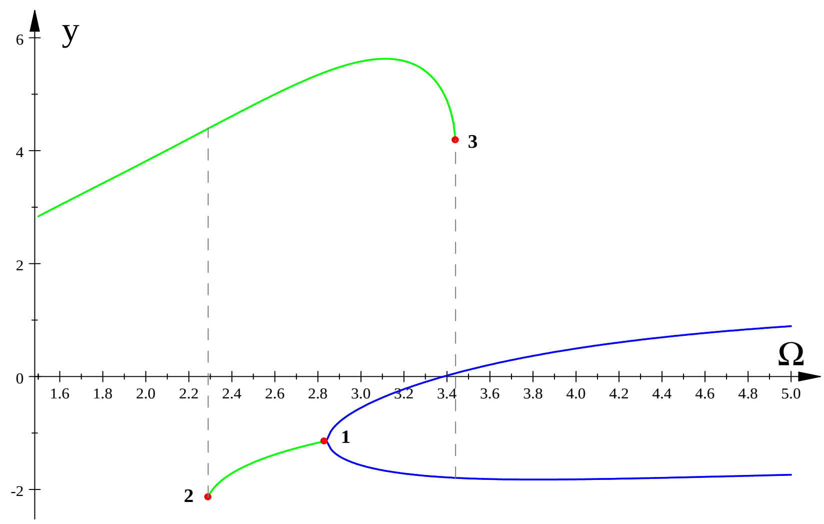

Figure 7: Bifurcation diagram $y(\Omega)$, $h = 0.5$, $c = 0.5$, $f = 10$.

The bifurcation diagram computed for Eq.(3) is shown in Fig.7. The transition between small and large orbits occurs indeed near the critical value $\Omega = 2.836$.

Moreover, we have used equations (10) and (16) to study jump phenomena. The computed points of jumps (at vertical tangencies) and the corresponding points present in the bifurcation diagram are denoted in Figs.6 and 7 as "2" and "3".

We have also determined the onset of bistability for large orbits. In Figure 8 below, we show the implicit functions $L_2(A, \Omega;\ 1.446, 0.5, 10) = 0$ (the onset of bistability, magenta), $L_2(A, \Omega;\ 1.20, 0.5, 10) = 0$ (blue-green), as well as the bifurcation diagrams computed for Eq.(3), the same color lines correspond to the same states.

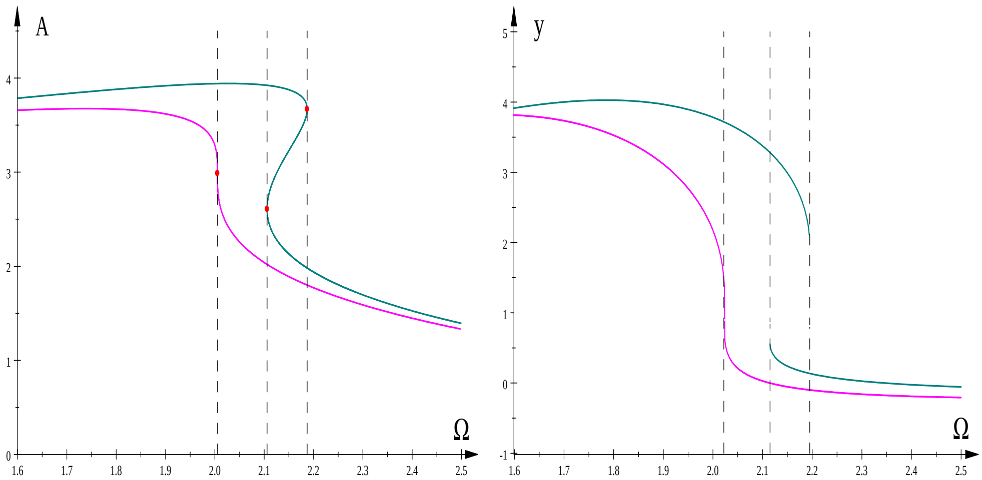

Figure 8: Functions $L_2(A, \Omega) = 0$: $c = 0.5$, $f = 10$, $h = 1.446$ (magenta), and $h = 1.20$ (blue-green); bifurcation diagrams $y(\Omega)$: $h = 1.43$ (magenta) and $h = 1.20$ (blue-green).

We can now describe a sequence of events, predicted by the form of the implicit functions $L_1 = 0$, $L_2 = 0$, cf. Fig.6, and confirmed by the bifurcation diagram, Fig.7, computed from Eq.(3).

Let $h = 0.5$, $c = 0.5$, $f = 10$, and $\Omega = 4.0$. In this case, the dynamics settles on either of two small orbits (blue), see Figs.6, 7. Then, for the decreasing values of Ω, the small orbit transforms into a large orbit of small amplitude (green) at point "1" (singular point). This large orbit, upon further decreasing of Ω, jumps at point "2" (vertical tangency point) to the large orbit with large amplitude (green). If the value of Ω is increased now, another vector tangency point ("3") is reached and the large orbit with large amplitude falls onto either of the small orbits (blue).

6 Conclusion

In this work, we have investigated several bifurcations present in the twin-well Duffing equation (1). We based our approach on the known steady-state asymptotic solution of the nondimensional Duffing equation (3) computed in implicit form, see Eqs.(4), (5a), (5b), and (6), (7).

Working in the framework of the differential properties of implicit functions [11–13], we have computed (i) singular points in the $3D$ formulation and (ii) $2D$ singular points in

Sections 3, 4, (iii) the points of vertical tangencies, and (iv) the double points of vertical tangencies in Section 4.

Case (i) corresponds to the small orbit – large orbit transition (escape phenomenon), see point "1" in Figs.6, 7. Case (ii) is a rupture of a stable branch of a small orbit solution, see Figs.2, 3, while case (iii) corresponds to jumps, see for example points "2", and "3" in Figs.6, 7. Finally, case (iv) coincides with the onset of bistability, after which jumps are possible, see Fig.4 and Figs.6, 8.

Our analytical predictions correlate well with the numerical computations carried out for the Duffing equation (3) and are reported in Section 5, the agreement is very good in the case of the large orbit and satisfactory for the small orbit (this shows that the large orbit asymptotic solution 7 is definitely more exact than the small orbit one 6).

References

[1] W. Szemplińska-Stupnicka. *Chaos, Bifurcations and Fractals Around Us: A Brief Introduction*. Vol. 47. World Scientific, 2003.

[2] S. Lenci and G. Rega. Forced harmonic vibration in a Duffing oscillator with negative linear stiffness and linear viscous damping. In: *The Duffing Equation: Nonlinear Oscillators and Their Behavior* (Eds.: I. Kovacic, M.J. Brennan). John Wiley & Sons, Hoboken, New Jersey, 2011, 277–322.

[3] P.J. Holmes. A Nonlinear Oscillator with a Strange Attractor. *Phil. Trans. R. Soc. Lond.* A **292** (1979) 419–448.

[4] F.C. Moon and P.J. Holmes. A Magnetoelastic Strange Attractor. *Journal of Sound and Vibration* **65** (1979) 275-296.

[5] I. Kovacic and M.J. Brennan, Eds. *The Duffing Equation: Nonlinear Oscillators and Their Behavior*. John Wiley & Sons, Hoboken, New Jersey, 2011.

[6] J. Kyziołand A. Okniński. Asymmetric Duffing Oscillator: Jump Manifold and Border Set. *Nonlinear Dyn. Syst. Theory* **23** (2023) 46–57.

[7] J. Awrejcewicz, Modified Poincaré method and implicit function theory. In: *Nonlinear Dynamics: New Theoretical and Applied Results* (Ed.: J. Awrejcewicz). Akademie Verlag, Berlin, 1995, 215-229.

[8] Nayfeh, A.H. *Introduction to Perturbation Techniques*. John Wiley & Sons, 2011.

[9] M. Wali Ullah, M. Alhaz Uddin and M. Saifur Rahman. A Modified Harmonic Balance Method for Solving Strongly Generalized Nonlinear Damped Forced Vibration Systems. *Nonlinear Dyn. Syst. Theory* **21** (2021) 544–552.

[10] D.W. Jordan and P. Smith. *Nonlinear ordinary differential equations*. Oxford University Press Inc., New York, Fourth edition, 2007.

[11] G.M. Fikhtengol'ts, (I.N Sneddon, Ed.). *The fundamentals of mathematical analysis*. Vol. 2, Elsevier, 2014 (Chapter 19).

[12] E. Hartmann. *Geometry and Algorithms for Computer-Aided Design*. Darmstadt University of Technology, Darmstadt, 2003.

[13] C.T.C. Wall. *Singular Points of Plane Curves*. Cambridge University Press, New York, 2004.

[14] P.J. Holmes and D.A. Rand. The bifurcations of Duffing's equation: an application of Catastrophe Theory. *J. Sound Vib.* **44** (1976) 237-253.

[15] T. Kalmár-Nagy and B. Balachandran. Forced harmonic vibration of a Duffing oscillator with linear viscous damping. In: *The Duffing Equation: Nonlinear Oscillators and Their Behavior* (Eds.: I. Kovacic, M.J. Brennan). John Wiley & Sons, 2011, 139–174.

[16] A.K. Mallik. Forced harmonic vibration of a Duffing oscillator with different damping mechanisms. In: *The Duffing Equation: Nonlinear Oscillators and Their Behavior* (Eds.: I. Kovacic, M.J. Brennan). John Wiley & Sons, Hoboken, New Jersey 2011, 175–217.

[17] J. Kyzioł. Metamorphoses of resonance curves for two coupled oscillators: The case of small non-linearities in the main mass frame. *Int. J. Nonlinear Mech.* **76** (2015) 164–168.

[18] W. Szemplinska-Stupnicka. Bifurcations of harmonic solution leading to chaotic motion in the softening type Duffing's oscillator. *Int. J. Nonlinear Mech.* **23** (1988) 257–277.

[19] M.P. Markakis. The jump phenomenon associated with the dynamics of the duffing equation. *Physics Open* **5** (2020) 100042.

[20] S. Janson. Resultant and discriminant of polynomials. Lecture notes, 2010. Available at `http://www2.math.uu.se/~svante/papers/sjN5.pdf`

Nonlinear Dynamics and Systems Theory, **24** (2) (2024) 193–204

Application of Mamdani Fuzzy Method in Herbal Soap Production Planning

I. H. Santoso [1], P. Katias [2], T. Herlambang [3], M. Tafrikan [4], K. Oktafianto [5], A. A. Firdaus [6*] and H. Arof [7]

[1] *Department of Accounting Magister, University of Wijaya Kusuma, Surabaya, Indonesia.*
[2] *Department of Management, Universitas Nahdlatul Ulama Surabaya, Indonesia.*
[3] *Department of Information System, Universitas Nahdlatul Ulama Surabaya, Indonesia.*
[4] *Department of Mathematics, Universitas Islam Negeri Walisongo, Indonesia.*
[5] *Department of Mathematics, University of PGRI Ronggolawe, Indonesia.*
[6*] *Department of Engineering, Faculty of Vocational, Airlangga University, Indonesia.*
[7] *Department of Electrical Engineering, University of Malaya, Malaysia.*

Received: August 23, 2023; Revised: February 26, 2024

Abstract: Fuzzy logic is a logic that has a value of fuzzyness between true or false. This study discusses the application of the Mamdani fuzzy logic in solving production planning problems based on demand, remains and stock shortages. The variables used for the production of herbal soap are 4 variables, namely 3 input variables which consist of the demand variable, residual variable and shortage variable, and 1 output variable, the production variable. The demand variable consists of 3 fuzzy sets, namely decreasing, fixed and increasing, residual and shortage variables consist of 3 fuzzy sets, namely little, moderate and many, while the production variable consists of 3 fuzzy sets, namely reduced, fixed and added. Therefore, a system is needed to determine the amount of herbal soap production so that there will be no problems. The results of this study aim to apply the Mamdani fuzzy logic method in predicting the amount of herbal soap production based on demand, remains and stock shortage data. Based on the calculations carried out, there were only 8,333% of the data that had actual results. At the same time, the remaining 91.667% are the data that have planned results that are not in accordance with the actual data.

Keywords: *fuzzy inference system; determination of production quantities; Mamdani fuzzy logic.*

Mathematics Subject Classification (2010): 03B52, 03E72, 94D05.

* Corresponding author: mailto:aa.firdaus@vokasi.unair.ac.id

1 Introduction

Bath soap products have developed into the primary needs of people of all social classes. Soap can be used to treat diseases such as skin diseases caused by bacteria or fungi. In other words, soap can be used as a medicine cleaning the body to minimize the possibility of suffering from diseases. The advantages of herbal soap compared to common soaps are: it is easy to carry, it is easy to store, it offers various uses and benefits, and it has an exclusive packaging appearance. Based on the data obtained, the producers often experienced either shortages of products or overproduction in their day to day production.

Determining the production target or the number of products by the application of the method allows membership values between 0 and 1 [1]. Various theories in the development of fuzzy logic show that basically, fuzzy logic can be used to model various systems [2]. Fuzzy logic is believed to be very flexible and has tolerance for existing data. Based on the fuzzy logic, a model of a system capable of estimating the number of product units to be produced will be generated [3–6].

The previous research has been carried out using the same method, that is, the Mamdani Fuzzy Method but with four variables, and each variable had only two sets. The residual variable had only two sets, that is, few and many. The sales and demand variable had two sets, that is, decreasing and increasing. And the order variable had two sets, decreasing and increasing. And in this study, there are four variables, and each has three sets [7–9].

Based on the description above, the researches in this paper are interested in carrying out a study entitled "The Application of the Fuzzy Mamdani Method in Herbal Soap Production Planning". The aim is to help determine the number of herbal soap product units to be produced and to introduce the Fuzzy Mamdani method to solve the herbal soap production problems.

2 Method

2.1 Research procedures

Software needs analysis is done to find out all the problems and requirements. The analysis is done by finding and determining the problems encountered, as well as all the requirements such as problem analysis, system analysis, system input and output, and the functions required [10, 11].

Based on the data obtained, the producer often experiences production shortages and excesses in the day to day production as shown in Table 1.

In general, the system to be developed attempts to apply the Mamdani Fuzzy method in the herbal soap production planning based on the demand for the product units, the remaining product units, and the shortages. The testing has to be carried out by comparing the number of product units at the shops to that of the production results planned. As a result, the system provides the output in the form of herbal soap production using the Fuzzy Mamdani method. The data used in this study are the production, demand, and shortage data in January-February, 2019 as shown in Table 1. The data indicate the remaining units of 29 out of 48 and the shortage of 19 out of 48.

2.2 Research Design

Context Diagram

Table 1: Data of Production for the January-February period.

Dates	Production	Demand	Remains	Shortage
03-Jan	610	211	399	0
04-Jan	399	944	0	545
05-Jan	655	201	454	0
07-Jan	454	1208	0	754
08-Jan	946	218	728	0
09-Jan	728	658	70	0
10-Jan	870	988	0	118
11-Jan	882	249	633	0
12-Jan	633	431	202	0
14-Jan	802	388	414	0
15-Jan	414	857	0	443
16-Jan	857	410	447	0
17-Jan	447	945	0	498
18-Jan	902	369	533	0
19-Jan	533	867	0	334
21-Jan	866	188	678	0
22-Jan	678	256	422	0
23-Jan	422	966	0	544
24-Jan	856	402	454	0
25-Jan	454	1157	0	703
26-Jan	997	310	687	0
28-Jan	657	1525	0	868
29-Jan	962	297	665	0
30-Jan	665	981	0	316
31-Jan	984	220	764	0
01-Feb	764	228	536	0
02-Feb	536	101	435	0
04-Feb	435	1139	0	704
06-Feb	896	1822	0	926
07-Feb	1074	454	620	0
08-Feb	620	198	422	0
09-Feb	422	603	0	181
11-Feb	819	336	483	0
12-Feb	483	1175	0	692
13-Feb	818	193	625	0
14-Feb	625	165	460	0
15-Feb	460	720	0	260
16-Feb	740	211	529	0
18-Feb	529	765	0	236
19-Feb	764	415	349	0
20-Feb	349	1408	0	1059
21-Feb	1141	299	842	0
22-Feb	842	180	662	0
23-Feb	662	218	444	0
25-Feb	444	910	0	466
26-Feb	734	154	580	0
27-Feb	580	206	374	0
28-Feb	374	897	0	523

Context diagram is an overview of the interactions occurring between the system and the user. The user enters the input variables, that is, the demand, the remains and the shortage for further processing. After the processing, the system produces the output in the form of the number of herbal soap units to be produced.

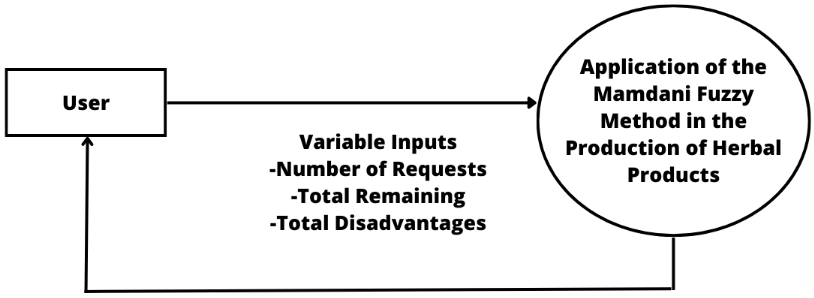

Figure 1: Context Diagram.

Interface Design.

We present the interface design for the production planning system into which the user enters the variables: the number of product units demanded, the number of the remaining product units and the number of shortages. The results of the calculations or the output for the production are immediately displayed in the form below.

Figure 2: Production Planning Form.

In the input column, there is the column matrix to be filled, that is, the first column for the demand variable value, the second column for the remains variable value, and the third column for the shortage variable value.

Data Analysis.

1. Determine the variables related to the process and the appropriate fuzzification function. There are 4 variables in the model, that is,

   - The demand variable consists of 3 fuzzy sets, that is, Decreasing, Fixed and Increasing.
     The function of the demand variable membership is

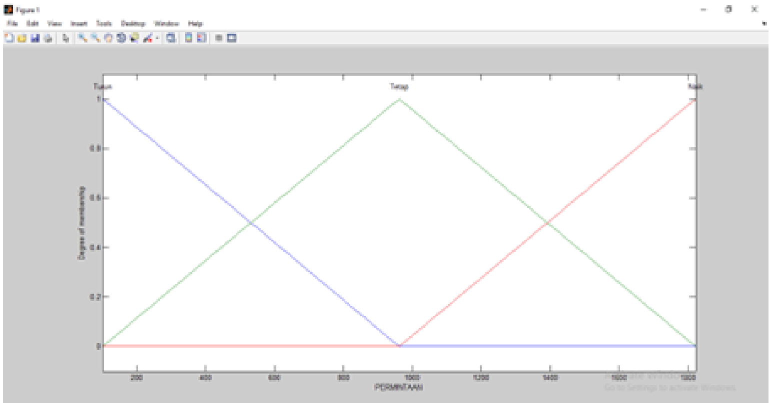

Figure 3: Demand Variable.

$$\mu_{decreasing\ demand} = \begin{cases} 1 & ; w \leq 101 \\ \frac{961.5-w}{961.5-101} & ; 101 \leq w \leq 961.5 \\ 0 & ; w \geq 961.5 \end{cases}$$

$$\mu_{fixed\ demand} = \begin{cases} 0 & ; w = 961.5 \\ \frac{w-101}{961.5-101} & ; 101 \leq w \leq 961.5 \\ \frac{1822-w}{1822-961.5} & ; 961.5 \leq w \leq 1822 \\ 1 & ; w \leq 101, w \geq 1822 \end{cases}$$

$$\mu_{increasing\ demand} = \begin{cases} 0 & ; w \leq 961.5 \\ \frac{w-961.5}{1822-961.5} & ; 961.5 \leq w \leq 1822 \\ 1 & ; w \geq 961.5 \end{cases}$$

   - The remains variable consists of 3 fuzzy sets, that is, **Few**, **Fair** and **Many**. The function of the remains variable membership is

$$\mu_{few\ remaining} = \begin{cases} 1 & ; x \leq 0 \\ \frac{421-x}{421-0} & ; 0 \leq x \leq 421 \\ 0 & ; x \geq 421 \end{cases}$$

$$\mu_{fair\ remaining} = \begin{cases} 0 & ; x = 421 \\ \frac{x-0}{421-0} & ; 0 \leq x \leq 421 \\ \frac{842-x}{842-421} & ; 421 \leq x \leq 842 \\ 1 & ; x \leq 0, x \geq 842 \end{cases}$$

$$\mu_{many\ remaining} = \begin{cases} 0 & ; x \leq 421 \\ \frac{x-421}{842-421} & ; 421 \leq x \leq 842 \\ 1 & ; x \geq 421 \end{cases}$$

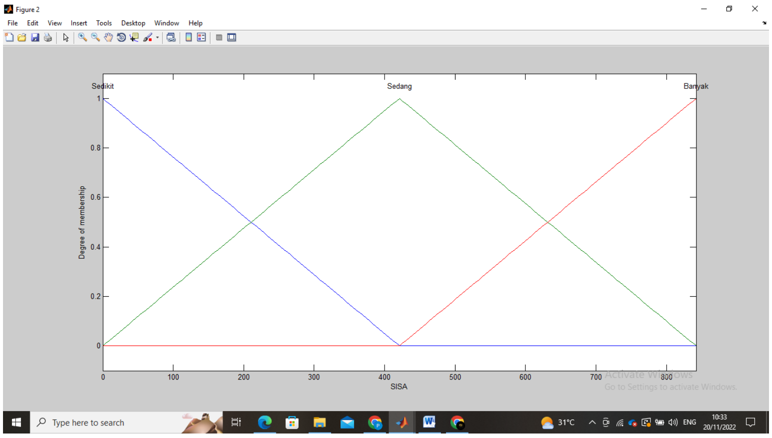

Figure 4: Remains Variable.

- The shortage variable consists of 3 fuzzy sets, that is, **Few**, **Fair** and **Many**.

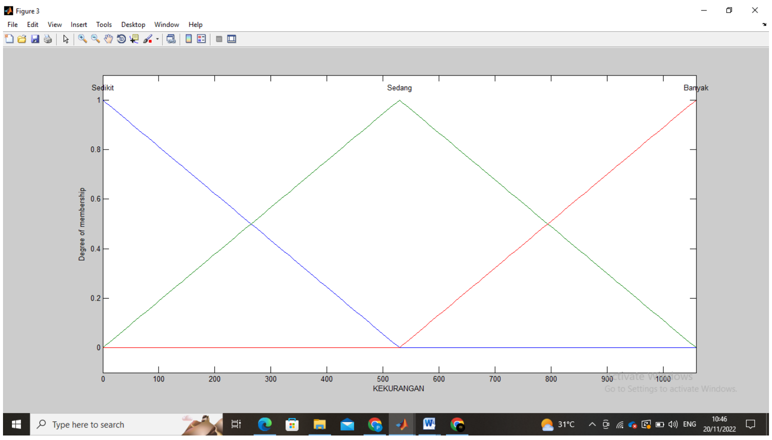

Figure 5: Shortage Variable.

The function of the shortage variable membership is

$$\mu_{few\ shortage} = \begin{cases} 1 & ; y \leq 0 \\ \frac{529.5-y}{529.5-0} & ; 0 \leq y \leq 529.5 \\ 0 & ; y \geq 529.5 \end{cases}$$

$$\mu_{fair\ shortage} = \begin{cases} 0 & ; y = 529.5 \\ \frac{y-0}{529.5-0} & ; 0 \leq y \leq 529.5 \\ \frac{1059-y}{1059-529.5} & ; 529.5 \leq y \leq 1059 \\ 1 & ; y \leq 0, y \geq 1059 \end{cases}$$

$$\mu_{many\ shortage} = \begin{cases} 0 & ; y \leq 529.5 \\ \frac{y-529.5}{1059-529.5} & ; 529.5 \leq y \leq 1059 \\ 1 & ; y \geq 529.5 \end{cases}$$

- The production variable consists of 3 fuzzy sets, that is, **Reduced**, **Fixed** and **Added**.

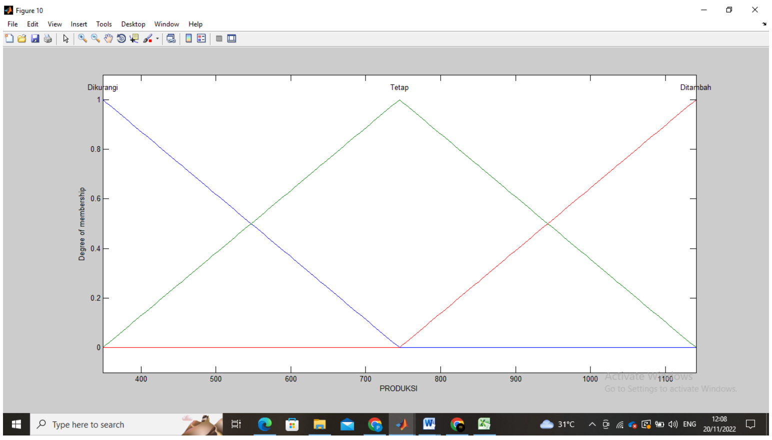

Figure 6: Production Variable.

The function of the production variable membership is

$$\mu_{reduced\ production} = \begin{cases} 1 & ; z \leq 349 \\ \frac{745-z}{745-349} & ; 349 \leq z \leq 745 \\ 0 & ; z \geq 745 \end{cases}$$

$$\mu_{fixed\ production} = \begin{cases} 0 & ; z = 745 \\ \frac{z-349}{745-349} & ; 349 \leq z \leq 745 \\ \frac{1141-z}{1141-745} & ; 745 \leq z \leq 1141 \\ 1 & ; z \leq 349, z \geq 1141 \end{cases}$$

$$\mu_{added\ production} = \begin{cases} 0 & ; z \leq 745 \\ \frac{z-745}{1141-745} & ; 745 \leq z \leq 1141 \\ 1 & ; z \geq 745 \end{cases}$$

Take the data on January 3, 2019, the value of the demand variable is 211, and the remains is 399. If the remains is known, the deficiency is automatically equal to 0 and vice versa. Fuzzification of the demand variable with the demand value 211 is

$$\mu_{decreasing\ demand}(211) = \frac{961.5 - 211}{961.5 - 101} = 0.872,$$

$$\mu_{fixed\ demand}(211) = \frac{211 - 101}{961.5 - 101} = 0.128.$$

Fuzzification of the remains variable with the remains value 399 is

$$\mu_{few\ remaining}(399) = \frac{421 - 399}{421 - 0} = 0.052,$$

$$\mu_{fair\ remaining}(399) = \frac{399-0}{421-0} = 0.948.$$

Based on the data analysis on the limits of each Fuzzy set of each variable, the fuzzy rules formed are as follows:
[$R1$] If (Demand is Decreased) And (Remains is Few) Then (Production is Fixed)
[$R2$] If (Demand is in Decreased) And (Remains is Fair) Then (Production is Reduced)
[$R3$] If (Demand is Decreased) And (Remains is Many) Then (Production is Reduced)
[$R4$] If (Demand is Fixed) And (Remains is Few) Then (Production is Added)
[$R5$] If (Demand is Fixed) And (Remains is Fair) Then (Production is Fixed)
[$R6$] If (Demand is Fixed) And (Remains is Many) Then (Production is Reduced)
[$R7$] If (Demand is Increasing) And (Remains is Few) Then (Production is Added)
[$R8$] If (Demand is Increasing) And (Remains is Fair) Then (Production is Added)
[$R9$] If (Demand is Increasing) And (Remains is Many) Then (Production is Fixed)
[$R10$] If (Demand is Decreased) And (Shortage is Few) Then (Production is Fixed)
[$R11$] If (Demand is Decreased) And (Shortage is Fair) Then (Production is Reduced)
[$R12$] If (Demand is Decreased) And (Shortage is Many) Then (Production is Reduced)
[$R13$] If (Demand is Fixed) And (Shortage is Few) Then (Production is Fixed)
[$R14$] If (Demand is Fixed) And (Shortage is Fair) Then (Production is Fixed)
[$R15$] If (Demand is Fixed) And (Shortage is Many) Then (Production is Added)
[$R16$] If (Demand is Increasing) And (Shortage is Few) Then (Production is Fixed)
[$R17$] If (Demand is Increasing) And (Shortage is Fair) Then (Production is Added)
[$R18$] If (Demand is Increasing) And (Shortage is Many) Then (Production is Added)

2. Implication Function Application.
   The function application we use is Minus function application:
   [$R1$] If (Demand is Decreased) And (Remains is Few) Then (Production is Fixed)

$$\alpha_1 = min(0.872; 0.052) = 0.052$$

   [$R2$] If (Demand is in Decreased) And (Remains is Fair) Then (Production is Reduced)

$$\alpha_1 = min(0.872; 0.948) = 0.872$$

   [$R4$] If (Demand is Fixed) And (Remains is Few) Then (Production is Added)

$$\alpha_2 = min(0.128; 0.052) = 0.052$$

   [$R5$] If (Demand is Fixed) And (Remains is Fair) Then (Production is Fixed)

$$\alpha_3 = min(0.128; 0.948) = 0.128$$

3. Rules of Composition.
   The MAX method is used to produce composition between all rules. $\mu_z =$

$max(0.052; 0.128) = 0.128$. It is known that the degree of the membership function for production is

$$\mu_{fixed\ production}(z) = \begin{cases} 0 & ; z = 745, \\ \frac{z-349}{745-349} & ; 349 \leq z \leq 745, \\ \frac{1141-z}{1141-745} & ; 745 \leq z \leq 1141, \\ 1 & ; z \leq 349, z \geq 1141, \end{cases}$$

$$\begin{aligned} \mu_z &= \frac{z-349}{745-349} = 0.128, \\ z - 349 &= 0.128 \times 396, \\ z - 349 &= 50.688, \\ z &= 399.688, \end{aligned}$$

$$\begin{aligned} \mu_z &= \frac{1141-z}{1141-745} = 0.128, \\ 1141 - z &= 0.128 \times 396, \\ 1141 - z &= 50.688, \\ z &= 1090.321. \end{aligned}$$

4. Defuzzification.
   The input of the defuzzification process is a fuzzy set obtained from the composition of the fuzzy rules, while the resulting output is a number in the domain of the fuzzy set. The method used for defuzzification is centroid.
   The calculation of Moment 1

$$\begin{aligned} M_1 &= \int_{349}^{399.688} \mu a_1 z dz \\ &= \int_{349}^{399.688} \frac{z-349}{745-349} z dz \\ &= \frac{1}{396} \int_{349}^{399.688} z^2 - 349 dz \\ &= 1241.7896439. \end{aligned}$$

   The calculation of Moment 2

$$\begin{aligned} M_2 &= \int_{399.688}^{1090.312} \mu a_2 z dz \\ &= \int_{399.688}^{1090.312} 0.128 z dz \\ &= 0.128 \frac{1}{2} \left[z^2\right]_{399.688}^{1090.312} dz \\ &= 65857.904637. \end{aligned}$$

   Thus, the value of each moment is

   - $M_1 = 1241.7896439$,
   - $M_2 = 65857.904637$.

3 Results and Discussion

3.1 Research Measurement

The pre-test and post-test are used in the measurement of this study. It aims to find out the difference test between the grouping of production ranges done manually based on the actual data and that of the prediction developed using the Mamdani fuzzy method.

Below is the percentage of the comparison between the manual grouping and the planning system developed:

1. The Results of the Comparison of the Groups under the Reduced category within the Range of 349-547.
   The results obtained from the Groups under the Reduced category indicate no data in conformance to those by manual grouping.
   Based on Table 2, out of 16 existing data, there is 1 planning result in conformance to the actual data, and the rest of 15 planning results do not conform to the actual data. It can be seen that the data in conformance is 6.25% and those which do not conform are 93.75%.

Table 2: Comparison of Groups under the Reduced category within the Range of 349-547.

No	Dates	Production	Demand	Remains	Shortage	Actual Group	Mamdani Fuzzy Group	Remark
1	4 Jan	399	944	0	545	Reduced	Fixed	Not match
2	7 Jan	454	1208	0	754	Reduced	Fixed	Not match
3	15 Jan	414	857	0	443	Reduced	Fixed	Not match
4	17 Jan	447	945	0	498	Reduced	Fixed	Not match
5	19 Jan	533	867	0	334	Reduced	Fixed	Not match
6	23 Jan	422	966	0	544	Reduced	Fixed	Not match
7	25 Jan	454	1157	0	703	Reduced	Fixed	Not match
8	2 Feb	536	101	435	0	Reduced	Reduced	Match
9	4 Feb	435	1139	0	704	Reduced	Fixed	Not match
10	9 Feb	422	603	0	181	Reduced	Fixed	Not match
11	12 Feb	483	1175	0	692	Reduced	Fixed	Not match
12	15 Feb	460	720	0	260	Reduced	Fixed	Not match
13	18 Feb	529	765	0	236	Reduced	Fixed	Not match
14	20 Feb	349	1408	0	1059	Reduced	Added	Not match
15	25 Feb	444	910	0	466	Reduced	Fixed	Not match
16	28 Feb	374	897	0	523	Reduced	Fixed	Not match

2. The Results of the Comparison of the Groups under the Fixed category within the Range of 547-943.
   The results obtained for the groups under the Fixed category indicate three of the data are in conformance to those by manual grouping. Based on Table 3, of 26 existing data, there are 3 planning results in accordance with the actual data, and 23 other data have the planning results which do not conform to the actual data. It can be seen that the data in conformance is 11.538%, those not in conformance are 88.462%.

3. The Results of the Comparison of the Groups under the Added category within the Range of 943-1141.

Table 3: Comparison of the groups under the Fixed category within the Range of 547-943.

No	Dates	Production	Demand	Remains	Shortage	Actual Group	Mamdani Fuzzy Group	Remark
1	3 Jan	610	211	399	0	Fixed	Reduced	Not match
2	5 Jan	655	201	454	0	Fixed	Reduced	Not match
3	9 Jan	728	658	70	0	Fixed	Reduced	Not match
4	10 Jan	870	988	0	118	Fixed	Fixed	Sesuai
5	11 Jan	882	249	633	0	Fixed	Reduced	Not match
6	12 Jan	633	431	202	0	Fixed	Fixed	Sesuai
7	14 Jan	802	388	414	0	Fixed	Reduced	Not match
8	16 Jan	857	410	447	0	Fixed	Reduced	Not match
9	18 Jan	902	369	533	0	Fixed	Reduced	Not match
10	21 Jan	866	188	678	0	Fixed	Reduced	Not match
11	22 Jan	678	256	422	0	Fixed	Reduced	Not match
12	24 Jan	856	40	454	0	Fixed	Reduced	Not match
13	28 Jan	657	1525	0	868	Fixed	Added	Not match
14	30 Jan	665	981	0	316	Fixed	Fixed	Match
15	1 Feb	764	228	536	0	Fixed	Reduced	Not match
16	6 Feb	896	1822	0	926	Fixed	Added	Not match
17	8 Feb	620	198	422	0	Fixed	Reduced	Not match
18	11 Feb	819	336	483	0	Fixed	Reduced	Not match
19	13 Jan	818	193	625	0	Fixed	Reduced	Not match
20	14 Feb	625	165	460	0	Fixed	Reduced	Not match
21	16 Feb	740	211	529	0	Fixed	Reduced	Not match
22	19 Jan	764	415	349	0	Fixed	Reduced	Not match
23	22 Feb	842	180	662	0	Fixed	Reduced	Not match
24	23 Feb	662	218	444	0	Fixed	Reduced	Not match
25	26 Feb	734	154	580	0	Fixed	Reduced	Not match
26	27 Feb	580	206	374	0	Fixed	Reduced	Not match

The results obtained for the groups under the Added category indicate no conformance to those by manual grouping at all. Based on Table 4, out of 6 existing data all have planning results not in accordance with those of the actual data. It can be seen that the data in conformance is 100%.

Table 4: Comparison of the Groups under the Fixed category within the Range of 943-1141.

No	Dates	Production	Demand	Remains	Shortage	Actual Group	Mamdani Fuzzy Group	Remarks
1	8 Jan	964	218	728	0	Added	Reduced	Not match
2	26 Jan	997	310	687	0	Added	Reduced	Not match
3	29 Jan	962	297	665	0	Added	Reduced	Not match
4	31 Jan	984	220	764	0	Added	Reduced	Not match
5	7 Feb	1074	454	620	0	Added	Reduced	Not match
6	21 Feb	1141	299	842	0	Added	Reduced	Not match

4 Conclusion

Based on the results above, we can see that only 8.333% of the data have the planning results matching the actual results. At the same time, the remaining 91.667% are the data having the planning results not in accordance with the actual ones. The presentage of the data having the planning results not in accordance with the actual results shows that before applying the Mamdani fuzzy method, the production planning resulted in a large number of the remaining product units unsold or shortages of herbal products. The contribution of the Mamdani fuzzy method is to minimize the remains and shortage of stocks, and its implementation helps to optimize capital, customer satisfaction is improved, and much more. And the producers can easily take advantage of this method to expand their business.

References

[1] M. Abrori and A. H. Prihamayu. Aplikasi Logika Fuzzy Metode Mamdani dalam Pengambilan keputusan Penentuan Jumlah Produksi. *Kaunia: Integration and Interconnection of Islam and Science Journal* **11** (2) (2015) 91–99.

[2] A. Alamsyah and I. H. Muna. Metode Fuzzy Inference System untuk Penilaian Kinerja Pegawai Perpustakaan dan Pustakawan. *Scientific Journal of Informatics* **3** (1) (2016) 88–98.

[3] N. Apriyanti and H. Aksad. Penerapan Metode Fuzzy Mamdani dalam Perencanaan Produksi Roti. *Progresif: Jurnal Ilmiah Komputer* **9** (1) (2013) 861–918.

[4] K. Harefa. Penerapan Fuzzy Inference System untuk Menentukan Jumlah Pembelian Produk Berdasarkan Data Persediaan dan Penjualan. *Jurnal Informatika Universitas Pamulang* **2** (4) (2017) 205–213.

[5] D. Much. Penentuan Jumlah Produksi Dengan Aplikasi Metode Fuzzy Mamdani. *Jurnal Ilmiah Teknik Industri* **4** (2) (2005) 95–104.

[6] M. Y. Anshori, I. H. Santoso, T. Herlambang, M. Tafrikan, M. Adinugroho, K. Oktafianto and A. A. Firdaus. Analysis of Customer Satisfaction Survey on E-Wallets Using Simple Additive Weighting and TOPSIS Methods. *Nonlinear Dynamics and Systems Theory* **24** (1) (2024) 28–40.

[7] D. Mulyadi. The Implementation of Logic Fuzzy Mamdani Method as the Decision Support on the Gradual Selection of New Students. *The Management Journal of Binaniaga* **3** (2) (2018) 23–38.

[8] A. H. Nasuha, M. Hutasuhut and M. Ramadhan. Penerapan Metode Fuzzy Mamdani Untuk Menentukan Stok Produk Herbal Berdasarkan Permintaan dan Penjualan. *Jurnal media informatika budidarma* **3** (4) (2012) 313–323.

[9] S. Rizvi, J. Mitchell, A. Razaque, M. R. Rizvi and I. Williams. A Fuzzy Inference System (FIS) to Evaluate The Security Readiness of Cloud Service Providers. *Journal of Cloud Computing: Advances, Systems, dan Applications* **9** (42) (2020) 1–17.

[10] A. Y. Asih, B. Gunawan, N. Hidayati, T. Herlambang, D. Rahmalia and K. Oktafianto. Weights Optimization Using Firefly Algorithm for Dengue Fever Optimal Control Model by Vaccination, Treatment, and Abateseae. *Nonlinear Dynamics and Systems Theory* **23** (3) (2023) 237–248.

[11] M. Y. Anshori, I. H. Santoso, T. Herlambang, D. Rahmalia, K. Oktafianto and P. Katias. Forecasting of Occupied Rooms in the Hotel Using Linear Support Vector Machine. *Nonlinear Dynamics and Systems Theory* **23** (2) (2023) 129–140.

Nonlinear Dynamics and Systems Theory, **24** (2) (2024) 205–216

Analysis and Numerical Approximation of the Variable-Order Time-Fractional Equation

Abdelwahab Zarour * and Mohamed Dalah

University Frères Mentouri Constantine 1,
Faculty of Exact Sciences, Department of Mathematics,
P.O. Box, 325 Ain El Bey Way, Constantine 25017, Algeria,
MAM and Differential Equations Laboratory.

Received: October 1, 2023; Revised: March 3, 2024

Abstract: In this paper, we investigate a fully implicit finite scheme approximation equation (IFSAE) of the 1-D linear variable-order time-fractional diffusion equation (VOTFDE). The numerical method of solving differential equations by approximating them with difference equations is called the implicit finite difference method (IFDM). The first-order numerical scheme, stability, consistency and convergence of the method are proven. Moreover, the scheme is implemented on two test problems and some graphical results are offered to verify the theoretical analysis of the above scheme and illustrate the effectiveness of the suggested schemes.

Keywords: *fractional derivatives; discretization; implicit numerical scheme; stability; convergence.*

Mathematics Subject Classification (2010): 70K75, 93A30, 34K37, 65N06.

1 Introduction

Applied mathematics is the application of mathematical methods in various fields such as physics, engineering, medicine, biology, finance, economics, computer science and industry. Thus, applied mathematics is a combination of mathematics and engineering. Operational calculus, also called operational analysis, is a technique used to transform analytical problems, especially differential equations, into algebraic problems, usually the problem of solving a polynomial equation. Numerical analysis is the study of algorithms that use numerical approximation (as opposed to symbolic manipulations) to the problems of mathematical analysis (as distinct from discrete mathematics). This is the study

* Corresponding author: mailto:zarour.abdelwahab@umc.edu.dz

of numerical methods that attempt to find approximate solutions rather than exact solutions to problems. Numerical analysis is used in all areas of engineering and natural sciences and, in the 21st century, also in life and social sciences, medicine, economics and even in the arts.

Nonlinear dynamics is a hot topic in physics, complexity science, and theoretical biology. Nonlinear dynamics offers new ways of studying the numerical solution of the variable-order time-fractional reaction-diffusion equation (VOTFRDE), namely implicit and explicit finite difference methods. Motivated by the above facts and the literature [3–8], namely in this work, we consider the numerical solution of the variable-order time-fractional reaction-diffusion equation (VOTFRDE) in one-dimensional space, where the parameter alpha is a function depending on x and t. A numerical scheme was given in [5]– [12] for approximating the variable-order time-fractional reaction-diffusion equation (VOTFRDE). An Implicit Finite Difference Scheme method was applied for the variable-order time-fractional reaction-diffusion equation (VOTFRDE) with the Coimbra derivative. Moreover, the scheme is implemented on two test problems and some graphical results are offered to verify the theoretical analysis of the above scheme and illustrate the effectiveness of the suggested schemes.

The paper is organized in a clear and comprehensive manner, as follows. The construction of our mathematical model with boundary conditions is presented in Section 2. Section 3 develops the implicit finite difference scheme, which utilizes forward finite difference approximations for space derivatives and Caputo's concept for time-fractional derivatives. In Section 4, we study the stability of the approximate scheme by using the method of Fourier. Next, in Section 5, we prove the convergence of the approximate scheme obtained in Section 3. The final Section 6 completes and summarizes several numerical problems addressed using the method developed in Section 2. The numerical solutions are obtained using MATLAB and graphically visualized to provide a clear understanding of the results.

2 Implicit Finite Difference Scheme

For the numerical solution of the space fractional diffusion equations, implicit and explicit finite difference methods have been proposed in the literature [7], [8], [11], [16], [18] and [20] for the numerical solution of the time-fractional diffusion equation. We augment the implicit numerical scheme in this section. Let us take a variable-order time-fractional diffusion equation as an example

$$\begin{cases} \frac{\partial^\beta u}{\partial t^\beta} + c\frac{\partial u}{\partial x} = 0 \;\; 0 < x < L, 0 < t < T, 0 < \beta < 1, \\ u(0,t) = u(L,t) = 0, \\ u(x,0) = u_0(x). \end{cases} \tag{1}$$

3 Discretization and Development of the Scheme

Let $[0, L]$ be the clomain of inerest, we discretise the domain first.We define

$$x_i = ih, \text{ where } i = \overline{0, M}, \text{ and } t_j = jk, \text{ where } j = \overline{0, N},$$

where k represents the time step size and h represents the space step length.

Let us assume that

$$u(x_i, t_j) = u_i^j,$$

note that u_i^j is the numerical approximation of $u(x_i, t_j)$. Next, we consider the fractional-order diffusion Equation (1), where β is the fractional order. The variable-order fractional derivative of order $\beta(x,t)$ is defined by the Coimbra derivative and is written as

$$\frac{\partial^{\beta(x,t)}u(x,t)}{\partial t^{\beta(x,t)}} = \begin{cases} \frac{1}{\Gamma(1-\beta(x,t))}\int_0^t \frac{u_\xi(x,\xi)}{(t-\xi)^{\beta(x,t)}}d\xi \ \text{ if } \ 0<\beta<1, \\ u_t(x,t) \ \text{ if } \ \beta(x,t)=1. \end{cases} \tag{2}$$

Initially, as the boundary value problem needs to be discretized to be able to solve (1), it is first necessary to discretize the variable-order time-fractional derivative (2) as follows:

$$\begin{aligned} \frac{\partial^{\beta(x_i,t_{j+1})}u(x_i,t_{j+1})}{\partial t^{\beta(x_i,t_{j+1})}} &= \frac{1}{\Gamma(1-\beta(x_i,t_{j+1}))}\int_0^{t_{j+1}} \frac{u_\xi(x_i,\xi)}{(t_{j+1}-\xi)^{\beta(x_i,t_{j+1})}}d\xi \\ &= \frac{1}{\Gamma(1-\beta(x_i,t_{j+1}))}\sum_{s=0}^{j}\int_{sk}^{(s+1)k} \frac{u_\xi(x_i,\xi)}{(t_{j+1}-\xi)^{\beta(x_i,t_{j+1})}}d\xi, \end{aligned}$$

then we obtain

$$\frac{\partial^{\beta(x_i,t_{j+1})}u(x_i,t_{j+1})}{\partial t^{\beta(x_i,t_{j+1})}} = \frac{1}{\Gamma(1-\beta(x_i,t_{j+1}))}\sum_{s=0}^{j}\int_{sk}^{(s+1)k} \left(\frac{\partial u}{\partial \xi}\right)_i^{s+1} \frac{d\xi}{(t_{j+1}-\xi)^{\beta(x_i,t_{j+1})}}.$$

The first-order spatial derivative can be approximated by the following expression:

$$\left(\frac{\partial u}{\partial \xi}\right)_i^{s+1} = \frac{u_i^{s+1}-u_i^s}{k} + \Delta(k). \tag{3}$$

Adopting the discrete scheme given in (7), we discretize the variable-order time-fractional derivative as

$$\begin{aligned} \frac{\partial^{\beta(x_i,t_{j+1})}u(x_i,t_{j+1})}{\partial t^{\beta(x_i,t_{j+1})}} &= \frac{1}{\Gamma(1-\beta(x_i,t_{j+1}))}\sum_{s=0}^{j}\frac{u_i^{s+1}-u_i^s}{k}\int_{(j-s)k}^{(j-s+1)k}\frac{dy}{y^{\beta(x_i,t_{j+1})}} \\ &= \frac{1}{\Gamma(1-\beta(x_i,t_{j+1}))}\sum_{n=0}^{j}\frac{u_i^{j-n+1}-u_i^{j-n}}{k}\int_{nk}^{(n+1)k}\frac{dy}{y^{\beta(x_i,t_{j+1})}} \\ &= \frac{k^{-\beta(x_i,t_{j+1})}}{(1-\beta(x_i,t_{j+1}))\Gamma(1-\beta(x_i,t_{j+1}))}\sum_{n=0}^{j}(u_i^{j-n+1}-u_i^{j-n})[(n+1)^{1-\beta(x_i,t_{j+1})}-n^{1-\beta(x_i,t_{j+1})}]. \end{aligned}$$

Let $y = t_{j+1}-\xi$. We have $\Gamma(1+\beta)=\beta\Gamma(\beta)$, and expanding the summation for $n=0$, we reach

$$\begin{aligned} \frac{\partial^{\beta(x_i,t_{j+1})}u(x_i,t_{j+1})}{\partial t^{\beta(x_i,t_{j+1})}} = \frac{k^{-\beta(x_i,t_{j+1})}}{\Gamma(2-\beta(x_i,t_{j+1}))}\Bigg[u_i^{j+1}-u_i^j + \sum_{n=1}^{j}(u_i^{j-n+1}-u_i^{j-n}) \\ [(n+1)^{1-\beta(x_i,t_{j+1})}-n^{1-\beta(x_i,t_{j+1})}]\Bigg], \end{aligned} \tag{4}$$

where $b_i^{j+1}(n) = (n+1)^{1-\beta(x_i,t_{j+1})}-n^{1-\beta(x_i,t_{j+1})}, \ \forall j = \overline{0, N-1}$.

We will use the forward difference approximation of space derivative as follows:

$$\frac{\partial u(x_i,t_{j+1})}{\partial x} = \frac{u_{i+1}^{j+1} - u_i^{j+1}}{h} + \Delta(h). \tag{5}$$

Using approximations (3) and (5), the semi-linear diffusion equation (1), we obtain

$$\frac{k^{-\beta(x_i,t_{j+1})}}{\Gamma(2-\beta(x_i,t_{j+1}))}\left[u_i^{j+1} - u_i^j + \sum_{n=1}^{j}(u_i^{j-n+1} - u_i^{j-n})b_i^{j+1}(n)\right] + c\frac{u_{i+1}^{j+1} - u_i^{j+1}}{h} = 0, \tag{6}$$

$\forall i = \overline{1,M}$ and $\forall j = \overline{1,N}$, where

$$a_i^{j+1} = \frac{c.k^{\beta(x_i,t_{j+1})}.\Gamma(2-\beta(x_i,t_{j+1}))}{h}.$$

The initial and boundary conditions are

$$u_0(x_i) = u_i^0, \;\; \forall i = \overline{0,M},$$

$$u_0^{j+1} = u_M^{j+1} = 0, \;\; \forall j = \overline{0,N-1}.$$

We obtain the following approximate scheme for equation (1):

$$\begin{cases} a_i^{j+1}u_{i+1}^{j+1} + (1-a_i^{j+1})u_i^{j+1} = u_i^j - \sum_{n=1}^{j}(u_{i+1}^{j-n+1} - u_i^{j-n})b_i^{j+1}(n), \\ \qquad \forall i = \overline{1,M-1}, \;\; \forall j = \overline{1,N-1}, \\ u_0^{j+1} = u_M^{j+1} = 0, \;\; \forall j = \overline{0,N-1}, \\ u_i^0 = u_0(x_i), \;\; \forall i = \overline{0,M}. \end{cases} \tag{7}$$

3.1 Properties

The coefficients $b_i^{j+1}(n)$ for all $i = \overline{0,M}$ and $j = \overline{0,N-1}$, satisfy

- **P1:** $b_i^{j+1}(0) = 1$.
- **P2:** $0 < b_i^{j+1}(0) < 1$.

4 Stability of the Approximate Scheme

In this section, we use the method of the Fourier analysis to discuss the stability of the approximate scheme (7). Consider the following equation:

$$a_i^{j+1}u_{i+1}^{j+1} + (1-a_i^{j+1})u_i^{j+1} = u_i^j - \sum_{n=1}^{j}(u_{i+1}^{j-n+1} - u_i^{j-n})b_i^{j+1}(n), \tag{8}$$

$$\forall i = \overline{1,M-1}, \;\; \forall j = \overline{1,N-1}.$$

Now, we define the following function:

$$\begin{cases} u^j(x) = u_i^j, \;\; \text{if } \; x_{i-\frac{1}{2}} < x < x_{i+\frac{1}{2}}, \;\; \forall i = \overline{1,M-1}, \\ 0, \;\; \text{otherwise}, \end{cases}$$

where $u^j(x)$ has the Fourier series expansion

$$u^j(x) = \sum_{m=-\infty}^{+\infty} \xi_j(m) e^{\frac{2\pi m}{L}x}, \ \ \forall j = \overline{1, N-1},$$

where

$$\xi_j(m) = \frac{1}{L}\int_0^L u^j(x) e^{-\frac{2\pi m}{L}x} dx.$$

After that, using Parseval's theorem, we get

$$\int_0^L |u^j(x)|^2 dx = \sum_{m=-\infty}^{+\infty} |\xi_j(m)|^2, \ \ \forall j = \overline{1, N-1}.$$

Then, we obtain the following expression:

$$\int_0^L |u^j(x)|^2 dx = \sum_{i=1}^{M-1} |hu_i^j|^2, \ \ \forall j = \overline{0, N},$$

and

$$\|u^j\|_2^2 = \sum_{i=1}^{M-1} |hu_i^j|^2 = \sum_{m=-\infty}^{+\infty} |\xi_j(m)|^2, \ \ \forall j = \overline{0, N}.$$

Now, assume that the solution of the equation (8) has the form

$$u_i^j = \xi_j e^{\nu\tau h i}, \tag{9}$$

where $\tau = \frac{2\pi m}{L}$ and $\nu^2 = -1$. Next, we replace (9) in equation (8), then we have

$$\xi_{j+1}(1 + a_i^{j+1}(e^{\nu\tau h} - 1)) = \xi_j - \sum_{n=1}^{j} (\xi_{j-n+1} - \xi_{j-n}) b_i^{j+1}(n). \tag{10}$$

Equation (10) can be rewritten as

$$\xi_{j+1} = \frac{\xi_j - \sum_{n=1}^{j} (\xi_{j-n+1} - \xi_{j-n}) b_i^{j+1}(n)}{(1 + a_i^{j+1}(e^{\nu\tau h} - 1))}, \ \ \forall j = \overline{0, N-1}. \tag{11}$$

We have the following first result.

Theorem 4.1 *The implicit finite difference scheme* (7) *is unconditionally stable for* $0 < \beta < 1$ *if*

$$\exists C > 0, \ \ \|u^j\|_2 = |\xi_j| \leq C\|u^0\|_2 = C|\xi_0|, \ \ \forall j = \overline{0, N-1}.$$

Proof. We use the proof by recurrence for $j = 1$, in view of (11), we obtain the following majoration:

$$\begin{aligned} |\xi_1| &= \left| \frac{\xi_0}{(1 + a_i^{j+1}(e^{\nu\tau h} - 1))} \right| = \frac{|\xi_0|}{\sqrt{[1 + a_i^1(cos(\tau h) - 1)]^2 + (a_i^1 \sin(\tau h))^2}} \\ &= \frac{|\xi_0|}{|1 - 2a_i^1 \sin(\frac{\tau h}{2})|} \leq C|\xi_0|. \end{aligned}$$

Now, let C^0 be given by

$$C^0 = C = \frac{1}{|1 - 2a^1 \sin(\frac{\tau h}{2})|} \text{ such that } a^1 = \min_{0 \le i \le M}(-a_i^1).$$

We assume that the statement defined in (12) is true,

$$|\xi_j| \le C|\xi_0|, \ \forall j = \overline{1, N}, \tag{12}$$

and we prove that the statement defined by (13) is true,

$$|\xi_{j+1}| \le C|\xi_0|, \ \forall j = \overline{1, N}. \tag{13}$$

$$\begin{aligned}
|\xi_{j+1}| &= \left| \frac{\xi_j - \sum_{n=1}^{j}(\xi_{j-n+1} - \xi_{j-n}) b_i^{j+1}(n)}{(1 + a_i^{j+1}(e^{\nu\tau h} - 1))} \right| \\
&= \frac{|\xi_j - \sum_{n=1}^{j}(\xi_{j-n+1} - \xi_{j-n}) b_i^{j+1}(n)|}{\sqrt{[1 + a_i^{j+1}(cos(\tau h) - 1)]^2 + (a_i^{j+1}\sin(\tau h))^2}} \\
&\le \frac{|\xi_j| + \sum_{n=1}^{j}|\xi_{j-n+1} - \xi_{j-n}||b_i^{j+1}(n)|}{\sqrt{[1 + a_i^{j+1}(cos(\tau h) - 1)]^2 + (a_i^{j+1}\sin(\tau h))^2}} \\
&= \frac{|\xi_j| + \sum_{n=1}^{j}(|\xi_{j-n+1}| + |\xi_{j-n}|)}{\sqrt{[1 + a_i^{j+1}(cos(\tau h) - 1)]^2 + (a_i^{j+1}\sin(\tau h))^2}} \\
&= \frac{2N - 1}{|1 - 2a_i^{j+1}\sin(\frac{\tau h}{2})|}|\xi_0| \\
&\le (2N - 1)C^j|\xi_0| \le [(2N - 1)\max_{0 \le j \le N-1} C^j]|\xi_0| \\
&= C|\xi_0|,
\end{aligned}$$

where

$$C^j = \frac{1}{|1 + 2a^{j+1}\sin(\frac{\tau h}{2})|} \text{ such that } a^{j+1} = \min_{0 \le i \le M}(-a_i^{j+1}), \ \forall j = \overline{0, N-1},$$

then we obtain $C = (2N - 1)\max_{0 \le j \le N-1} C^j$. Finally, we get

$$|\xi_{j+1}| \le C|\xi_0|, \ \forall j = \overline{0, N-1},$$

and the approximate scheme (7) is unconditionally stable, which concludes the proof of Theorem 4.1.

5 Convergence of the Approximate Scheme

In this section, we use the method of the Fourier analysis to discuss the convergence of the error e_i^j, which is given by

$$e_i^j = u(x_i, t_j) - u_i^j. \tag{14}$$

Replacing (14) in equation (8), we obtain

$$a_i^{j+1}e_{i+1}^{j+1} + (1 - a_i^{j+1})e_i^{j+1} = e_i^j - \sum_{n=1}^{j}(e_{i+1}^{j-n+1} - e_i^{j-n})b_i^{j+1}(n) + r_i^j \tag{15}$$

$\forall i = \overline{1, M-1}$ and $\forall j = \overline{1, N-1}$. Then we obtain

$$r_i^j = k^{\beta(x_i,t_{j+1})}\Gamma(2 - \beta(x_i, t_{j+1}))[\Delta(k) + \Delta(h)].$$

Next, we define the following grid functions as follows:

$$e^j(x) = \begin{cases} e_i^j, & \text{if } x_{i-\frac{1}{2}} < x < x_{i+\frac{1}{2}}, \ \forall i = \overline{1, M-1}, \\ 0, & \text{otherwise}, \end{cases}$$

and

$$r^j(x) = \begin{cases} r_i^j, & \text{if } x_{i-\frac{1}{2}} < x < x_{i+\frac{1}{2}}, \ \forall i = \overline{1, M-1}, \\ 0, & \text{otherwise}. \end{cases}$$

Then $e^n(x)$ and $r^n(x)$ have the Fourier series expansions as follows:

$$e^j(x) = \sum_{m=-\infty}^{+\infty} \gamma_j(m) e^{\frac{2\pi m}{L}x}, \quad r^j(x) = \sum_{m=-\infty}^{+\infty} \lambda_j(mp) e^{\frac{2\pi m}{L}x}, \ \forall j = \overline{0, N}, \tag{16}$$

and

$$\gamma_j(m) = \frac{1}{L}\int_0^L e^j(x) e^{-\frac{2\pi m}{L}x} dx,, \quad \lambda_j(m) = \frac{1}{L}\int_0^L r^j(x) e^{-\frac{2\pi m}{L}x} dx. \tag{17}$$

After that, using Parseval's thorem, we obtain

$$\int_0^L |e^j(x)|^2 dx = \sum_{m=-\infty}^{+\infty} |\gamma_j(m)|^2, \quad \int_0^L |r^j(x)|^2 dx = \sum_{m=-\infty}^{+\infty} |\gamma_j(m)|^2, \ \forall j = \overline{0, N},$$

then the errors e^j and r^j take the following form:

$$\|e^j\|_2^2 = \sum_{i=1}^{M-1} |he_i^j|^2 = \sum_{m=-\infty}^{+\infty} |\gamma_j(m)|^2, \ \forall j = \overline{0, N}, \tag{18}$$

and

$$\|r^j\|_2^2 = \sum_{i=1}^{M-1} |hr_i^j|^2 = \sum_{m=-\infty}^{+\infty} |\lambda_j(m)|^2, \ \forall j = \overline{0, N}. \tag{19}$$

Next, we suppose that

$$e_i^j = \gamma_j e^{\nu\tau hi} \ , r_i^j = \lambda_j e^{\nu\tau hi}, \tag{20}$$

we replace (20) in equation (15), then we get

$$\gamma_{j+1}(1 + a_i^{j+1}(e^{\nu\tau h} - 1)) = \gamma_j - \sum_{n=1}^{j}(\gamma_{j-n+1} - \gamma_{j-n})b_i^{j+1}(n) + \lambda_j,$$

then

$$\gamma_{j+1} = \frac{\gamma_j - \sum_{n=1}^{j}(\gamma_{j-n+1} - \gamma_{j-n})b_i^{j+1}(n) + \lambda_j}{(1 + a_i^{j+1}(e^{\nu\tau h} - 1))}, \ \forall j = \overline{0, N-1}. \tag{21}$$

We get the following result.

Theorem 5.1 *The implicit finite difference scheme* (7) *is convergent for* $0 < \beta < 1$ *if*

$$\|e^j\|_2 = |\gamma_j| \leq C_1(k+h), \ \ \forall j = \overline{1, N}.$$

Proof. We use the proof by recurrence for $j = 1$, we have

$$|\gamma_1| = \left| \frac{\gamma_0 + \lambda_0}{(1 + a_i^1(e^{\nu\tau h} - 1))} \right| \leq \frac{|\gamma_0| + |\lambda_0|}{|1 - 2a_i^1 \sin(\frac{\tau h}{2})|} \leq \frac{|\lambda_0|}{|1 - 2a_i^1 \sin(\frac{\tau h}{2})|},$$

where $\gamma_0 = e_i^0 = u(x_i, 0) - u_i^0 = 0$.

By the convergence of the series on the right-hand side of (19), there is a positive constant C_2 such that

$$\exists C_2 > 0, \ \ |r_i^0| \leq C_2(k+h), \ \ \forall i = \overline{0, M},$$

then we obtain

$$\exists C_2 > 0, \ \ \|r^0\|_2 = |\lambda_0| \leq C_2\sqrt{L}(k+h),$$

so

$$|\gamma_1| \leq \frac{C_2\sqrt{L}(k+h)}{|1 - 2a_i^1 \sin(\frac{\tau h}{2})|} \leq \frac{C_2\sqrt{L}(k+h)}{|1 - 2a^1 \sin(\frac{\tau h}{2})|} = C_1(k+h)$$

such that

$$a^1 = \min_{0 \leq i \leq M}(-a_i^1),$$

and

$$C^0 = \frac{1}{|1 - 2a^1 \sin(\frac{\tau h}{2})|} \ \text{ such that } \ C_1 = C^0 C_2\sqrt{L},$$

then we obtain

$$|\gamma_1| \leq C_1(k+h).$$

We assume that the following statement is true:

$$\|e^j\|_2 = |\gamma_j| \leq C_1(k+h), \ \ j = \overline{1, N}, \tag{22}$$

and we prove that the following statement is true:

$$\|e^{j+1}\|_2 = |\gamma_{j+1}| \leq C_1(k+h), \ \ j = \overline{0, N-1}. \tag{23}$$

One can see that $|\gamma_{j+1}|$ satisfies

$$\begin{aligned}
|\gamma_{j+1}| &= \left| \frac{\gamma_j - \sum_{n=1}^{j}(\gamma_{j-n+1} - \gamma_{j-n})b_i^{j+1}(n) + \lambda_j}{(1 + a_i^{j+1}(e^{\nu\tau h} - 1))} \right| \\
&= \left| \frac{\gamma_j - \sum_{n=1}^{j}(\gamma_{j-n+1} - \gamma_{j-n})b_i^{j+1}(n) + \lambda_j}{1 - 2a_i^{j+1} \sin(\frac{\tau h}{2})} \right| \\
&\leq \frac{|\gamma_j| + \sum_{n=1}^{j}(|\gamma_{j-n+1}| + |\gamma_{j-n}|)|b_i^{j+1}(n)| + |\lambda_j|}{|1 - 2a_i^{j+1} \sin(\frac{\tau h}{2})|} \\
&\leq \frac{2N - 1}{|1 - 2a_i^{j+1} \sin(\frac{\tau h}{2})|} C_1(k+h) + \frac{|\lambda_j|}{|1 - 2a_i^{j+1} \sin(\frac{\tau h}{2})|}.
\end{aligned}$$

By the convergence of the series on the right-hand side of (19), there is a positive constant C_2 such that

$$\exists C_2 > 0, \ |r_i^j| \leq C_2(k+h), \ i = \overline{0,M}, \ \forall j = \overline{0,N}.$$

Thereafter, we obtain

$$\exists C_2 > 0, \ \|r^j\|_2 = |\lambda_j| \leq C_2\sqrt{L}(k+h), \ \forall j = \overline{0,N},$$

then $|\gamma_{j+1}|$ becomes as follows:

$$\begin{aligned} |\gamma_{j+1}| &\leq \frac{2N-1}{|1-2a_i^{j+1}\sin(\frac{\tau h}{2})|}C_1(k+h) + \frac{1}{|1-2a_i^{j+1}\sin(\frac{\tau h}{2})|}C_2\sqrt{L}(k+h) \\ &\leq CC_1(k+h) + \frac{CC_2\sqrt{L}}{2N-1}(k+h) \end{aligned}$$

such that $C = (2N-1)\max_{0\leq j\leq N-1} C^j$, where C^j is given by

$$C^j = \frac{1}{|1+2a^{j+1}\sin(\frac{\tau h}{2})|} \ \text{ such that } \ a^{j+1} = \min_{0\leq i\leq M}(-a_i^{j+1}), \ j = \overline{0,N-1}.$$

Let

$$L = \left(\frac{C_1(1-C)(2N-1)}{CC_2}\right)^2.$$

Subsequently, we can obtain

$$|\gamma_{j+1}| \leq CC_1(k+h) + \frac{CC_2\sqrt{L}}{2N-1}(k+h) = C_1(k+h).$$

Finally, we obtain

$$\|e^j\|_2 \leq C_1(k+h), \ \forall j = \overline{0,N-1}.$$

So the implicit finite difference scheme (7) is convergent, which concludes the proof of Theorem 5.1.

5.1 Solvability of the approximate scheme

Theorem 5.2 *The approximate scheme* (24) *is uniquely solvable.*

It can be seen that the corresponding homogeneous linear algebraic equations for the approximate scheme (24) are

$$\begin{cases} a_i^{j+1}u_{i+1}^{j+1} + (1-a_i^{j+1})u_i^{j+1} = u_i^j - \sum_{n=1}^{j}(u_{i+1}^{j-n+1} - u_i^{j-n})b_i^{j+1}(n), \\ \forall i = \overline{1,M-1} \ \text{ and } \ \forall j = \overline{1,N-1}, \\ u_0^{j+1} = u_M^{j+1} = 0, \ \forall i = \overline{0,M} \ \text{ and } \ \forall j = \overline{0,N-1}, \\ u_i^0 = 0, \ \text{ for all } \ i = \overline{0,M}. \end{cases} \tag{24}$$

Proof. Similar to the proof of Theorem 4.1, we can also verify the solutions of the equations (24) satisfy $\|u^j\|_2 \leq C\|u^0\|$, for all $j = \overline{1,N}$, we have $u^0 = 0$, so we get $u^j = 0$ for all $j = \overline{1,N}$.

This indicates that the equations (24) have only zero solutions, the approximate scheme (24) is uniquely solvable. We now easily conclude the proof of Theorem 5.2.

6 Numerical Experiments

In this section, two numerical examples are discussed to confirm the effectiveness of the developed implicit difference scheme (IFDS).

Example 1. This first example is concerned with the numerical solution of the linear variable-order time-fractional diffusion equation with initial and boundary conditions, where the first order derivative is substituted by a Caputo fractional derivative of order β $(0 < \beta < 1)$. Consider the 1-D linear variable-order time-fractional diffusion equation with initial and boundary conditions:

$$\begin{cases} \frac{\partial^\beta u}{\partial t^\beta} + c\frac{\partial u}{\partial x} = 0 \ \ 0 < x < L, 0 < t < T, 0 < \beta < 1, \\ u(0,t) = u(L,t) = 0, \\ u(x,0) = u_0(x). \end{cases} \tag{25}$$

Specifically, we consider the model problem in (25) over $x \in [0;1]$, $t \in [0;1]$, $L = 1$, $T = 1$, $\beta = e^{-x-t}$, $c = 0.5$, $N = M = 50, 100, 150, 200$ and $u_0(x) = 1 - 0.3 * \cos(pi * x)$. We present several numerical experiments to support the theoretical and numerical analyses of the previous sections.

Example 2. We first fix in the mathematical model defined by (26), the values of $x \in [0;1]$, $t \in [0;1]$, $L = 1$, $T = 1$, $\beta = e^{-x*t}$, $c = 0.75$, $N = M = 20, 30, 40, 50$ and $u_0(x) = 1 - 0.5 * pi * x$. We present several numerical experiments to support the theoretical and numerical analyses of the previous sections.

$$\begin{cases} \frac{\partial^\beta u}{\partial t^\beta} + c\frac{\partial u}{\partial x} = 0 \ \ 0 < x < L, 0 < t < T, 0 < \beta < 1, \\ u(0,t) = u(L,t) = 0, \\ u(x,0) = u_0(x). \end{cases} \tag{26}$$

In this example, we present different numerical experiments to support the theoretical and numerical analyses of the previous sections.

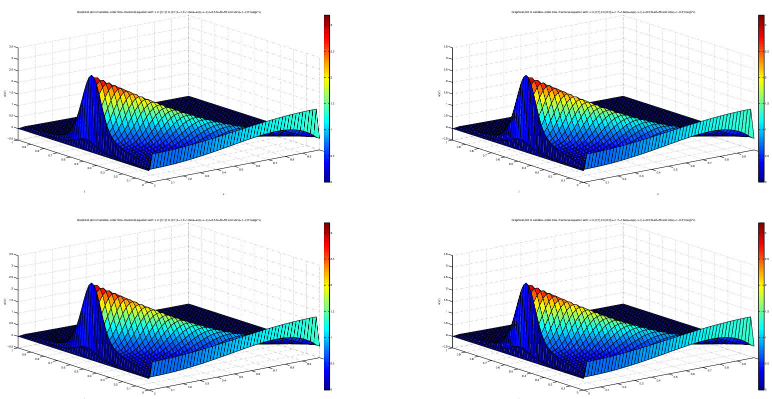

Figure 1. Example 1: Plot of LVTFDE: $\beta = e^{-x-t}$, $c = 0.50$, $u_0(x) = 1 - 0.3 * cos(pi * x)$ $N = M = 50, 100, 150, 200$, $L = T = 1$, $0 < \beta < 1$.

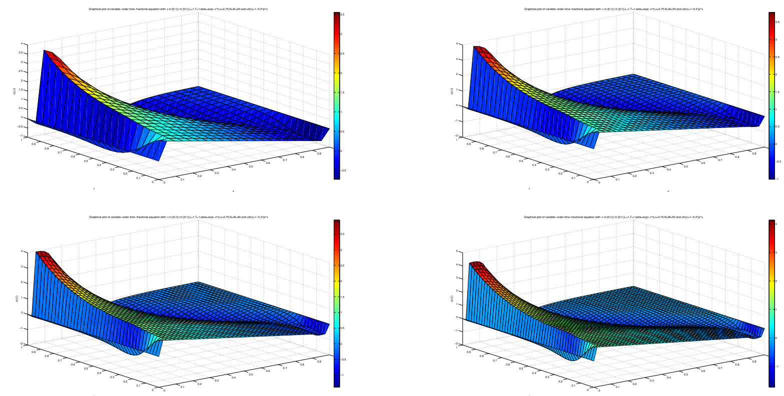

Figure 2. Example 2: Plot of LVTFDE: $\beta = e^{-x*t}$, $c = 0.75$, $u_0(x) = 1 - 0.5 * pi * x$, $N = M = 20, 30, 40, 50$, $L = T = 1$, $0 < \beta < 1$.

Conclusion

In this paper, we consider a numerical approximation method to solve a fractional model for the advection-reaction-diffusion equation with the Coimbra derivative. By using finite difference schemes and obtaining the operational matrix, all that remains is to solve fractional partial differential equations. Some examples are given to illustrate the effectiveness of the proposed numerical algorithm. In several cases, the capabilities of the program developed with MATLAB were reached in terms of meshes and calculation times.

Acknowledgment

We thank the referee for the careful and insightful review of our manuscript. We address all of the concerns of the referee here. The author thanks the anonymous referees for their helpful comments that improved the quality of the manuscript. We revised the manuscript according to your respected advice and the referee's detailed suggestions.

References

[1] K. B. Oldman and J. Spanier. *The Fractional Calculus.* Academic Press, 1974.

[2] K. S. Miller and B. Ross. *An Introduction to the Fractional Calculus and Fractional Differential Equations.* John Wiley, New York, London, 1993.

[3] S. G. Samko, A. A. Kilbas and O. I. Marichev. *Fractional Integrals and Derivatives.* Gordon and Breach Sciences Publishers, 1993.

[4] I. Podlubny. *Fractional Differential Equations.* Academic Press. 1999.

[5] R. D. Richtmyer and K. W. Morton. *Difference Methods for Initial-Value Problems.* Interscience Publishers, New York, 1967.

[6] K. Diethelm and A. D. Freed. On the solution of nonlinear fractional order differential equations used in the modelling of viscoplasticity Scientific Computing in Chemical Engineering II: In: *Computational Fluid Dynamics, Reaction Engineering and Molecular Properties, Springer Verlag, Heidelberg*, 1999, 217–224.

[7] F. Liu, P. Zhuang, V. Anh and I. Turner. A fractional-order implicit difference approximation for the space-time fractional diffusion equation. *ANZIAM J.* **47** (2006) 48–68.

[8] T. A. M. Langlands and B. I. Henry. The accuracy and stability analysis of an implicit solution method for the fractional diffusion equation. *J. Comp. Phys.* **205** (2005) 719–736.

[9] D. Y. Goos and G. F. Reyero. Mathematical analysis of a cauchy problem for the time-fractional diffusion-wave equation with α in [0, 2]. *J. Fourier. Anal.* (2016) 1–23.

[10] Z. Wang and S. Vong. Compact difference schemes for the modified anomalous fractional sub-diffusion equation and the fractional diffusion-wave equation. *J. Comput. Phy.* **277** (2014) 1–15.

[11] E. Afshari, B. Sepehrian and A. M. Nazari. Finite difference method for solving the space-time fractional wave equation in the Caputo form, *Fract. Diff. Eqn.* **5** (1) (2015) 55–63.

[12] U. Ali, M. Sohail, M. Usman, F. A. Abdullah, I. Khan and K. S. Nisar. Fourth-Order Difference Approximation for Time-Fractional Modified Sub-Diffusion Equation. *Syemmetry* **12** (2020) 1–11.

[13] M. Dehghan, J. Manafian and A. Saadatmandi. Solving nonlinear fractional partial differential equations using the homotopy analysis method. *Numerical Methods Partial Diff. Eqs.: Int. J.* **26** (2) (2010) 448–479.

[14] M. Dehghan, J. Manafian and A. Saadatmandi. The solution of the linear fractional partial differential equations using the homotopy analysis method. *Zeitschrift für Naturforschung-A* **65** (11) (2010) 935–949.

[15] J. Singh, D. Kumar, Z. Hammouch and A. Atangana. A fractional epidemiological model for computer viruses pertaining to a new fractional derivative. *Appl. Math. Comput.* **316** (2018) 504–515.

[16] S. A. Osman and T. A. M. Langlands. An implicit Keller Box numerical scheme for the solution of fractional sub-diffusion equations. *Appl. Math. Comput.* **348** (2019) 609–626.

[17] K. D. Dwivedi, S. Das and D. Baleanu. Numerical Solution of Nonlinear Space-Time Fractional-Order Advection-Reaction-Diffusion Equation, *J. Comput. Nonlinear Dyn.* **15** (6) (2020) 1–8.

[18] M. Meerschaert and C. Tadjeran. Finite difference approximations for two-sided space-fractional partial differential equations. *Appl. Numer. Math.* **56** (2006) 80–90.

[19] J. H. He. Approximate analytical solution for seepage flow with fractional derivatives in porous media. *Comput. Methods Appl. Mech. Eng.* **167** (1–2) (1998) 57–68.

[20] C. Tadjeran and M. M. Meerschaert. A second-order accurate numerical method for the two dimensional fractional diffusion equation. *J. Comput. Phys.* **220** (2007) 813–823.